

**A solar assisted high temperature refrigeration system for
postharvest pre-storage fruit cooling**

By

FOUAD M. ALKILANI

Thesis submitted in fulfilment of the requirements for the degree

Master of Engineering: Mechanical Engineering

in the Faculty of Engineering at the

Cape Peninsula University of Technology

Supervisor: Mr. Kant. Kanyarusoke

Co-supervisor: Dr. O. Nemraoui

Bellville

February 2017

CPUT copyright information

The dissertation/thesis may not be published either in part (in scholarly, scientific or technical journals), or as a whole (as a monograph), unless permission has been obtained from the University

DECLARATION

I, FOUAD M. ALKILANI, declare that the contents of this dissertation/thesis represent my own unaided work, and that the dissertation/thesis has not previously been submitted for academic examination towards any qualification. Furthermore, it represents my own opinions and not necessarily those of the Cape Peninsula University of Technology.

Signed

Date

ABSTRACT

Agriculture has emerged as a major economic activity in the African continent. Therefore, fruits and vegetables are considered as essential source of vitamins, minerals and proteins. However, fruits and vegetables are perishing rapidly. Thus, the adequate handling starts from the field, by applying appropriate method of storage and preservation in order to reduce post-harvest losses and extend its shelf life.

Preservation by removing heat from the products is the most common method of preservation. In rural areas, the access to the grid is expensive or in some cases impossible. Therefore, researchers have been paying more attention to find alternative sources of power to run the cooling units.

This study provides proof of a concept for the use of solar energy to cool down harvested fruits and vegetables at the farm level to an adequate farm storage temperature. The target storage temperature range is between 5 and 15 °C. A model refrigerator was designed and constructed in the mechanical engineering workshop of Cape Peninsula University of Technology. It was installed and tested in outdoor conditions to get the effect of different weather conditions. The model consists of a typical vapour compression system powered by a 12 V solar PV system. A DC compressor was used, and therefore, there is no inverter. The model was first tested without a product and then with 20 kg batches of different fruits for a period of two weeks in April 2016. Wind speed, ambient temperature and solar radiation intensity data were monitored and collected from a Campbell Scientific weather station mounted on the roof adjacent to the model. By monitoring the temperatures and compressor current hourly, the refrigeration effect, power consumption and coefficient of performance were determined. The overall COP based on input solar energy was 2.8. It was thus proved that a suitably sized PV system could be designed and implemented at farm level to cool harvested fruits from ambient to storage temperature without the use of an inverter. This could go some way to helping retard deterioration of fruits and vegetables before delivery to a marketplace or to storage.

ACKNOWLEDGEMENTS

I wish to thank and express my gratitude to

- Messrs. Kant. Kanyarusoke and D. O. Nemraoui for their supervision of this thesis. I wish to thank them for all their advice, counselling, support, guidance and constructive criticism which helped to accomplish this work.
- The staff of the Mechanical Engineering Workshop for their assistance.

DEDICATION

I would like to dedicate this thesis to my family and friends.

TABLE OF CONTENTS

DECLARATION.....	II
ABSTRACT	III
ACKNOWLEDGEMENTS.....	IV
TABLE OF CONTENTS	VI
CHAPTER 1 INTRODUCTION	1
1.1 BACKGROUND OF THE RESEARCH PROBLEM	1
1.1.1 Food processing	1
1.1.2 Refrigeration.....	2
1.1.3 Temperature ranges of refrigeration systems	3
1.1.3.1 High-temperature refrigeration applications	3
1.1.3.2 Medium-temperature refrigeration	5
1.1.3.3 Low-temperature refrigeration	5
1.1.3.4 Cryogenics.....	6
1.1.4 Problem Statement.....	7
1.1.5 Post-harvest losses	7
1.1.5.1 Post-harvest loss causes.....	8
1.1.5.2 Preservation processes	8
1.1.5.3 Precooling process	9
1.1.6 Solar Energy.....	10
1.1.7 Solar Radiation	10
1.1.8 Solar PV collector.....	12
1.1.8.1 Grid- connected systems.....	13
1.1.8.2 1.1.8.2 Hybrid PV systems	13
1.1.8.3 Stand-alone systems	14
1.1.9 Solar refrigeration.....	14
1.1.9.1 Solar thermal refrigeration.....	14
1.1.9.2 Solar electric refrigeration	15
1.1.9.3 Vapor-compression cycle	15
1.1.10 Thermodynamic analysis of vapor-compression refrigeration cycle	17
1.1.11 Practical vapour-compression refrigeration system.....	18
1.2 PROJECT OBJECTIVES.....	19
1.2.1 Main objective	19
1.2.2 Specific objectives.....	19
1.3 DELIMITATION OF THE RESEARCH	19
1.4 THESIS ORGANIZATION	20
CHAPTER 2 DESIGN AND CONSTRUCTION OF THE SOLAR PV REFRIGERATION SYSTEM	21
2.1 INTRODUCTION.....	21
2.2 DESIGN COOLING SYSTEM	21
2.2.1 Cabinet construction.....	21
2.2.1.1 Cabinet size	22
2.2.1.2 Cabinet volume	22
2.2.2 Heat load in cooling unit.....	23
2.2.2.1 Transmission load.....	23
2.2.2.2 Infiltration load.....	25
2.2.2.3 Product heat load.....	25
2.2.2.4 Miscellaneous load.....	27

2.2.3	<i>Temperature establishment</i>	28
2.2.4	<i>Heat load calculation</i>	28
2.2.5	<i>Compressor selection and specification</i>	30
2.2.6	<i>Evaporator design</i>	31
2.2.7	<i>Condensing unit</i>	32
2.2.8	<i>Throttling device</i>	33
2.3	SOLAR PV SYSTEM	33
2.3.1	<i>PV modules</i>	33
2.3.2	<i>Charge controller</i>	35
2.3.3	<i>Solar batteries</i>	36
2.4	SIZING SOLAR PV SYSTEM	37
2.4.1	<i>Estimate solar radiation at the site</i>	37
2.4.2	<i>Determine the total power demands</i>	37
2.4.3	<i>Sizing PV modules</i>	38
2.4.4	<i>Battery sizing</i>	38
2.4.1	<i>Refrigeration system construction</i>	39
CHAPTER 3 EXPERIMENTAL SETUP AND METHODOLOGY		42
3.1	MODEL TESTING	42
3.1.1	<i>Testing procedure</i>	42
3.1.2	<i>Measured data and instrumentation</i>	42
3.2	EXPERIMENTAL SETUP AND METHODOLOGY	47
3.3	SOLAR RADIATION ESTIMATION	49
3.4	COEFFICIENT OF PERFORMANCE OF THE REFRIGERATION SYSTEM	52
CHAPTER 4 RESULTS AND DISCUSSION		54
4.1	INTRODUCTION	54
CHAPTER 5 CONCLUSIONS AND RECOMMENDATIONS		65
5.1	SUMMARY	65
5.2	CONCLUSION	65
5.3	RECOMMENDATION FOR FUTURE WORK	66
	• AN INVESTIGATION ON THE EFFECT OF THE DIRECT SUNLIGHT INCIDENT ON THE COOLING COMPARTMENT WALLS COULD INCREASES THE HEAT LEAKAGE TO THE SYSTEM AND INFLUENCES ON THE SYSTEM PERFORMANCE	66
REFERENCES		63
APPENDICES		70

LIST OF FIGURES

FIGURE 1.1: MAGNETIZING AND DEMAGNETIZING PROCESS	4
FIGURE 1.2: (A) SCHEMATIC DIAGRAM OF A TWO-STAGE VAPOUR-COMPRESSION SYSTEM, (B) TEMPERATURE-ENTROPY (T-S) DIAGRAM.....	6
FIGURE 1.3: WORLD SOLAR RADIATION MAP	11
FIGURE 1.4: SOLAR PV COMBINATION.....	13
FIGURE 1.5: (A) SCHEMATIC DIAGRAM OF A VAPOR-COMPRESSION REFRIGERATION SYSTEM, (B) THE TEMPERATURE - ENTROPY (T-S) DIAGRAM.....	16
FIGURE 1.6: AN IDEAL VAPOR-COMPRESSION REFRIGERATION SYSTEM AND (T – S) DIAGRAM.	19
FIGURE 2.1: CROSS SECTION OF A CABINET’S SURFACE.....	22
FIGURE 2.2: AIR-COOLED EVAPORATOR	32
FIGURE 2.3: THE MAIN COMPONENTS IN PV MODULE.	34
FIGURE 2.4: SOLAR PV SYSTEM COMPONENTS.....	39
FIGURE 2.5: THE PIPES ALIGNMENT OF THE REFRIGERATION SYSTEM.....	40
FIGURE 2.6: OXY-ACETYLENE WELDING.....	40
FIGURE 2.7: REFRIGERATION SYSTEM CHARGING PROCESS.....	41
FIGURE 3.1: CAMPBELL SCIENTIFIC WEATHER STATION.....	43
FIGURE 3.2: SCHEMATIC DIAGRAM OF THE KIPP & ZONEN CMP06 PYRANOMETER	44
FIGURE 3.3: KIPP & ZONEN SP-LITE SILICON PYRANOMETER	44
FIGURE 3.4: 03101 R.M YOUNG ANEMOMETER.....	45
FIGURE 3.5: ETEKCITY MSR-C600 DIGITAL CLAMP METER	46
FIGURE 3.6: DIGITAL THERMOMETERS.....	47
FIGURE 3.7: EXPERIMENTAL SET-UP: (A) ACTUAL LAYOUT, (B) WIRING DIAGRAM.....	48
FIGURE 3.9: SOLAR ANGLES ON INCLINED PV PANEL.....	51
FIGURE 3.10: ACTUAL VAPOUR-COMPRESSION SYSTEM AND ITS T-S DIAGRAM.....	53
FIGURE 4.1: VARIATION OF WEATHER CONDITION WITH LOCAL TIME ON 18APRIL 2016 AT CAPE PENINSULA UNIVERSITY OF TECHNOLOGY.....	55
FIGURE 4.2: VARIATION OF SOLAR RADIATION ON HORIZONTAL SURFACE AND INCLINED PV PANEL MEASURED ON 18 APRIL 2016.....	56
FIGURE 4.3: VARIATION OF BEAM, DIFFUSE AND DIRECT SOLAR RADIATION WITH LOCAL TIME ON 19 APRIL 2016	57
FIGURE 4.4: VARIATION OF THE TEMPERATURE OF THE OUTSIDE SURFACES OF THE COOLING ROOM WALLS	57
FIGURE 4.5: VARIATION OF AMBIENT AND PRODUCT TEMPERATURE ON 18 APRIL 2016	58
FIGURE 4.6: VARIATION OF THE STACKED FRUIT AT FIRST DAY OF STORAGE	59
FIGURE 4.7: VARIATION OF THE TEMPERATURE DISTRIBUTION IN THE SECOND DAY OF STORAGE.....	59
FIGURE 4.8: THE DIFFERENCE BETWEEN AMBIENT AND FRUIT TEMPERATURE IN THE SECOND DAY OF STORAGE	60
FIGURE 4.9: VARIATION OF AMBIENT, OUTSIDE WALL AND INSIDE COOLING ROOM TEMPERATURE.....	61
FIGURE 4.10: VARIATION OF COEFFICIENT OF PERFORMANCE OF THE COOLING SYSTEM ON 18 APRIL 2016	61
FIGURE 4.11: THE TOTAL HEAT LOAD DURING THE FIRST DAY OF STORAGE.....	62
FIGURE 4.12: COMPARISON BETWEEN A HEAT LOAD OF THE PV REFRIGERATION MODEL WITH LOADED AND EMPTY COOLING SPACE	62

FIGURE 4.13: THE IMPACT OF AMBIENT TEMPERATURE ON TOTAL HEAT LOAD OF REFRIGERATION SYSTEM. 63

FIGURE 4.14: COMPARISON BETWEEN COMPRESSOR POWER CONSUMPTION..... 64

LIST OF TABLES

Table 1.1: The storage condition of some fruits and vegetables.....	10
Table 2.1: Cabinet surface specification.....	24
Table 2.2: The coefficients f and g for various products.....	25
Table 2.3: Heat of respiration of some fruits and vegetables in different storage temperature.....	26
Table 2.4: Evaporator fan specification.....	27
Table 2.5: Allowance for sun effect.....	28
Table 2.6: The respiration heat load for different type of products.....	29
Table 2.7: Compressor specification.....	30
Table 2.8: PV module specification.....	34
Table 2.9: Comparative between the two types of charge controller.....	35
Table 2.10: Annual solar radiation of CPUT Bellville.....	36
Table 3.1: Value of n	37
Table D-1: Measured data on 11 April 2016.....	82
Table D-2: Measured data on 12 April 2016.....	83
Table D-3: Measured data on 13 April 2016.....	84
Table D-4: Measured data on 14 April 2016.....	85
Table D-5: Measured data on 15 April 2016.....	86
Table D-6: Measured data on 18 April 2016.....	87
Table D-7: Measured data on 19 April 2016.....	88
Table D-8: Measured data on 20 April 2016.....	89
Table E-1: Measured data on 12 April 2016.....	90
Table E-2: Measured data on 13 April 2016.....	90
Table E-3: Measured data on 14 April 2016.....	91
Table E-4: Measured data on 18 April 2016.....	91
Table E-5: Measured data on 19 April 2016.....	92
Table E-6: Measured data on 20 April 2016.....	92
Table E-7: Ampere-hour consumed by the DC compressor.....	93

Nomenclature

Symbol	Description	Unit
\dot{m}	Mass flow rate	kg/s
h	Enthalpy	kg/kJ
A	Area	m^2
U	Heat transfer coefficient	$W/m^2.K$
K	Thermal conductivity	$W/m.K$
m	Mass	kg
I	Solar radiation flux	W/m^2
c_p	Specific heat	$kJ/kg.k$
Q	Heat energy	kJ
T	Temperature	$^{\circ}C$
n	Day of year	
R_b	Ratio of beam radiation on inclined Surface to that on horizontal plane	-
H	Altitude	m
L	Latitude	degree
I_{sc}	Solar constant	W/m^2
ρ_g	Ground reflectivity	-

Greek symbols	Description	Unit
β	Solar still cover inclination	Degrees
θ_i	Incident angle	Degrees
θ_z	Zenith angle	Degrees
ω	Hour angle	Degrees
δ	Declination angle of the sun	Degrees

Chapter 1 Introduction

1.1 Background of the research problem

1.1.1 Food processing

Food, air, and water are essential to human life. Food provides energy to our bodies and supplies necessary chemicals for growth and protection against diseases. Thus the need for fresh food has continuously grown due to high demand for healthy and convenient diets in urban fast-paced daily life. Fresh fruits and vegetables are the most consumed food products. They are rich with minerals and vitamins which are necessary for the body's activities. Because most fruit and vegetable products are perishable by nature and they are seasonal, they must be preserved and stored in controlled conditions before long term consumption.

For hundreds of years, our predecessors have found several ways to protect their food from spoilage. Drying, smoking, salting, and pickling are the most common methods that they used. In addition to that, some of those living in cold areas used cold caves as storage areas to preserve their food. Despite the variety in fruit preservation methods, preservation by removing heat is considered the most common method. This method reduces the activity of microorganisms and enzymes of fruits. It also depresses the chemical reaction rates (Berk, 2013). As a result, fruits can keep their nutritional value and sensory quality (taste, texture, flavor, color and appearance) in desirable conditions.

The growing demand for fresh fruits has encouraged researchers to become interested in each process of preservation. Precooling is the first of these processes. It should be done as soon after harvest as possible. The main purpose of this process is to remove field heat and keep the product in a precooling unit before loading into a transport vehicle or even a larger on-farm storage room. Precooling units can be installed close to the field to reduce delay in cooling process. Because most fields are located far away from urban areas, access to grid service is difficult or expensive. The need for an alternative energy source has motivated researchers to try to find a solution to this challenge. Renewable energy forms such as wind, solar, biomass, and hydro are considered to provide the best source of power for this purpose.

1.1.2 Refrigeration

Hundreds of years ago, people noticed an interesting phenomenon of water producing a cooling effect when it is evaporating. At the beginning, they did not attempt to understand or explain of this phenomenon. But in earlier times, the ancient Egyptians used evaporation to chill jars of water. After that, Indians employed this method to make ice (Dincer & Kanoglu, 2010). They were keeping water in the porous pots open during the night. The evaporation of water in cool dry air caused the formation of ice (Prasad, 2006).

The first attempts to produce cold by mechanical processes was in 1784, when William Coolen at the University of Glasgow produced refrigeration by creating partial vacuum over ethyl ether (Arora, 2010). He used a hand-operated compressor machine to run the system.

All of this led to the appearance and development of artificial refrigeration and air conditioning systems. In terms of comfort, residential air conditioning took place in the United States of America in the late of 1950s (Whitman, Johnson, & Tomczyk, 2005).

In the last few decades, there has been considerable diversification in the development of refrigeration systems leading to new inventions such as solar power vapor-absorption system, steam-jet refrigeration, cryogenics, etc. Now a day, refrigeration and air conditioning application plays a remarkable role in our daily lives whether in domestic or commercial application such as food preservation, comfort control, food and beverage production, gas liquefaction, medicine purposes, electronic cooling, and so on. Refrigeration and air conditioning systems can be classified according to their application as follows:

- **Domestic refrigeration**

Domestic refrigeration refers to units which are designed for household uses such as refrigerators, freezers, window type air conditioning, and other unit with low capacity. These units are plug-in appliance which can be moved from one position to another (Whitman, Johnson, Tomczyk & Silberstein, 2012).

- **Commercial refrigeration**

Commercial refrigeration refers to units with large capacity than the domestic units. They are used by retailer outlets for storage and display frozen and fresh food and beverages.

- **Industrial refrigeration**

Industrial refrigeration refers to units providing cooling for large-scale processes such as food manufacturing and other similar processes which require controlled temperature.

- **Transport refrigeration and air conditioning**

Transport refrigeration refers to units that have been designed to control the temperature of any food stuff during transportation. It is considered a link between the food centers and the consumer's out-let point. It includes trucks, containers and trailers. All of these can be called reefer units.

1.1.3 Temperature ranges of refrigeration systems

The temperature ranges for refrigeration systems refer to the temperature of the refrigerated chamber. To be more specific, it is the boiling temperature of the refrigerant in the evaporator. In this field of industry, the temperature ranges of refrigeration can be divided into:

1.1.3.1 High-temperature refrigeration applications

High-temperature refrigeration applications involve a cooling space temperature range of 8 °C to 15 °C (Whitman *et al.*, 2012). Air-conditioning is one example of high-temperature refrigeration applications. The term air-conditioning refers to the automatic control of atmospheric environment (air temperature, humidity, and air distribution) for purposes of human comfort and for some industrial applications (Jones, 2011). Vapour compression cycle is one of the most common cycles utilised to achieve a cooling effect in air conditioning applications. Another example of high temperature refrigeration is magnetic refrigeration. It is one of the magneto-caloric effect (MCE) applications. Magneto-caloric effect MCE comes from the ability of magnetic materials to absorb or dissipate heat in magnetising or demagnetising process (Liu, Fullerton, Gutfrisch & Sellmyer 2010). If a magnetic material is exposed to an external magnetic field, a temperature change occurs corresponding to change in thermodynamic state. Based on this phenomenon, many refrigeration cycles have been designed and developed (Scarpa, Tagliafico & Tagliafico 2015). Figure 1.1 demonstrates the magnetising and demagnetising process.

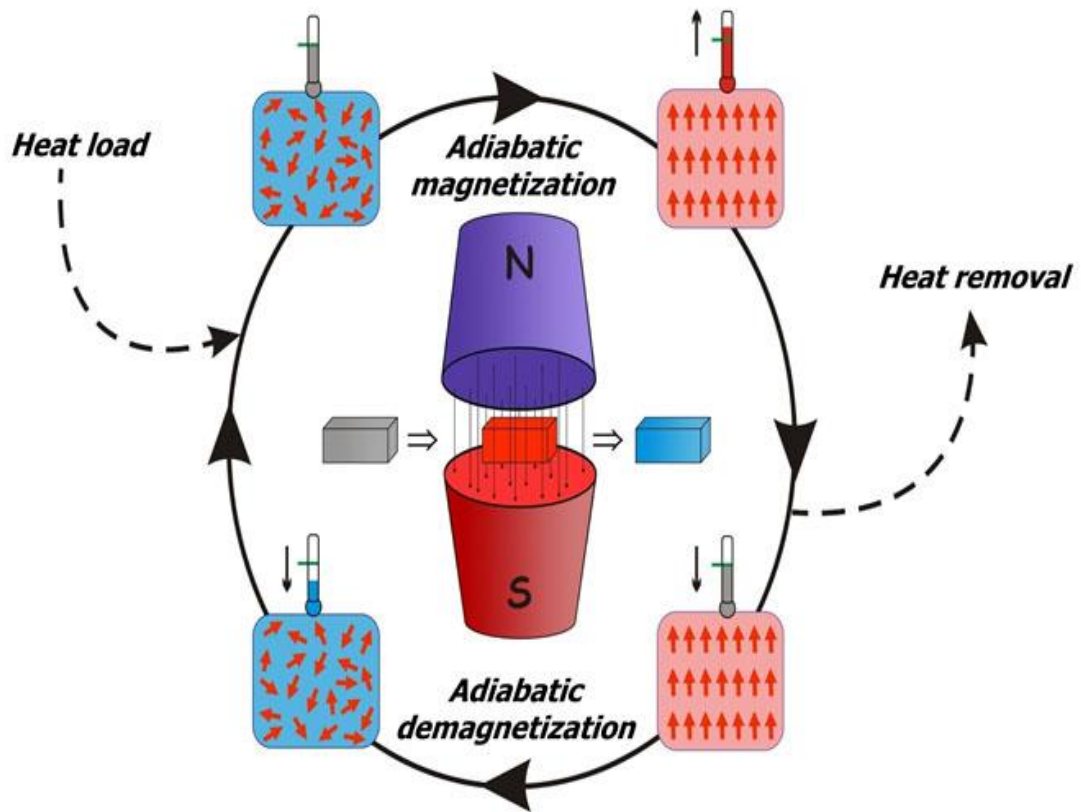


Figure 1.1: Magnetising and demagnetising process.

Source (Shatruk, 2014)

Magneto-caloric materials (MCM) are considered to be at the heart of every magnetic refrigeration or heat-pump applications (Kitanovski, Tusek, Tomc, Plaznik, Ozbolt & Poredos, 2014). Magnetic refrigeration technology has a long history. It was first studied 130 years ago (He, Gong, Zhang, Dai, Shen & Wu, 2013). In the last few decades, magnetic refrigeration has been employed in the room-temperature range. (Brown, 1976) achieved 47 K no-load temperature span in magnetic field of 7 T by using gadolinium (Gd) as the working material. (Zimm, Jastrab, Sternberg, Pecharsky, Gschneider, Osborne & Anderson, 1998) attained a cooling power of 500W in a magnetic field of 5T. They developed a reciprocating magnetic refrigerator and used gadolinium (Gd) as the working material. (Zimm, Boede, Chell, Sternberg, Fujita, Fujieda & Fukamichi 2006) designed and experimented with a rotary magnetic refrigerator (RMR) using gadolinium alloy. They obtained cooling power of 49 W in a permanent magnetic field of 1.5T. (He et al., 2013) designed and built hybrid refrigerator which combined an active magnetic refrigeration effect with the stirling

gas regenerative refrigeration effect. They achieved a cooling temperature of 3.5 °C and improved the cooling performance by 24% for a hybrid system compared to a pure stirling system. Most of the applications of magnetic refrigeration at room temperature use permanent magnets as a source of magnetic field (Kitanovski et al., 2014). Thus different design of permanent magnetic circuits have been considered and developed for magnetic refrigeration systems. They include; halbach cylinder, c-shaped halbach, nested halbach, rotor-stator and coaxial permanent circuit.

1.1.3.2 Medium-temperature refrigeration

Medium-temperature refrigeration applications which involve cooling space temperature range of -2 °C to 5 °C. Household refrigerators and supermarket display refrigerators are an example of medium-temperature applications (Whitman et al., 2012). Medium temperature refrigeration can be achieved by different refrigeration cycles. Absorption and adsorption cycles are thermally driven systems used to produce medium temperature refrigeration (Edenhofer et al., 2011).

1.1.3.3 Low-temperature refrigeration

Low-temperature refrigeration applications are those which involve cooling space temperature range of 0 °C to -50 °C. In air conditioning, chilled water at 0 °C is considered low temperature refrigeration. In industrial refrigeration, blast freezing at -45 °C is considered low as well (Whitman et al., 2005). In this temperature range, a simple vapour-compression cycle may not be suitable to use. Therefore, a more advanced refrigeration system can be used. In industry, different types of systems are considered to achieve low temperature refrigeration. Multistage compression systems and cascades are widely used (Dincer & Kanoglu, 2010). In multistage system, two or more compressors are connected in series as shown in Figure 1.2. This system can attain an evaporator temperature of approximately -60 °C (Khurmi & Gupta, 2006). A cascade refrigeration cycle is employed to achieve a high-temperature differential between the cooling space and ambient (Dincer & Kanoglu, 2010). Cascades systems have two separate refrigerant circuits, a high temperature circuit and low temperature circuit (Rudy, 2000). They basically employ two separate vapour compression systems with different types of refrigerants.

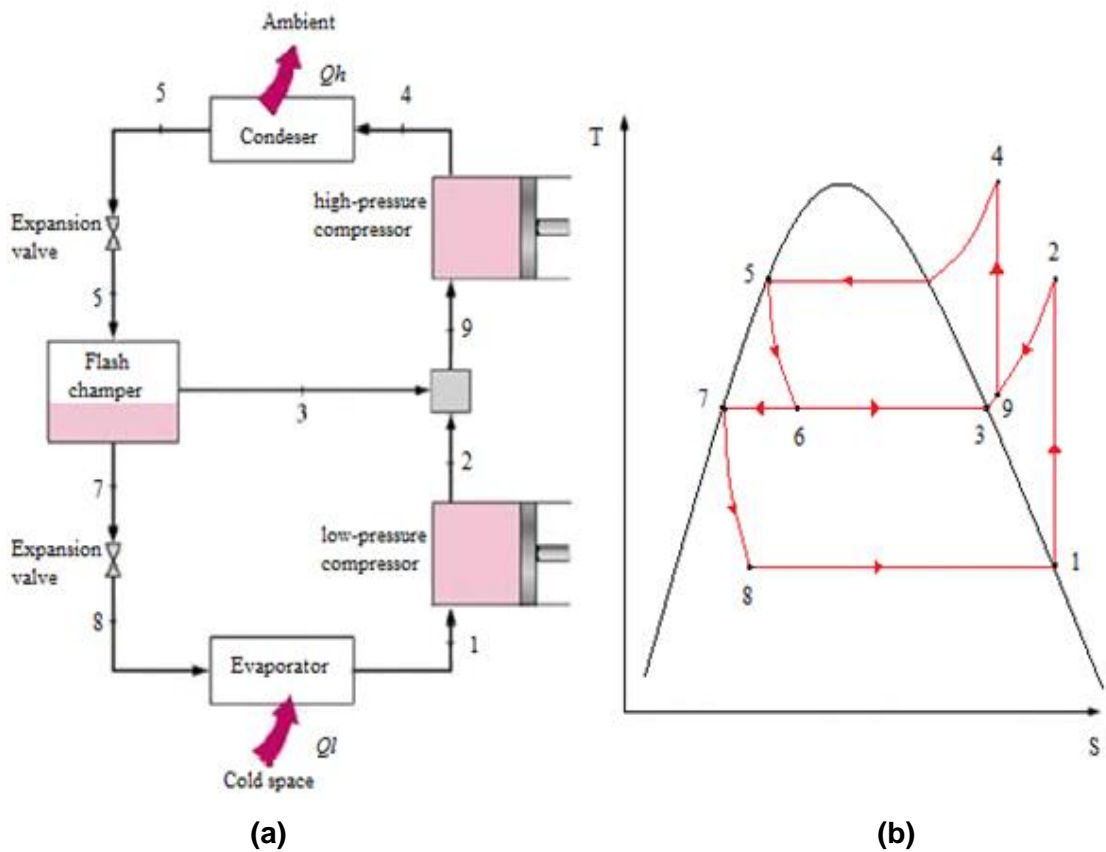


Figure 1.2: (a) Schematic diagram of a two-stage vapour-compression system, (b) temperature-entropy (T-S) diagram.

Adapted from (Corner, 2015)

1.1.3.4 Cryogenics

Cryogenics is the science and technology of a very low temperature below $-150\text{ }^{\circ}\text{C}$. The term cryogenic originates from the Greek words (kryos) which means frost and (genic) which means to produce. One of the most important features of cryogenic refrigeration application is a liquefaction of natural gas (LNG). Natural gas is considered as a clean energy source so that, its demand in global market has increased. To transport natural gas overseas, it should be cooled at very low temperature (cryogenic) of about $-162\text{ }^{\circ}\text{C}$ and loaded in special vessels called (LNG carriers) (Karakurt, Gunes, Arda & Ust, 2014). These processes reduce the volume of natural gas by a factor of about 600 times in order to make the transportation more economical (Wang, Zhang & Xu, 2012). There is different refrigeration cycles operated with different refrigerants for natural gas liquefaction (Kanoglu, 2002). Multistage cascade refrigeration was the first cycle used and is still commonly used in liquefaction of natural gas (Göktun & Yavuz, 2000) (Wang, et al., 2012). Linde-

Hampson cycle is also employed for the same purpose (Dincer & Kanoglu, 2010). Other Applications of cryogenic refrigeration include separation of gases such as oxygen and nitrogen from the air, fast freezing of some foods and preservation of biological materials such as human blood and tissues. In the area of tactical and space application, cryo-coolers are required on many satellites in order to cool infrared and microwave detectors (Zhi, Han, Dietrich, Gan, Qiu, & Thummes, 2013) .

1.1.4 Problem Statement

The problem addressed by this research is that in most African rural areas, there are no modern fruit preservation methods because of the lack of grid supply. Yet, production takes place in such areas. The effect has been large post-harvest losses of fruit. This project is intended to provide a model design that could be used to reduce these losses at a small-sized farm level.

1.1.5 Post-harvest losses

The world's population is increasing rapidly. In 2011, the United Nation estimated the total human population to be 7 billion and predicted the number would increase to reach 10 billion by the end of the century (Pimentel & Peshin, 2014). Therefore, the demand for food production will rise by about 70 % in the next few decades (Tefera, 2012). The biggest challenge for the agriculture society worldwide is how to expand crop production and ensure food security.

The term food security can be defined as the ability of all people to have access (physical, social, and economical) to sufficient, safe, and nutritious food necessary to lead healthy lives (McDonald, 2013). The World Food Summit (WFS) has defined food security as the availability at all times of convenient world food supplies of basic food stuffs to maintain and sustain a steady expansion of food consumption and offset fluctuation in production and prices (Haen, Thomas, Huddleston, Sharma & Ramesh, 2002). Crop yield protection is one of the key components of food security (Savary, Ficke, Aubertot, Hollier & Clayton, 2012).

Reductions in crop losses and food processing technologies have significant impact on food production (Pedreschi, Lurie, Hertog, Nicolai, Mes & Woltering, 2013). Since 1977, the Food and Agriculture Organization (FAO) has given priority to the prevention of crop losses, particularly post-harvest losses (Burden, Wills, & Smith, 1989).

The term post-harvest refers to the period between the maturity of crops and the time of their consumption. During this period, the crop can be exposed to several risks such as spoilage, mishandling, and pest infestation. On the African continent, more

than half of the people live in rural areas where they make a living from agricultural activities (Tefera, 2012). Post-harvest losses have been estimated as 25 % (Burden, et al., 1989). This threatens stability of the food production. Therefore, many procedures have been considered in order to save money and efforts, and reduce poverty and hunger. Pedreschi et al. reported that in developing countries, crop losses occur early in the food supply chain at post-harvest processes (Pedreschi, et al., 2013).

FAW reports that fruit, vegetables, and root crops are more susceptible to damage during the harvest, handling, and transport. Products such as tomatoes, sweet potatoes, plantain, and bananas are most affected by post-harvest processes (Burden, et al., 1989). (Indira & Sudheer, 2007) classified post-harvest losses as economic, quantitative, pilferage, qualitative, and nutritive loss.

1.1.5.1 Post-harvest loss causes

The causes of post-harvest loss of fruits and vegetables can be divided into two categories; primary and secondary causes. The former include mechanical, physiological, pathological, and environmental causes. Secondary causes include mishandling of products and inadequate transport, storage, and marketing.

In the first category, mechanical loss such as cracking and bruising can happen during the picking and packaging. Birds and insects are other reasons for mechanical loss. Pathological loss caused by fungi and bacteria activity can occur rapidly and cause spacious break down of the product. The environmental factors such as temperature and humidity play a significant role during the storage period of the product. Temperature is considered as the most important factor. The appropriate storage temperature extends shelf life and decreases the growth of pathogens.

In the second category, inappropriate harvesting, transportation, and the marketing system lead to increased possibilities of contamination with organisms and decrease the quality of the product (Indira & Sudheer, 2007) (Kader, 2004).

1.1.5.2 Preservation processes

As stated in the previous section, fruits and vegetables constitute an important item of our system of nutrition. They play a significant role in the human diet through the supply of vitamins and minerals (Bhattarai, Rijal, & Mishra, 2013). The need for fresh fruits and vegetables has grown in world markets. To keep fruits and vegetables in safe and unspoiled conditions, preservation should be applied especially for perishable fruits. Also because most of the fruit and vegetable products are consumed in areas of the world far distant from their production sites, preservation processes should take place. The main purpose of preservation is to protect fruits

from spoilage. Spoilage is defined as any process leading to the deterioration of safety, sensory quality (taste, flavour, texture, colour and appearance) or nutritional value of fruits and vegetables. According to (Berk, 2013) there are four different types of food spoilage which include:

- Microbial spoilage - deterioration due to the activity and/or presence of microorganisms.
- Enzymatic spoilage - undesirable changes due to enzyme catalysed reactions.
- Chemical spoilage – reactions between food components.
- Physical spoilage - undesirable changes in the physical structure of the food

The most important type of deterioration in food is microbial spoilage, since it may affect both the quality and the safety of food. He has demonstrated that the main preservation technologies by which the various types of food spoilage can be controlled as following:

- Preservation by heat (thermal processes).
- Preservation by removal of heat (low temperature processes).
- Preservation by reduction of water activity.
- Ionising radiation.
- Chemical preservation

The preservation by removal of heat is the most common means. Low temperature depresses the activity of microorganisms and enzymes. In contrast to heat, a low temperature does not destroy microorganisms and enzymes to any significant extent. The improvement in the cold distribution chain has made international trade of fruits and vegetables possible. Precooling is one of the important processes in cold chain processes

1.1.5.3 Precooling process

The removal of heat through the process of precooling to a recommend storage temperature and relative humidity is suggested as a means to maintain the quality of fruits and vegetables (World Health Organization, 2007). The quality of most fruits will rapidly deteriorate if heat is not removed before loading into transportation equipment. The main objective of precooling is to extend life of products by reducing: heat, rate of respiration, loss of moisture, production of ethylene, and spread of decay.

According to the report of World Health Organization (WHO) (Heyman, 2007), precooling should occur as soon as possible after harvesting. For most products, harvesting should be done in the early morning hours to minimize field heat and

refrigeration load on precooling equipment. The important factors such as mold growth and injuries caused by the chilling process must be taken into account as well as the required period of storage. Table 1.1 demonstrates required conditions for cold storage of some fruits and vegetables (Dossat & Horan, 2002).

Table 1.1: The storage conditions of some fruits and vegetables

Fruit & Veg	Temperature range °C	Relative humidity %	Approximate storage life	Water content %
Avocados	5 - 13	90 - 95	2 - 8 weeks	84
Bananas	10 - 15	85 - 90	1 - 2 weeks	75
Green bananas	13 - 15	80 - 90	1 - 2 weeks	75
Dates	6 - 10	70 - 75	6 months	20
Lemons	11 - 13	85 - 90	1 - 4 months	89
Oranges	7 - 12	85 - 90	3 - 6 weeks	86
Mangoes	10 - 13	85 - 90	2 - 3 weeks	81
Pomegranates	5 - 8	90 - 95	2 - 3 months	82
Cucumbers	8 - 10	85 - 90	10 - 14 days	96
Potatoes	10 - 13	85 - 90	4 - 7 months	69

1.1.6 Solar Energy

The sun provides most of the energy sources on earth directly or indirectly (except nuclear and geothermal). It supplies a vast amount of energy to the surface of the earth. It drives the climate and weather systems. The availability of solar energy has ensured it is the most capable and promising future energy solution (Narasimhan, Jiang, & Park, 2016) (Kosmopoulos, Kazadzis, Lagouvardos, Kotroni, & Bais, 2015). There are plenty of technologies currently available to capture and harvest solar energy in order to convert it to thermal or electrical energy forms. Photovoltaic (PV), Thermal collectors, thermos-chemical reaction, and PV-Thermal are examples of solar energy collecting devices (Kosmopoulos et al., 2015).

1.1.7 Solar Radiation

Sunshine reaches the earth as a type of energy called radiation. Radiation is composed of millions of high energy particles called photons. Each unit of solar radiation or photon carries a certain amount of energy. Solar radiation reaches the

earth surface in various form ranging from gamma and x-ray to ultraviolet (UV) and radio wave (Badescu, 2008). Figure 1.3 illustrates world solar radiation map.

The rate of the energy emission from the sun is 3.8×10^{23} kW, which results from the conversion of $(4.7 \times 10^6 \text{ ton/s})$ of mass to energy. Despite the earth being located 150 million km from the Sun, it receives approximately 1.7×10^{17} kW (Kreith & Krumdieck, 2014).

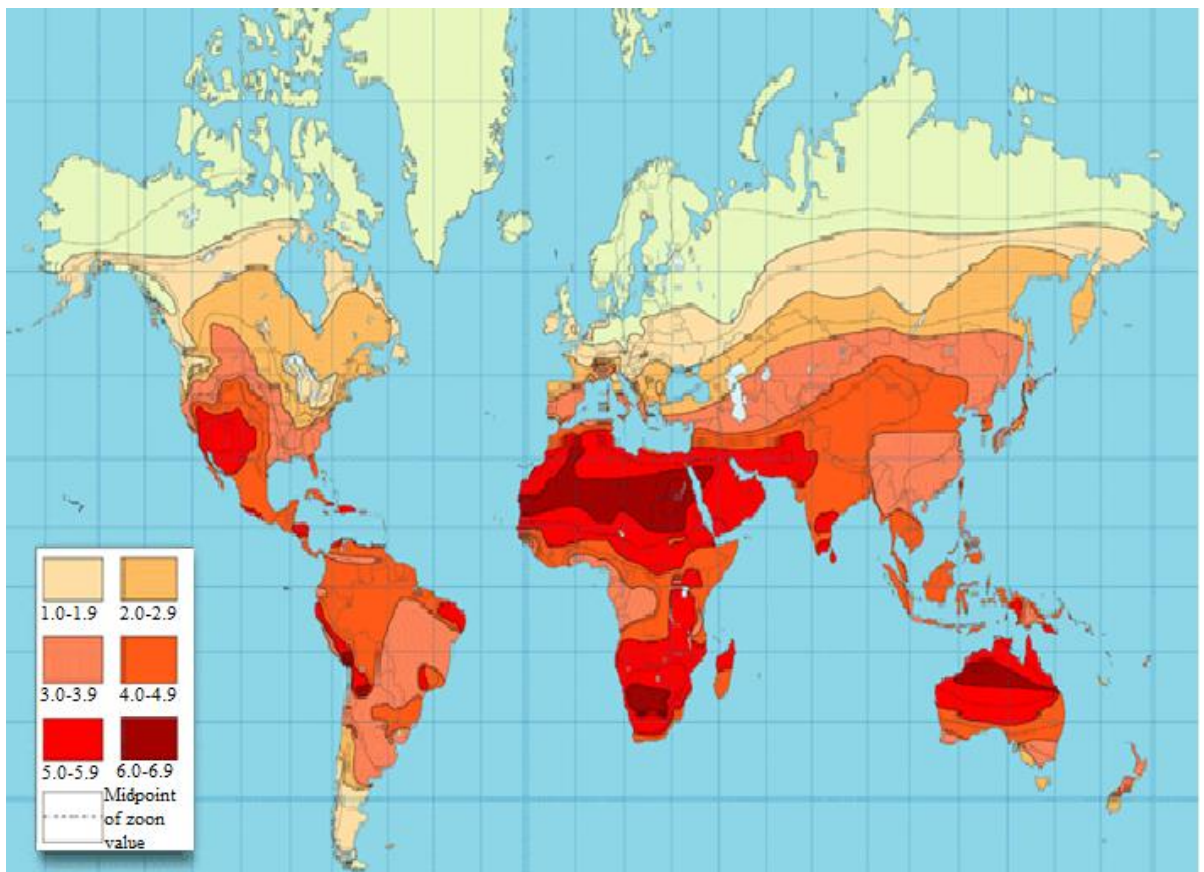


Figure 1.3: World solar radiation map

Adapted from (Open Electrical, 2013)

The distance between the sun and the earth is not fixed (Sonnenenergie, 2012). As a result the irradiance fluctuates between 1325 W/m^2 and 1412 W/m^2 . The average value is referred to as solar constant I_{sc} . It is standardised at 1367 W/m^2 . The solar constant is the energy from the sun per unit time received on unit area of surface perpendicular to the direction of propagation of the radiation at mean earth-sun distance outside the atmosphere (Duffie & Beckman, 2013). In practical experiments, (Duffie & Beckman, 2013) have suggested using the formula of Perez (1996) to calculate the total solar radiation.

$$I_{panel} = I_{bh}R_b + I_d(1 - F_1)\left(\frac{1 + \cos \beta}{2}\right) + I_dF_1\frac{a}{b} + I_dF_2 \sin \beta + I_h\rho_g\left(\frac{1 - \cos \beta}{2}\right) \quad (1.1)$$

Where: I_{panel} is total radiation on the tilted surface,

I_{bh} is horizontal incident beam flux,

R_b is panel to horizontal incident beam flux ratio,

β is panel slope,

ρ_g is ground reflectivity,

b is dependent on zenith angle,

a is dependent on incident angle at panel,

I_d is general incident diffuse flux,

I_h is total horizontal incident radiation flux

f_1, f_2 circumsolar horizontal incident radiation flux

1.1.8 Solar PV collector

Solar PV modules are solid-state semiconductor devices which convert solar radiation into usable electrical power. Materials such as mono crystalline silicon, polycrystalline silicon, micro-crystalline silicon, copper indium selenide, and cadmium telluride are used in a PV panel (Devabhaktuni, Alam, Depuru, Green, Nims, & Near. 2013). Figure 1.3 illustrates a solar cell, a module, and an array. When a photovoltaic cell is exposed to sun rays, negatively charged electrons absorb the energy of light photons. They gather at the negative pole of the PV cell and form a negative electrical charge. Due to the drain of electrons, the opposite end of the cell creates a positive charge. This separation of electrical charges is called potential difference or electric tension. The effort of these separated charges to reunite is called electric voltage. This voltage can be measured with a voltmeter. As long as light reaches the photovoltaic cell, the separated charge cannot return to the cell and recombine.

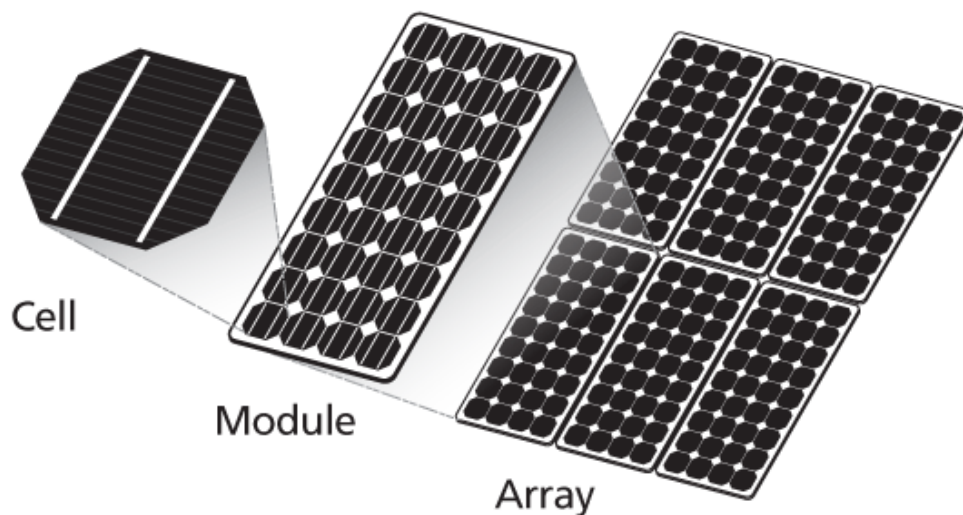


Figure 1.4: Solar PV combination

Adapted from (Samlexsolar, 2004)

When a conductive wire connects the two poles, negative electrons can flow back to the positive pole. This flow of electrons is known as electrical current. It can be measured with an ammeter. There are three common types of solar PV systems. Each type is characterized by unique considerations in design, installation and operation (Fang & Li, 2013).

1.1.8.1 Grid- connected systems

In grid connected systems, PV supplies the generated power directly to a utility grid. The central element of this system is the inverter that converts direct current into alternative current. This system can be subdivided into two categories: complete feed in and self-consumption plus feed in. In the first category all generated power feed into the grid. In the second category, when there is more generated power than the consumer need, the excess power can be fed into the grid. The possibility to consume solar energy during the whole day and at night requires some sort of energy storage. Lead accumulators are still the first choice for solar systems. They represent a reasonable cost performance value and are very reliable when the maintenance is good.

1.1.8.2 Hybrid PV systems

Hybrid systems use more than one energy technology as a power source. The combination of wind generators and PV carries the advantage that in many regions both resources are complementary in their availability. PV can also combine with a

fuel engine generator as an auxiliary supply. This system requires sophisticated controls (Reddy, 2010).

1.1.8.3 Stand-alone systems

In this configuration the photovoltaic system represents the only available electrical power resource. A direct connection to the grid is not possible or it is uneconomical. Stand-alone PV systems are not synchronised with the frequency and amplitude of the utility grid and therefore must always be installed in a separate electrical circuit. These systems are suitable for some applications such as camping, irrigation systems and for water pumping, lighting, and cooling purposes. It can also provide a house's facilities with electrical power in remote areas.

1.1.9 Solar refrigeration

Solar energy has become more attractive for cooling purposes today. It can provide cheap and clean source for cooling and refrigeration application all over the world. Solar refrigeration technologies harness the energy of the sun and use it to run the cooling system. This type of solar application is an attractive option for food and vaccines preservation in areas with a high intensity of solar radiation and instability in electricity supply or in areas which are located far from the grid. A solar refrigeration system can be divided into two main categories: the one as a thermal driven and the other as electricity driven system.

1.1.9.1 Solar thermal refrigeration

In solar thermal refrigeration, the refrigeration effect can be produced through solar thermal gain. The main parts of this system are: a solar collector array, a tank for thermal storage, a thermal AC unit, a heat exchanger and connecting pipe (Ullah, Saidur, Ping, Akikur, & Shuvo, 2013). Flat-plate collectors and Evacuated tube collectors are the most common types of collectors (Kim & Ferreira, 2008).

We will briefly demonstrate how this system works. The solar collector transforms solar radiation into heat and transfers that heat to a heat transfer fluid (refrigerant) in the collector. The fluid is stored in a thermal storage tank. This hot refrigerant is used to run the AC (air-conditioning) unit. It then circulates through the entire system. The heat exchanger is responsible for transferring heat between the hot and cold spaces (Ullah, et al., 2013) . For commercial and household purposes, four major solar thermal driven cooling systems are available with absorption, adsorption, desiccant and ejector cooling systems.

1.1.9.2 Solar electric refrigeration

This system uses photovoltaic (PV) panels to power a conventional refrigeration machine (Bilgili, 2011). The output of the PV system can be utilised to run the cooling unit directly by using a DC motor or indirectly by using an inverter. The system consists of four basic components: PV modules, storage system, inverter circuit, and vapor-compression unit (Sarbu & Sebarchievici, 2013).

1.1.9.3 Vapour-compression cycle

Vapor-compression refrigeration (VCR) cycles are considered to be the most commonly used in domestic and industrial refrigeration and air-conditioning (Jain, Kachhwaha, & Sachdeva, 2013) (Mopab & Shapiro, 2000) (Dincer & Kanoglu, 2010). The term vapor compression refers to the way the cooling liquid is circulated through the system components. The four key components of the (VCR) system are; the compressor, the condenser, the evaporator, and the throttling device (Silbrestein, 2015).

Figure 1.4 (a) shows a schematic diagram of a simple vapour-compression refrigeration cycle. In this cycle, the vapour refrigerant enters the compressor through the suction line as a low pressure and low temperature superheated vapour and it leaves through the discharge line as a high pressure and high temperature superheated vapor.

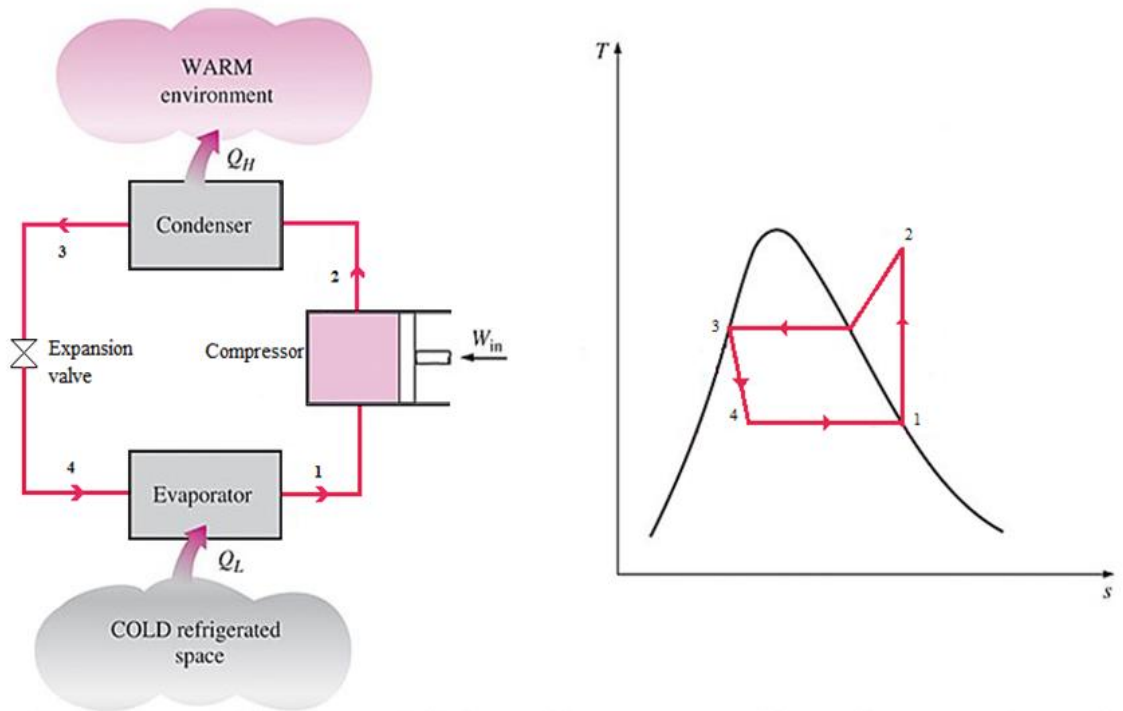


Figure 1.5: (a) Schematic diagram of a vapor-compression refrigeration system, (b) the temperature - entropy ($T-S$) diagram.

Adapted from (Dincer & Kanoglu, 2010)

Once the high pressure and high temperature refrigerant reaches the condenser it starts to change its state into liquid by losing heat. The condensing temperature of the refrigerant is higher than the ambient temperature and therefore heat transfer condenses the high pressure refrigerant vapour into a high pressure saturated liquid. After the condensing process, the refrigerant sub-cools and continues dissipate sensible heat. Sensible heat refers to the change in temperature that can be measured by a thermometer. After that the refrigerant moves to a throttling device in order to reduce its pressure to the low pressure point and the boiling temperature of the refrigerant is lower than that of the heat source. As long as the refrigerant passes the evaporator, it absorbs a considerable amount of heat and boiling occurs producing a low pressure saturated vapor. The low pressure vapour enters the compressor repeating the cycle. (Schmidt, 2007) (Silbrestein, 2015).

To illustrate VCR simply, the ideal vapour-compression refrigeration cycle is shown in temperature-entropy ($T - s$) diagram in figure 1.4 (b). The cycle consists of the following summarized processes:

- Process 1-2: reversible adiabatic compression. The low pressure vapour passes into the compressor.
- Process 2-3: reversible condensation. The high pressure, high temperature vapour passes from the compressor into the condenser to reject the heat.
- Process 3-4: irreversible expansion. From the condenser, the high pressure liquid refrigerant passes into the throttling device to drop its pressure and temperature.
- Process 4-1: reversible heat gain. From the throttling device, the low pressure liquid refrigerant passes through the evaporator and boils by absorbing heat from the surrounding ambient to complete the cycle.

1.1.10 Thermodynamic analysis of vapour-compression refrigeration cycle

As mentioned in the previous section, the ideal VCR consists of number of flow processes. These processes can be analyzed thermodynamically by applying steady-state operation. Assuming that, the kinetic and potential energy changes are negligible.

Let us start with the compressor.

$$\begin{aligned}\dot{E}_{in} &= \dot{E}_{out} \\ \dot{m}h_1 + \dot{W} &= \dot{m}h_2 \\ \dot{W} &= \dot{m}(h_2 - h_1)\end{aligned}\tag{1.2}$$

Where: \dot{m} is mass flow rate of refrigerant (kg/s),

h is enthalpy (kJ/kg),

\dot{W} is compressor power input (kW).

For the condenser

$$\begin{aligned}\dot{m}h_2 &= \dot{m}h_3 + Q_h \\ Q_h &= \dot{m}(h_2 - h_3)\end{aligned}\tag{1.3}$$

Where: Q_H is the heat rejection from the condenser

For the throttling device

$$\begin{aligned}\dot{m}h_3 &= \dot{m}h_4 \\ h_3 &= h_4\end{aligned}\tag{1.4}$$

For the evaporator

$$\begin{aligned}\dot{m}h_4 + Q_L &= \dot{m}h_1 \\ Q_L &= \dot{m}(h_1 - h_4)\end{aligned}\quad (1.5)$$

Where: Q_L is heat extracted from cooling space.

The energy balance for the entire refrigeration system can be written as

$$\dot{W} + Q_L = Q_h \quad (1.6)$$

Therefore, the coefficient of performance (COP) of the refrigeration system is

$$COP = \frac{Q_L}{\dot{W}} \quad (1.7)$$

The value of enthalpy can be determined by using the log P-h (pressure-enthalpy) diagram or/and the tabulated numerical values of the thermodynamic properties of the refrigerants.

1.1.11 Practical vapour-compression refrigeration system

According to (Dincer & Kanoglu, 2010) there are some differences between the practical VCR cycle and the ideal VCR cycle (mentioned above). In the practical VCR cycle, there are two processes which should be considered. The first process is superheating which refers to superheating of the refrigerant vapour in the evaporator. The second process is subcooling which refers to subcooling of the refrigerant liquid in the condenser. Figure (1.5) shows the practical VCR cycle. In this cycle, at the suction line, the refrigerant vapour entering the compressor is superheated. During the process, the heat transfer to/from the surrounding leads to an increase/decrease in the entropy as illustrated by the lines 1-2 and 1-2'. At the outlet of the condenser, the pressure of the liquid becomes less than the vapour entering and the temperature of the refrigerant is a bit higher than the ambient temperature therefore the heat is being transferred. The subcooling process may occur before the refrigerant enters the throttling device leading to cooling the refrigerant below its condensing temperature. Subcooling ensures that the liquid refrigerant has no vapour bubbles entering the throttling device. Moreover, the temperature may drop in the piping between the condenser and the throttling device. After the expansion process therefore, the refrigerant entering the evaporator with lower enthalpy as a result of heat transfer, which leads the refrigerant to absorb more heat in the evaporator. The superheating may occur when the refrigerant leaving the evaporator through heat transfer from the ambient in the piping between the evaporator and compressor.

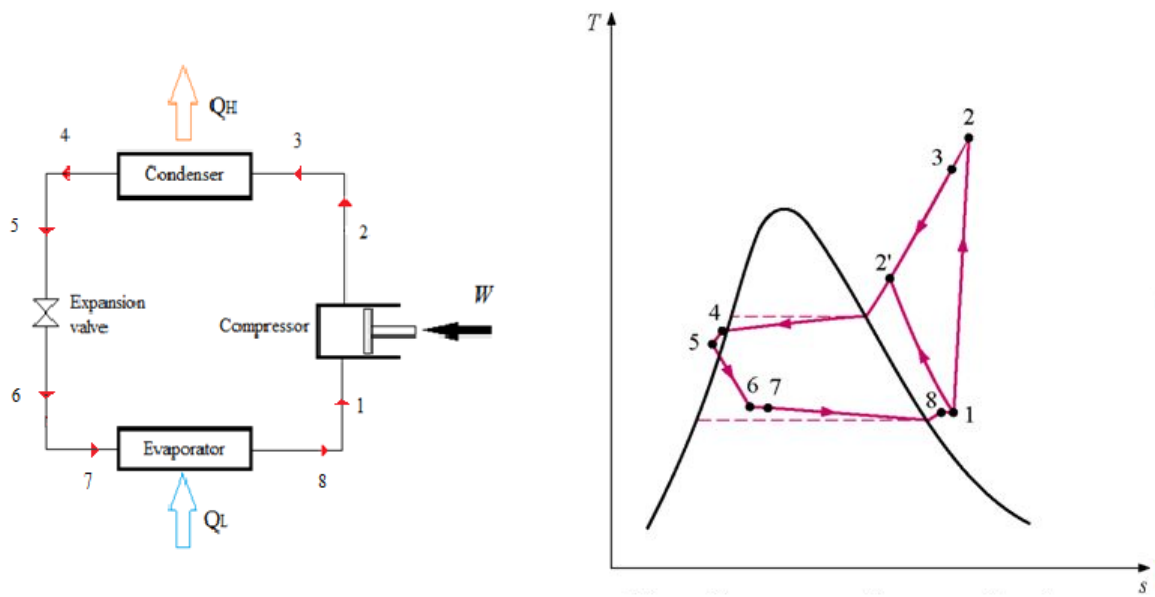


Figure 1.6: An ideal vapor-compression refrigeration system and (T – s) diagram.

Adapted from (Dincer & Kanoglu, 2010)

1.2 Project objectives

1.2.1 Main objective

The main objective of this study is to design and develop a cooling unit which uses solar energy as the source of power in order to provide a fruit producer with clean and cheap source of energy.

1.2.2 Specific objectives

The specific objectives of this study are the following

- To design and manufacture a solar refrigeration system.
- To model the solar refrigeration system.
- To test the model

1.3 Delimitation of the research

In this research:

1. The model cooling room will be between 1 and 2 m³.
2. We will use a DC compressor as alternative to conventional compressors.

3. Target temperature will be between 5 and 15 °C
4. Refrigerant will be R-134a

1.4 Thesis Organization

Chapter one has given general back ground information on solar refrigeration systems. It has highlighted food preservation methods and the advantages of pre-cooling as well. The basic principles of solar PV refrigeration are also demonstrated.

Chapter two presents the heat load calculation of the system and describes the design of a solar PV refrigeration system and the size of the PV system components.

Chapter three demonstrates the experimental methodology and set up. It gives the method of measurements and testing of a PV refrigeration system. Data collection is also examined.

Chapter four discusses the results from the testing of the solar PV refrigeration system.

Chapter five offers the conclusion and the recommendation emanating from the investigation into the system.

Chapter 2 DESIGN AND CONSTRUCTION OF THE SOLAR PV REFRIGERATION SYSTEM

2.1 Introduction

A solar electric refrigeration system consists of two systems, namely: solar PV system and refrigeration system. Each of these systems was designed and sized according to specific considerations. Therefore, several techniques were considered in order to minimise energy losses, reduce the capital cost and increase system performance. The following section demonstrates and describes the considerations for the design and material selection of the solar PV refrigeration system.

2.2 Design cooling system

For the purpose of experimentation, a vapour-compression cycle was utilised to produce the desired cooling and dehumidification. The four main components of this cycle are the compressor, evaporator, expansion device, and condenser. To select the appropriate size of these components, the cooling space geometry and the heat load of the system were determined first.

2.2.1 Cabinet construction

Selection of appropriate materials to build a refrigerated space is a major factor in terms of energy saving. To ensure a good insulation and body stiffness, several materials were considered for the construction of the cabinet surfaces. It is mainly consists of three layers of materials as shown in Figure 2.1.

- **Interior surface**

The interior surfaces were made from plastic panels (Polypropylene, PP). Polypropylene is light, impact resistant, moisture resistant, easy to clean and strong enough to support the evaporator.

- **External surface**

The external surfaces are made from aluminum sheets. Aluminum is considered to be the best choice for the following reasons: it is light, capable of supporting the cabinet structure which needs to hold the condensing unit, and its anticorrosive.

- **Insulation material**

The selection of insulation is very important in order to reduce the heat leakage into the refrigerated space. There is a variety of insulation materials. Polyurethane is

selected for many reasons. It is an excellent insulator, structurally strong, safe, very light, and affordable.

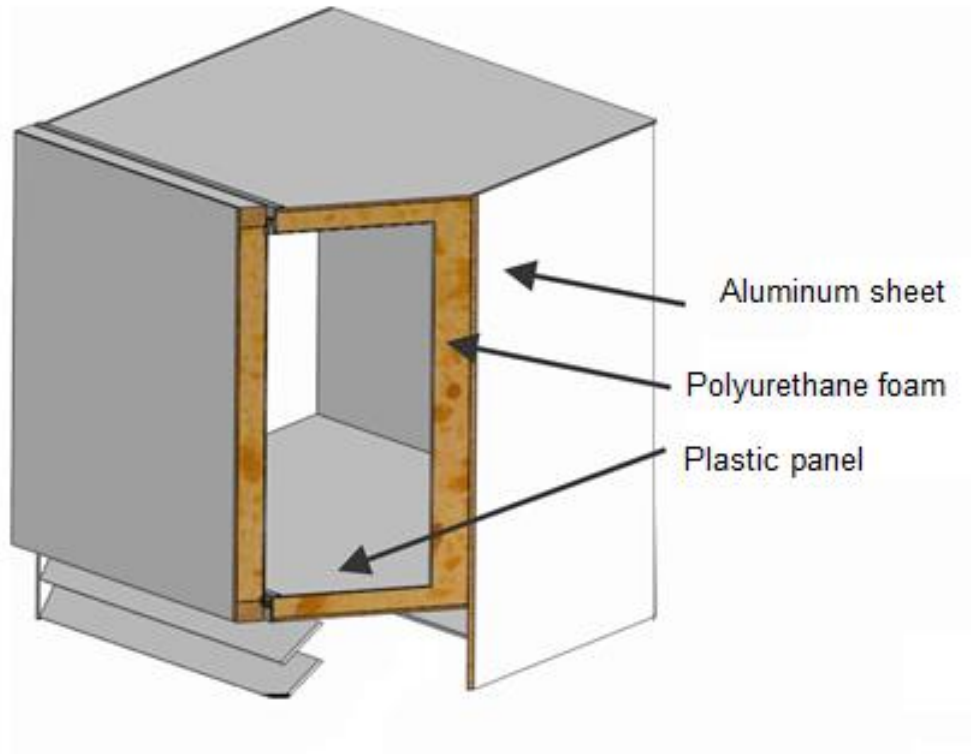


Figure 2.1: Cross section of a cabinet's surface

2.2.1.1 Cabinet size

The dimension of the cooling cabinet will be as follows:

The area of the ceiling is 1 m².

The area of the floor is 1 m².

The areas of each sidewall are 1m² and each end wall 1 m².

The total outside area of the cabinet is 6 m².

2.2.1.2 Cabinet volume

The cabinet volume is used to estimate the air change and product load. It is calculated from the interior dimensions as follows:

The total volume is 0.729 m³.

2.2.2 Heat load in cooling unit

In order to design and select the refrigeration equipment, the heat load estimation was done. To establish the heat load in a cooling unit, the total amount of heat that must be removed during a certain period of time was determined. It included the heat leakage and the heat usage loads.

The heat leakage (transmission) load is a sensible heat that leaks through the walls, ceiling, floor and roof of the cabinet per unit of time.

The heat usage (service) load includes the sum of the following heat loads:

- Infiltration load – sensible and latent heat that is carried into the cabinet.
- Product load – respiration heat that must be removed from fresh products such as fruits, vegetables and meat.
- Miscellaneous load –load from electric lights, motors and working people.

The heat leakage load is considered as a major factor in the design of a refrigeration system. Therefore, refrigeration companies and manufactures determine the amount of heat leakage through the surfaces of refrigerated space. They establish tables and charts based on these calculations which can be used by researchers.

There are a number of factors that affect the heat leakage load that have to be taken into account in calculation (Althouse, Turnquist, Bracciano, Bracciano, & Bracciano, 2013). There are:

- Time. More heat will leak in long-term storage than short-term.
- Temperature difference. The heat leakage will be more when the difference between the refrigerated space and ambient temperature is great.
- Type of insulation. Expanded polyurethane foam is one of the insulation materials which is commonly used.
- Thickness of insulation.
- External area of cabinet.

2.2.2.1 Transmission load

The sensible heat gain through the surfaces is calculated in a steady state as following:

$$Q_{leak} = UA\Delta T \quad (2.1)$$

Where:

Q_{leak} is heat gain (W),

A is outside area (m²),

ΔT is temperature difference (°C),

U is overall heat transfer coefficient

The overall heat transfer coefficient U of the surfaces can be calculated by the following equation:

$$U = \frac{1}{\frac{1}{h_i} + \frac{x}{k} + \frac{1}{h_o}} \quad (2.2)$$

Where

x = Wall thickness (m)

k = Thermal conductivity (W/m .k)

h_i = Inside surface conductance (W/m².k)

h_o = Outside surface conductance (W/m².k)

According to (ASHRAE, 2002), U factor for the flat parallel multi-surfaces can be calculated by the following equation:

$$U = \frac{1}{\frac{x_1}{k_1} + \frac{x_2}{k_2} + \frac{x_3}{k_3}} \quad (2.3)$$

Where:

x_1 , x_2 and x_3 are the thickness of material 1, 2, and 3 respectively.

k_1 , k_2 and k_3 are the thermal conductivity of material 1, 2 and 3 respectively.

The thermal conductivity refers to the ability of material to allow heat to flows through the surfaces. It can be determined by the Fourier's law of heat transfer.

$$q = -k \frac{dT}{dx} \quad (2.4)$$

Where:

q is heat transfer rate per unit area (W/m²),

dT/dx is temperature gradient per unit length (°K/m),

k is thermal conductivity (W/m.K)

As mentioned in the previous section, the surfaces are made from three layers of materials. The specification of each material is shown in Table 2.1.

Table 2.1: Cabinet surface specification

Type of material	Thickness(m)	<i>k</i> (W/m.K)
Plastic panel	0.003	0.23
Polyurethane expanded foam	0.045	0.02
Aluminum sheet	0.002	205

Adapted from (Peter Beck, 2008) (Mark, 2007)

2.2.2.2 Infiltration load

Infiltration load refers to the heat gain from the air flow into the refrigerated space during the loading or unloading the products. In many cases, the door will only be open for short period of time (Sun, 2012). Thus, in the calculation of the total heat load, the infiltration load was assumed to be negligible.

2.2.2.3 Product heat load

The product heat load is considered the main contributor to the heat load in refrigerated space. In order to simplify the calculation, the product heat load was divided into two types of load as follows:

- **Sensible heat load**

Sensible heat load refers to an amount of heat that must be removed from the product to reach the desired cooling temperature. It can be estimated with the following equation:

$$Q_{p-sen} = mc_p (T_1 - T_2) \quad (2.5)$$

Where:

Q_{p-sen} is Heat removed (kJ),

m is Mass of product (kg),

c_p is Specific heat of product [kJ (kg.C)],

T_1 is initial temperature of product (°C),

T_2 is Storage temperature (°C),

To get Q_{p-sen} in watt

$$Q_{p-sen} (W) = \frac{1000Q_p(kJ)}{3600}$$

(2.6)

- **Respiration heat load**

Heat respiration refers to the amount of heat that is generated from living food products such as fruits and vegetables. The correlation between the carbon dioxide production rates and the commodity's heat generation has led to develop mathematical formula which can be used to calculate the heat of respiration (Gopala Rao, 2015). This formula as following:

$$Q_{p-res} = \frac{10.7f}{3600} \left(\frac{9\theta}{5} + 32 \right)^g \quad (2.6)$$

Where:

Q_{p-res} is Heat generation rate (W/kg),

f , g are respiration coefficients,

θ is average temperature of products in °C

Table (2.2) gives the respiration coefficients for various commodities.

Table 2.2: The coefficients f and g for various products

Products	Respiration coefficients		Products	Respiration coefficients	
	f	g		f	g
Apples	5.68×10^{-4}	2.5917	Limes	2.983×10^{-8}	4.7329
Blueberries	7.25×10^{-5}	3.2585	Onions	3.668×10^{-4}	2.538
Cabbage	6.08×10^{-5}	2.6183	Oranges	2.805×10^{-4}	2.684
Carrots	5.002×10^{-3}	1.7926	Peaches	1.299×10^{-5}	3.6417
Grape fruit	3.582×10^{-3}	1.9982	Pears	6.361×10^{-5}	3.203
Grapes	7.065×10^{-5}	3.033	Plums	8.608×10^{-5}	2.972
Lemons	1.119×10^{-2}	1.7710	Tomatoes	2.007×10^{-4}	2.835

Adapted from (Gopala Rao, 2015)

After harvesting, most vegetables have high respiration rates. Within a few days, the respiration rate decreases quickly. Fruits, however, are different from other food products. Fruits such as grapes and citrus which do not ripen during cold storage, have a constant respiration rate. Those fruits which ripen during cold storage, such as peaches and apples manifest an increase in respiration rate (Gopala Rao, 2015). Table 2.3 gives the heat of respiration rates as a function of temperature for some fruits and vegetables.

Table 2.3: Heat of respiration of some fruits and vegetables in different temperatures

product	Heat of respiration (mW/kg)					
	0 °C	5 °C	10 °C	15 °C	20 °C	25 °C
Apples	10.7	16.0	-	-	-	-
Bananas, green	-	-	-	59.7-130.9	87.3	155.2
Bananas, ripe	-	-	-	37.3-164.9	-	97-242.5
Mangoes	-	-	-	133.4	226.6-449	356
Onions	6.8-9.2	10.7-19.9	-	14.7-28.1	-	-
Potatoes	-	17.5-20	19.7-29.6	19.7-34	19.7-40	-
Tomatoes	-	-	-	79.1	120.3	143

Adapted from (Gopala Rao, 2015)

2.2.2.4 Miscellaneous load

Miscellaneous load includes heat load from evaporator fan, lights and people. The heat load from light and people will be neglected in the calculation.

Evaporator fan produces a considerable heat amount in a refrigeration system. Thus, a selection of an appropriate fan is important in terms of energy saving. In many refrigeration applications, conventional shaded-pole AC motors have been replaced with DC electronically commutated motors.

In this project, a DC fan motor with the following specifications was used.

Table 2.4: Evaporator fan specification

Specification	Description	Specification	Description
Power	2 W	Dimension	92×92×25 mm
Voltage rate	12 V	Type	Tube axial
Air flow	1.46 m ³ /min	Operation temperature	-10 ~ 70 °C

Adapted from (Digi-Key, 1995)

In general, the actual heat load calculation is more complex and a safety factor has to be considered in the calculation. According to (ASHRAE, 2002), the total heat load is increased by 10% to avoid any incompatibility between the design criteria and actual operation.

2.2.3 Temperature establishment

The desirable temperature in the refrigerated space was considered as a reference point in refrigeration system design and heat load calculation. The outside temperature during the day and night varies greatly, especially in the summer. When this is the case, in heat load calculations, the highest ambient temperature is considered as a reference. In order to determine the temperature difference (ΔT) between the ambient and refrigerated room temperature, the highest ambient temperature of the Belleville suburb in the Western Cape Province was considered to be 35 °C in summer season. For short-term preservation of fruits and vegetables, 5 °C is considered the average of refrigerated space temperature.

2.2.4 Heat load calculation

For the purpose of experimentation, the following calculation will encounter the approximate refrigeration system requirement.

- **Transmission load**

From Table 2.1 and equation 2.3:

$$x_1 = 0.003 \text{ m}, x_2 = 0.045 \text{ m and } x_3 = 0.002 \text{ m}$$

$$k_1 = 0.23 \text{ W/m.K}, k_2 = 0.02 \text{ W/m.K and } k_3 = 205 \text{ W/m.K}$$

Therefore:

$$U = 0.522 \text{ W/ (m}^2\text{.K)}$$

To estimate the temperature of cooling unit walls, Table 2.4 gives the degrees C should be added to normal temperature difference.

Table 2.5: Allowance for sun effect

Colour of surface	East wall	North wall	West wall	North wall
Dark	4.4	2.8	4.4	11.1
Medium	3.3	2.2	3.3	8.3
Light	2.2	1.1	2.2	5

From equation (2.1), the sensible heat gain through the surfaces is

$$Q_{leak} = 0.522 \times 6 \times (38 - 5)$$

$$= 103.3 \text{ W}$$

- **Sensible product load**

To calculate the sensible heat of a product, It was assumed that, the product mass was 50 kg (harvest per day), the average of specific heat of many products considered, the initial temperature of product after harvest was 25 °C and the compressor run 12 hours per day considering the heat losses during the night will be low.

From equation 2.5, the sensible heat from the product is:

$$Q_{p-sen} = mc_p (T_1 - T_2)$$

$$= 50 \times 3.77 \times (25 - 5)$$

$$= 3770 \text{ kJ}$$

Heat removal rate in 12 hour = 3770/12 = 314.16 kJ/h

$$= 87 \text{ W}$$

- **Respiration load**

From equation (2.6) and Table 2.3, the respiration heat load for the variable product will be as in Table 2.5.

Table 2.6: The respiration heat load for different types of products

product	Respiration heat load	product	Respiration heat load
Apples	0.03293	Limes	0.00698
Blueberries	0.05888	Onions	0.01870
Cabbage	0.04220	Oranges	0.02505
Carrots	0.01455	Peaches	0.04596
Grape fruit	0.02296	Pears	0.04172
Grapes	0.02409	Plums	0.05647
Lemons	0.02997	Tomatoes	0.03202

Note that, the previous table gave the respiration in W/kg for different types of fruits and vegetables. The highest heat load highlighted in brown, is considered in the calculation.

From Table 2.6, the respiration heat load of 50 kg of product is:

$$\begin{aligned} Q_{p-res} &= 50 \times 0.05888 \\ &= 2.94 \text{ W} \end{aligned}$$

- **Evaporator fan load**

From Table 2.4, the evaporator fan load is 2 W.

Therefore the total heat load is expressed in equation (2.7).

$$\begin{aligned} Q_{ref} &= \sum Q_{leak} + \sum Q_{p-sen} + \sum Q_{fan} + \sum Q_{p-res} & (2.7) \\ &= 103.3 + 87 + 2.94 + 2 \\ &= 195.2 \text{ W} \end{aligned}$$

An additional 10% was taken as a safety factor. So that would bring the total heat load to 214.72 W.

2.2.5 Compressor selection and specification

The compressor is considered the heart of the vapour compression cycle. Its principal purpose is to change the refrigerant vapour pressure from low level to high

during the cycle. It is designed to handle peak load conditions, which means that it runs at the peak load whether it is in summer or winter. Thus, the compressor capacity was selected to have a higher capacity than the total heat load to avoid overloading the compressor motor.

For the purpose of experimentation, the DC compressor is considered to encounter more than 214.4 W of refrigeration load which was calculated in the previous section. There are many types of DC compressors available in markets. The most suitable one has the following specifications:

Table 2.7: Compressor Specification.

Compressor specification	Description
Compressor rotation	2000 ~ 3500 rpm
Cooling capacity	175 ~ 224 W
Power supply	DC 12 V
Refrigerant	R134a
Displacement	2.5 cm ³
Working current	2.2 ~ 9 A
Dimension	204×130×137 mm
Net weight	4.3 kg

Adapted from: (Compressor, 2003)

For more technical specifications, see appendix A-1.

2.2.6 Evaporator design

The principal purpose of the evaporator is to remove heat from the refrigerated space. The second purpose is to maintain humidity. In the experiment, a forced circulation finned evaporator was used.

A finned evaporator consists of rows of round copper tubes placed in rows of uniformly spaced aluminium flat plates. This arrangement allows the air to pass between them. The tubes are interconnected by bent tubes to create multiple fluid-passes. A fan, driven by a DC motor is enclosed with the finned evaporator in aluminium housing. The fan rotates at a low speed to avoid dehydration of the product.

The main advantages of these types of evaporators are that they take up little space in the cooling room, have a low frost creation, and there is no space needed between the product's loads.

The pressure-temperature (or pressure - enthalpy) chart of R-134a was used to determine the evaporator pressure and temperature.

2.2.7 Condensing unit

The main function of the condenser is to reject heat that is absorbed by the evaporator and that from the compressor. Condensers can be classified according to the cooling medium into four categories; water-cooled, air-cooled, evaporative air and water, and refrigerant cooled (ASHRAE, 2008).

An air-cooled condenser is the most commonly used in a small compression system. It relies on gravity circulation of the ambient air. So, it was used in the experiment. Figure 2.2 illustrates the air-cooled condenser.

Basically, the air-cooled condensers consist of a brazed-steel tube with aluminium fins bounded to it and sprayed with an anti-corrosion protective.

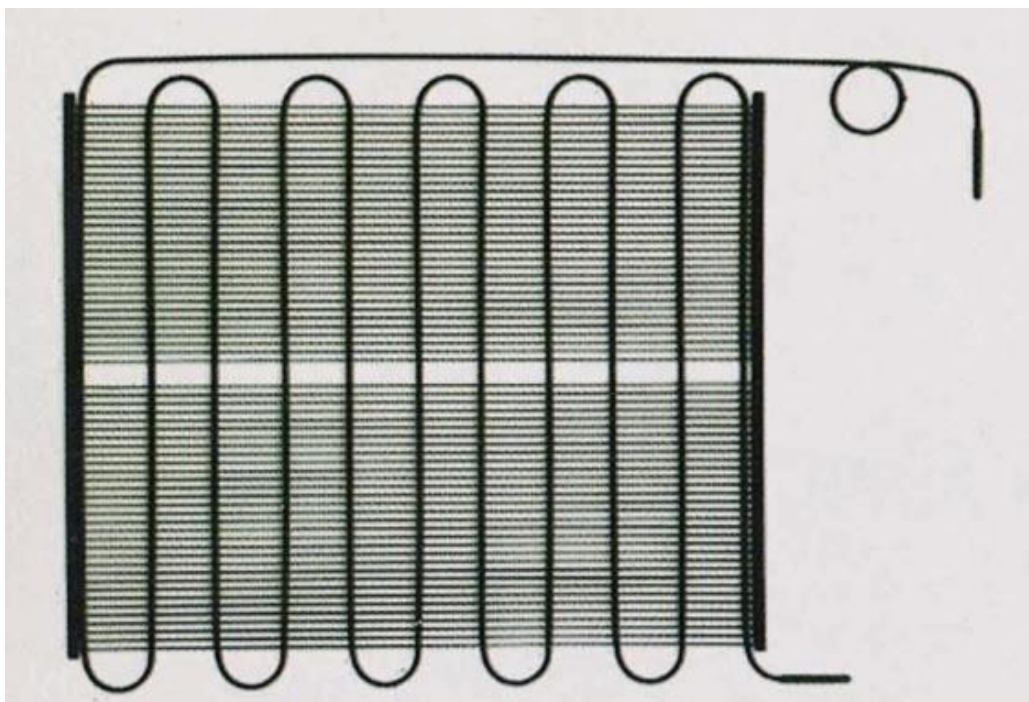


Figure 2.2: Air-cooled evaporator

2.2.8 Throttling device

The principal function of a throttling device (refrigerant control) is to change the refrigerant pressure from high level (condenser) to low ready to enter the evaporator.

In compression systems, throttling devices can be divided into three categories which depend on the following: pressure change, temperature change, and volume change.

Capillary tubes are considered as throttling devices in cooling system design. They are lengths of seamless tubes with narrow and accurate diameters.

A capillary tube system is known a critically charged system. The amount of refrigerant is charged very carefully.

2.3 Solar PV system

A solar PV system includes different components which are selected according to considerations such as system type, site location and applications. The major components are PV panels, charge controller and batteries bank. These components are electrically connected to each other and form a single unit with interdependent parts.

2.3.1 PV modules

A PV module consists of specific number of PV cells connected in parallel to increase current and in series to produce high voltage. The module is encapsulated in tempered glass on the front side, and with protective sheet on the back side. These components are sealed from the edges and held together in an aluminum frame as illustrated in Figure 2.3. The module is attached with a wiring box from the back side.

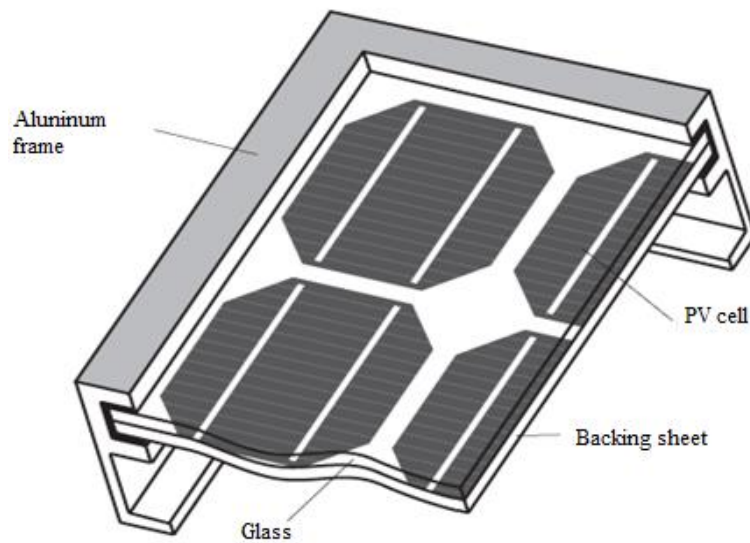


Figure 2.3: The main components in PV module.

Adapted from (Samlexsolar, 2004)

There are a myriad of variables that are taken into account when buying PV modules. They include performance, efficiency and quality to name a few. There are different types of PV panels on the markets currently, Polycrystalline, monocrystalline, hybrid and black frames panels are examples of commercially available modules (Direct, 1986). In this experiment, monocrystalline modules were used. The main advantages of a monocrystalline module are the following: it has the highest efficiency rates, it is space-efficient and last longer (Maehlnm, 2015). The performance of monocrystalline module characteristics are derived at standard test condition (STC): irradiance of 1000W/m^2 and module cell temperature of $25\text{ }^\circ\text{C}$. The following table demonstrates the performance of a monocrystalline PV module.

Table 2.8: PV module specification

PV module	Specification
Nominal power P_n	90 W
Maximum power voltage V_{pm}	18.40 V
Maximum power current I_{pm}	4.90 A
Open circuit voltage V_{oc}	22.40 V

Short circuit current I_{sc}	5.50 A
Net module surface	1.57 m ²

Monocrystalline module (Data sheet of PV module)

2.3.2 Charge controller

The charge controller is a key component of a solar PV system. It is basically a voltage and/or current regulator in the PV power system in order to protect batteries from overcharging or completely draining.

Despite the variety in charge controllers, there are two types that are most commonly used in PV power installations. The first one is the pulse width modulation (PWM) and the second one is the maximum power tracking (MPPT). To specify the suitable one for the system, some requirements have to be analysed. Both of them adjust charging rates and monitor the battery's temperature to prevent overheating. Also each one of them has its own advantages. Thus, the selection depends on system components, site condition, size of array and load, and the cost. The following table demonstrates a comparison between the two types of charge controller.

Table 2.9: Comparative between the two types of charge controller

	Pulse width modulation (PWM)	Maximum power point tracking (MPPT)
Array voltage	PV voltage and battery voltage have to be matched	PV array voltage can be higher than battery voltage
Battery voltage	Good performance in warm temperature and when battery is almost fully charged	It can be operated above battery voltage so that, it enhances the performance in cold temperature and when the charge in battery is lower
System size	More suitable in small system	It has capacity to handle more than what the PWM regulator does.
PV array sizing method	PV array sized in Amps (based on current produced when PV array is operating at battery voltage)	The temperature compensated V_{oc} of the array should be less than the maximum input voltage of the regulator.
Grid connection	Off-grid	Off-grid and on-grid
Cost	low	high

Adapted from: (Solarcraft, 2014) (Vader, 2014)

The maximum power point tracking MPPT was selected in the experiment.

2.3.3 Solar batteries

Solar storage batteries are essential component of the solar PV system. It stores the excess energy which is produced by PV panels. This energy would compensate the leakage of power during the cloudy days and/or use during the night. In PV system installation, there are two main categories of battery: grid-tie and off-grid.

In markets globe, there are different types of batteries available. Deep-cycle and lead-acid batteries are the most commonly used in the renewable energy field. In this project, deep-cycle batteries are selected in order to build batteries bank.

2.4 Sizing solar PV system

The following steps are based on the training course in PV installation and solar PV manufacture's recommendations. It is meant to meet the requirement in solar PV system sizing.

2.4.1 Estimate solar radiation at the site

The following table gives the annual solar radiation of the Cape Peninsula University of Technology site based on NATIONAL RENEWABLE ENERGY LABORATORY data collection and PVWATTS calculator (NREL, 2014).

Table 2.10: Annual solar radiation at CPUT Bellville

Month	Solar radiation per day (kW/m ²)	Energy (kWh)
January	7.91	755
February	7.53	644
March	6.49	626
April	5.08	474
May	4.12	403
June	3.28	317
July	3.33	332
August	4.49	447
September	5.49	521
October	6.57	637
November	7.57	712
December	7.65	722

2.4.2 Determine the total power demands

The total power needed to run the system equals the input power of the compressor and evaporator fan. This load has to be supplied by the PV system. Then, the total load are multiplied by 1.1 (energy losses) to calculate the total watt-hour per day needed from the PV modules.

From Appendix 1 and Table 2.4, the maximum power input for the compressor at evaporator temperature of -5 °C and the motor speed 2500 rpm is 74.3 W. The evaporator fan is 2 W. Therefore, the total power is 76.3 W. The running time of the compressor was estimated at about 12 hours a day.

Therefore,

$$76.3 \times 12 = 915.6 \text{ Wh/day}$$

$$915.6 \times 1.3 = 1190.28 \text{ Wh/day}$$

2.4.3 Sizing PV modules

In order to size PV array, the total peak watt that the PV module produces is needed. From Table 2.8, the total peak watt is 90 W. The average solar radiation for the CPUPT Bellville site is 5.79 KW/day.

$$\begin{aligned} \text{The number of PV panels needed} &= 1190.28/90 \times 5.79 \\ &= 2.28 \end{aligned}$$

The actual number is 3 modules

2.4.4 Battery sizing

To size the battery bank, the total load should be converted to amp-hours as follows:

$$\text{The total appliance} = 76.3 \times 12 = 915.6 \text{ Wh}$$

$$\text{Nominal battery voltage} = 12 \text{ V}$$

$$\text{Days of autonomy} = 2 \text{ days}$$

$$\text{Battery efficiency} = 0.75$$

$$\text{Depth of discharge DOD} = 60\%$$

$$\text{Battery capacity (Ah)} = \frac{\text{total watt-hour} \times \text{days of autonomy}}{\text{battery losses} \times \text{DOD} \times \text{nominal battery voltage}}$$

$$\begin{aligned} \text{Battery capacity} &= (915.6 \times 2) / (0.75 \times 0.6 \times 12) \\ &= 339.11 \text{ Ah} \end{aligned}$$

The battery should be rated 12 V 400 Ah for 2 days of autonomy. For more technical specification of the batteries that have been chosen, see Appendix A-2.

From the previous calculations, we conclude that the components of solar PV system are, three 90 W PV panels, MPPT charge regulator and four deep cycle batteries with capacity of 100 Ah connected to the load as shown in Figure 2.4.

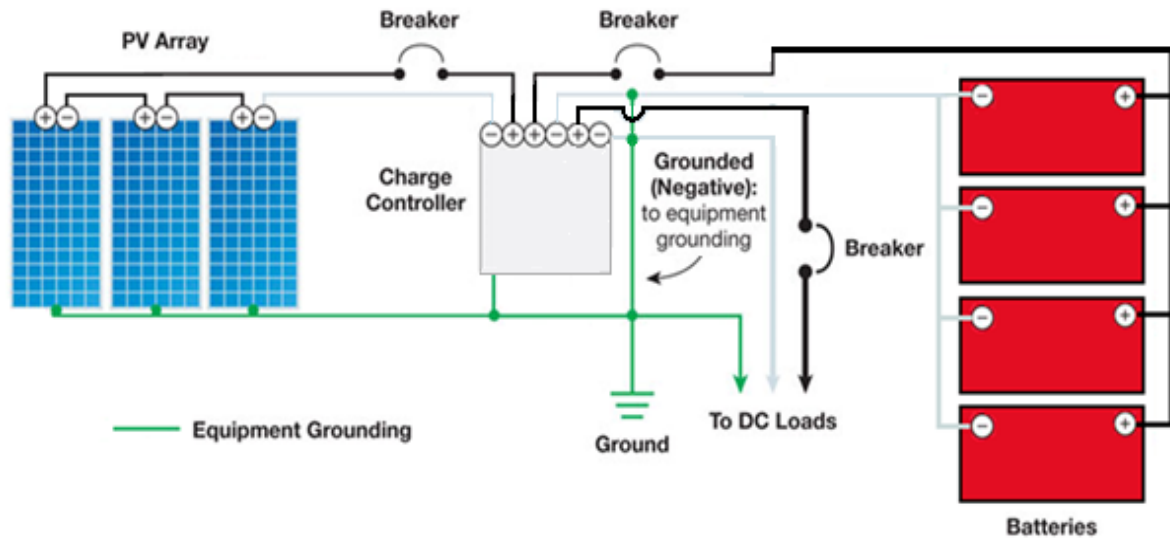


Figure 2.4: Solar PV system components

2.4.1 Refrigeration system construction

The refrigeration system was installed in a thermodynamic laboratory. For cost purpose, a deep freeze chest container was used as a cooling room. A flat evaporator was attached to the back wall of the cooling room. In order to ensure smooth circulation of the air, a small gap about 3 cm was lift between the evaporator and the wall. The outlet of the evaporator was welded to the suction line with dimensions of 6.2 mm in diameter and 15 cm in length. The other end of the suction line was welded to the compressor. The air forced cooled condenser attached to side wall and its inlet welded to the discharge line dimension of 5 mm in diameter and 5cm in length. The other end of the discharge line was welded to the compressor. The outlet of the condenser was welded to the dryer filter. A capillary tube was welded to the dryer filter and the other end to the inlet of evaporator. For purpose of charge and discharge the system with refrigerant, 10 cm pipe was welded to the process connector of the compressor. Figure 2.5 shows the pipes alignment of the refrigeration system. Oxy-acetylene welding used to weld the refrigeration system components as shown in Figure 2.6.

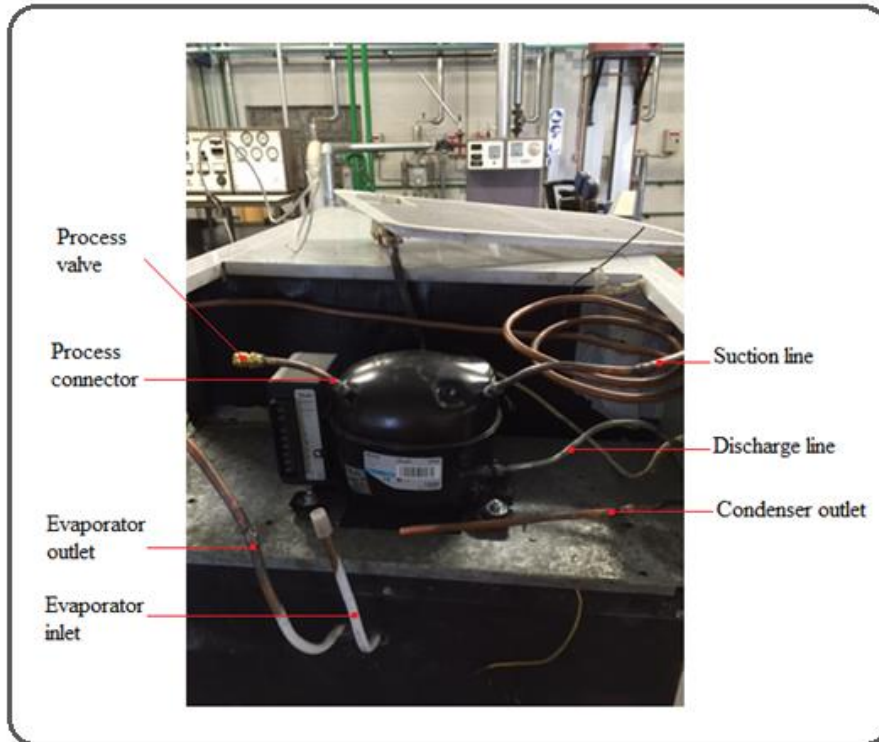


Figure 2.5: The pipes alignment of the refrigeration system

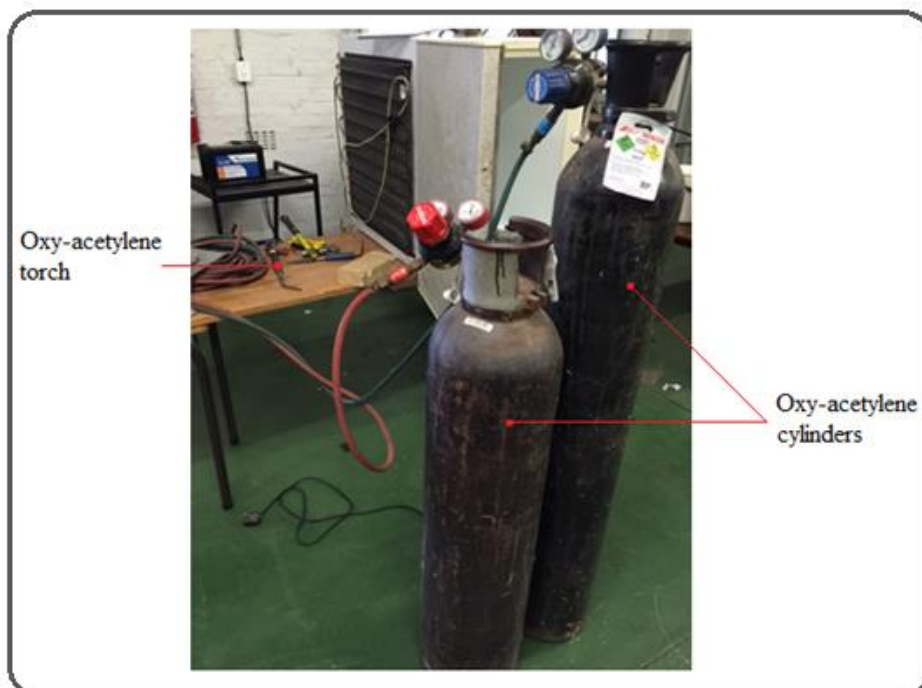


Figure 2.6: Oxy-acetylene welding

To charge the system with refrigerant, a vacuum pump was used to evacuate the refrigeration system. It takes about ten minutes for complete evacuation to ensure

removal of as many contaminants and moisture as possible. After the evacuation, a test gauge was attached to the process valve and R134 refrigerant gas cylinder. The system was charged with about 800 g of the refrigerant. The refrigerant cylinder was weighed before and after the process to ensure that the specific amount of refrigerant flowed into the system. Figure 3.3 shows the charging process.

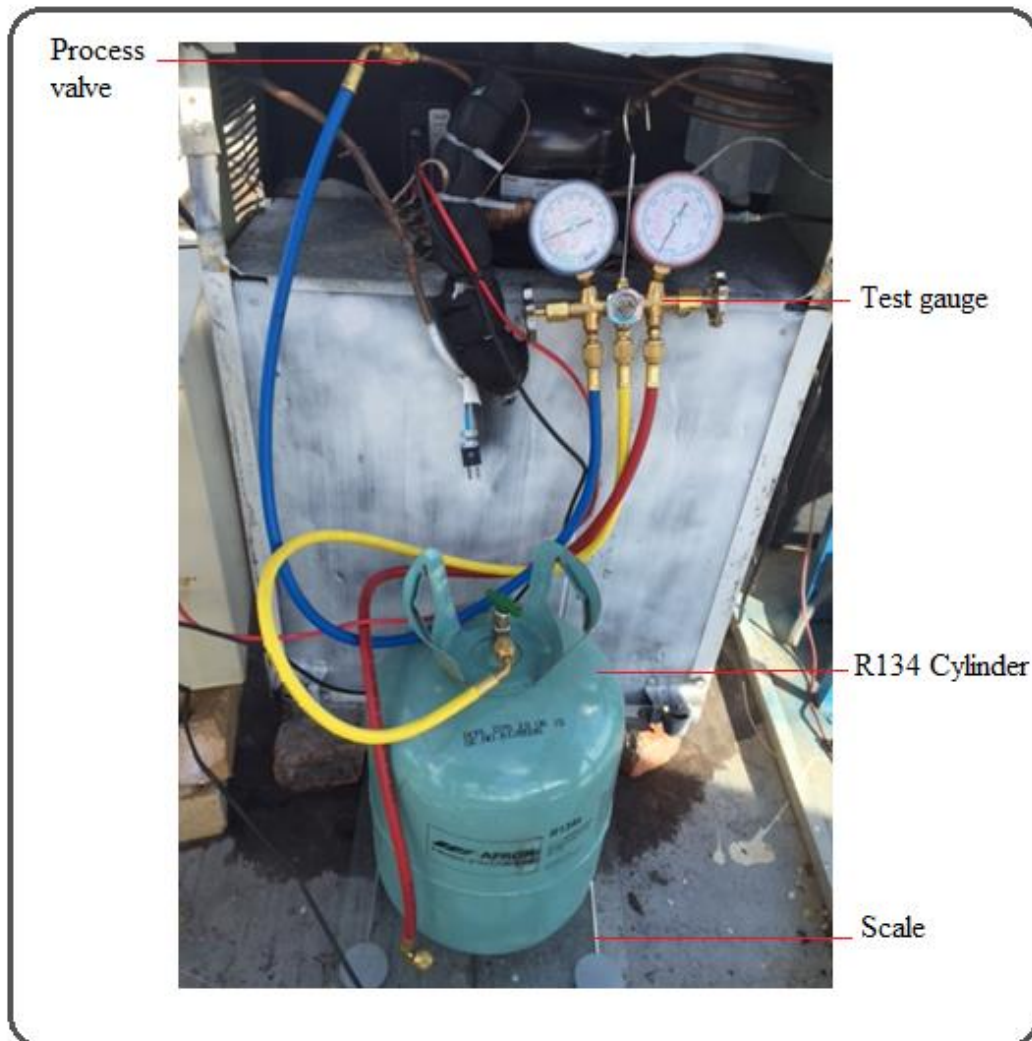


Figure 2.7: Refrigeration system charging process

Chapter 3 EXPERIMENTAL SETUP AND METHODOLOGY

The refrigeration system described in CHAPTER 2 was assembled in a Thermodynamics laboratory in the mechanical engineering department and then attached to the solar system on the top roof of the building. The experiments were performed in April 2016 for a period of 26 days. The experiments were run in weather condition in Bellville, Cape Town. Firstly, the performance of the system was tested with an empty cooling space. Secondly, the performance of the system was tested with a fully loaded cooling space. This chapter presents the experimental setup and the data collection methodology in order to investigate the coefficient of performance and then to calculate the total heat load of the cooling system. Instrumentation and testing procedures are described as well.

3.1 Model testing

3.1.1 Testing procedure

The experiments were implemented under the atmospheric conditions on the roof of the mechanical department building, Bellville, Cape Town. The data collection was done during the day between 8:00 to 17:00 during the month of April 2016.

3.1.2 Measured data and instrumentation

During the period of experimentation, solar radiation intensity, ambient temperature and wind speed were collected from the weather station on the roof of the building. This station consists of two pyranometers and an anemometer as shown in Figure 3.3. The first pyranometer with a shading ring measured diffuse radiation. The other one measured the total solar radiation (diffuse and beam). The anemometer measured the air velocity. All of them were connected to the data logger.

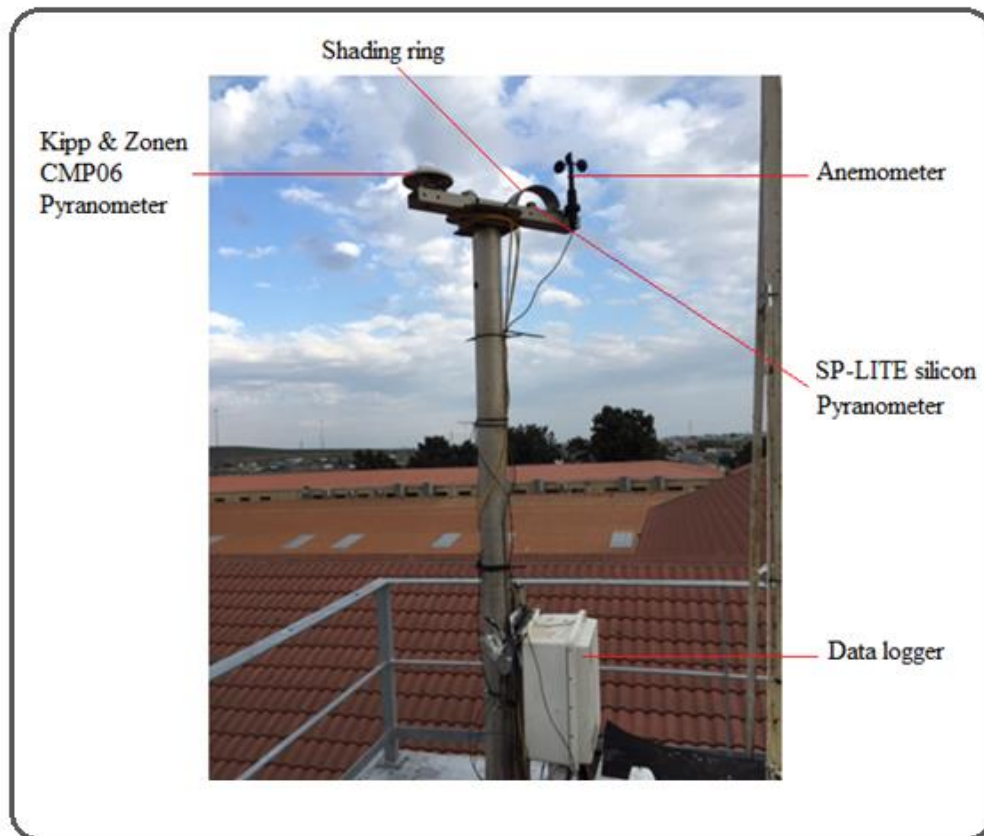


Figure 3.1: Campbell Scientific weather station

- **Solar radiation measurements**

During the period of experimentation, the solar radiation was measured by using two different types of pyranometers

The Kipp & Zone CMP6 pyranometer was used to measure the total solar radiation intensity. It consists of a high quality blackened thermopile sensor, two glass domes, housing and cable as shown in Figure 3.2. Its flat spectral sensitivity ranged from 285 to 2800 nm. For more technical specification, see Appendix B-1.

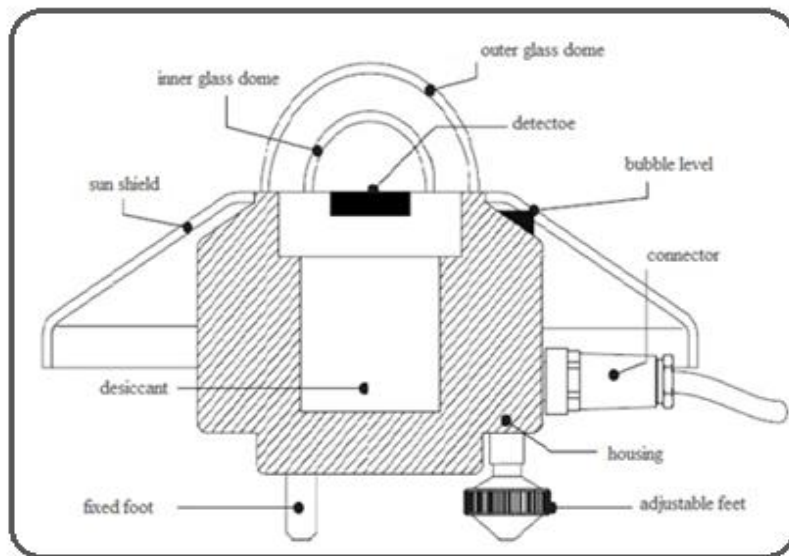


Figure 3.2: Schematic diagram of the Kipp & Zonen CMP06 Pyranometer

Adapted from (Omni, 2009)

The Kipp & Zonen SP-LITE Silicon pyranometer (Figure 3.3) was used to measure the diffuse solar radiation. It consists of a photodiode complete with frame and cable. In order to produce a voltage output, the electrical circuit of the photodiode includes a shunt resistor. The photodiode electrical sensitivity changes with the temperature. A nominal value of this change is about 0.2 % per °C. For more technical specification, see appendix B-2.



Figure 3.3: Kipp & Zonen SP-LITE silicon Pyranometer

Adapted from (campbell, 2015)

- **Wind speed measurement**

A 03101 Young three cup anemometer (Figure 3.4) was used to measure the wind speed. It consists of three cups connected to the shaft. The rotation of the shaft generates a sine wave voltage with a frequency proportional to wind speed. The data logger which was directly connected to the anemometer measures the pulse signals and gives the reading of m/s. Appendix B-3 gives more technical specifications of the 03101 anemometer.

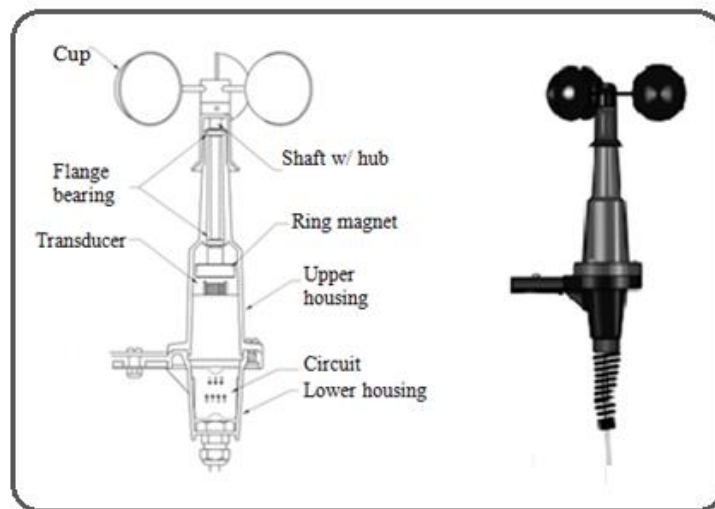


Figure 3.4: 03101 R.M Young Anemometer

Adapted from (campbell, 2015)

- **Electrical current measurement**

Etekcity MSR-C600 Digital Clamp Meter & Multimeter with AC / DC Voltage Test (Figure 3.5) was used to measure the current consumption of the refrigeration system. The meter has two jaws that close around the conductor measuring the current. The jaw diameter ranged up to 28 mm.



Figure 3.5: Etekcity MSR-C600 Digital Clamp Meter

- **Temperature measurements**

Different types of thermometers (Figure 3.6) were used to measure the temperature of the refrigeration system. Four of 5 PCS/LOT TPM-10 Embedded Digital Thermometers were attached to the inside walls. Two of the T-type (Copper/Constantan) thermocouples were attached to the inlet and outlet of the evaporator. Another two were used to measure the fruit temperature. The temperatures of the outside walls and the condenser were measured by an infrared digital thermometer. See Appendix B-4 and Appendix B-5 for technical specifications of the thermometers. The temperatures distribution was as following:

1. The left side of the inner wall temperature (T_{lin})
2. The right side of the inner wall temperature (T_{rin})
3. The inner side of the door temperature (T_{din})
4. The cooling room temperature (T_{in})
5. The evaporator inlet temperature (T_{ein})
6. The evaporator outlet temperature (T_{eout})
7. The left side of the outer wall temperature (T_{lout})
8. The right side of the outer wall temperature (T_{rout})
9. The upper side of the outer wall temperature (T_{up})
10. The back side of the outer wall temperature (T_b)
11. The outer side of the door temperature (T_{dout})
12. The condenser inlet temperature (T_{cin})
13. The condenser outlet temperature (T_{cout})

14. Ambient temperature (T_a)

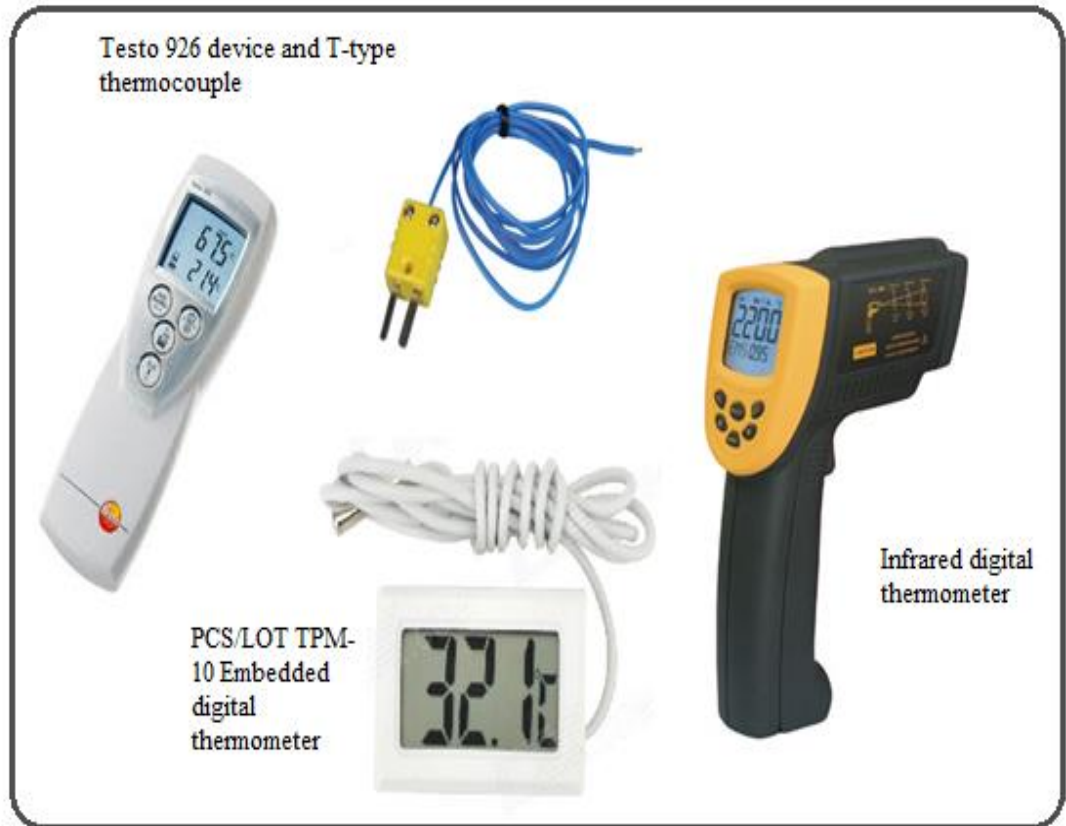


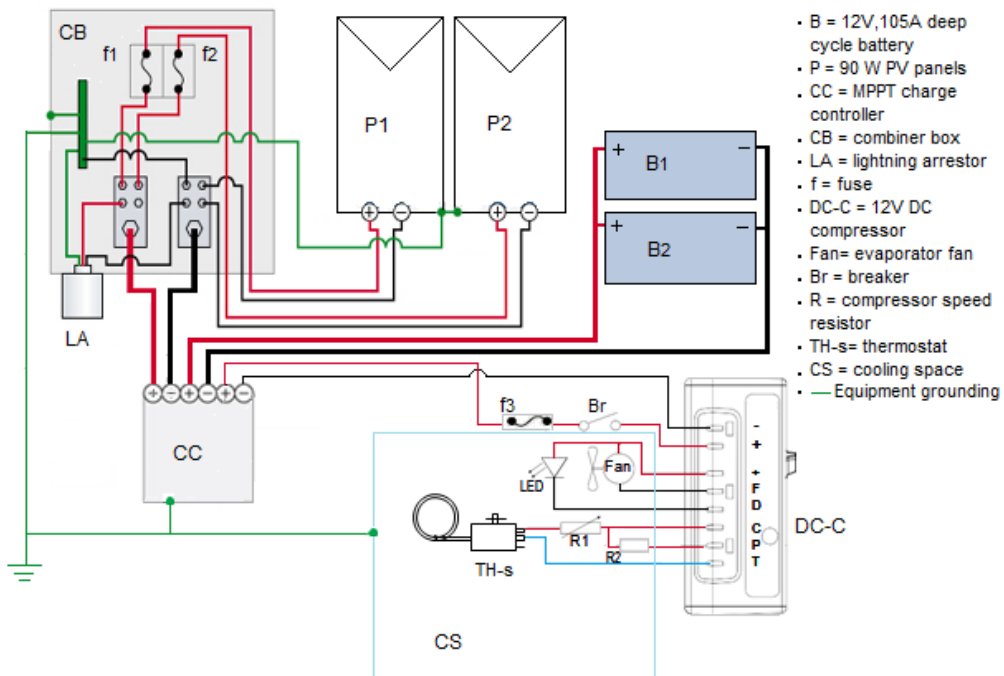
Figure 3.6: Digital thermometers

3.2 Experimental setup

A solar PV system consists of two 90W PV panels, ten A MPPT charge controller and two 12V; 105A deep cycle batteries wired up as shown in Figure 3.7. The panels were installed on a metal frame facing north at a slope of 30° from the horizontal. The charge controller, main switcher, and the other electronic components were installed in the protected box as illustrated in Figure 3.7 (a). In the refrigeration system, a 12V DC compressor has eight terminal plugs. Two terminals were connected to the charge controller. The rest were connected to the evaporator fan, led light, compressor speed controller and thermostat as demonstrated in Figure 3.7 (b). A set of thermocouples were attached to the cooling system components in order to measure the temperature. The weather data (horizontal radiation, diffuse radiation and ambient temperature) were recorded in the data logger.



(a)



(b)

Figure 3.7: Experimental set-up: (a) Actual layout, (b) Wiring diagram

3.3 Solar radiation estimation

The data collected from the Campbell Scientific weather station shows the solar radiation on a horizontal surface. For a tilted surface therefore, the total incident solar radiation is the sum of the beam and diffuse component. It can be expressed as follows:

$$I_T = I_{T,b} + I_{T,d} \quad (3.1)$$

In recent studies of the clear sky, the intention is to divide the diffuse into an isotropic diffuse ($I_{T,d,iso}$), circumsolar diffuse ($I_{T,d,cs}$), horizon brightening ($I_{T,d,hb}$) and the reflected radiation ($I_{T,d,g}$) (Loutzenhiser, et al., 2007). Therefore, equation 3.1 can be written as following:

$$I_T = I_{T,b} + I_{T,d,iso} + I_{T,d,cs} + I_{T,d,hb} + I_{T,d,g} \quad (3.2)$$

By applying the geometrical relationship, the solar azimuth and altitude can be determined for the location (longitude and latitude).

Loutzenhiser and others examined seven solar radiation models on tilted surfaces. They included Isotropic sky, Klucher, Hay-Davies, Reindle, Muneer, and Perez models. They concluded that the Perez model represents a more detailed analysis of solar radiation diffuse. In the experiment therefore, the Perez 1990 model was used to estimate the solar radiation on tilted PV panels (Perez, et al., 1990). It is expressed as following:

$$I_T = I_b R_b + I_d \left[(1 - f_1) \left(\frac{1 + \cos\beta}{2} \right) + F_1 \frac{a}{b} + F_2 \sin\beta \right] + I_h \rho_g \left(\frac{1 - \cos\beta}{2} \right) \quad (3.3)$$

(a) and (b) take into account the incidence angle of the sun on the sloped and horizontal surfaces. F_1 and F_2 are circumsolar and horizon brightness coefficients. The value of (a) and (b) is computed as follows:

$$a = \max(0, \cos\theta_i) \quad (3.4)$$

$$b = \max(\cos 85^\circ, \cos\theta_z) \quad (3.5)$$

The coefficients F_1 and F_2 depend on the sky clearness factor ϵ and the brightness factor Δ . These factors are computed as follows:

$$\varepsilon = \frac{\frac{I_d + I_{b,n}}{I_d} + 5.535 \times 10^{-6} \times \theta^3}{1 + (5.535 \times 10^{-6} \times \theta^3)} \quad (3.6)$$

$$I_{b,n} = \frac{I_b}{\cos\theta_z} \quad (3.7)$$

Where, $I_{b,n}$ is normal incidence beam.

$$\Delta = m \frac{I_d}{I_{on}} \quad (3.8)$$

$$m = \frac{1}{\cos\theta_z} \quad (3.9)$$

$$I_{on} = I_{sc} \left(1 + 0.33 \cos \frac{360n}{365} \right) \times \cos\theta_z \quad (3.10)$$

Where, m is the air mass. I_{on} is the extra-terrestrial normal incidence radiation; I_{sc} is the solar constant (1367 W/m²).

Therefore, F_1 and F_2 are computed as following:

$$F_1 = \max \left[0, \left(f_{11} + f_{12}\Delta + \frac{\pi\theta_z}{180} f_{13} \right) \right] \quad (3.11)$$

$$F_2 = \left(f_{21} + f_{22}\Delta + \frac{\pi\theta_z}{180} f_{23} \right) \quad (3.12)$$

The factors F_{11} , F_{12} , F_{13} , F_{21} , F_{22} and F_{23} were derived by (Perez, et al., 1990) based on a statistical analysis of the clearness. These factors are given in Appendix C-1.

The beam radiation ratio R_b on tilted surface is calculated as following:

$$R_b = \frac{\cos\theta_i}{\cos\theta_z} \quad (3.13)$$

θ_z is the zenith angle and θ_i is the incident angle. This is shown in Figure 3.8.

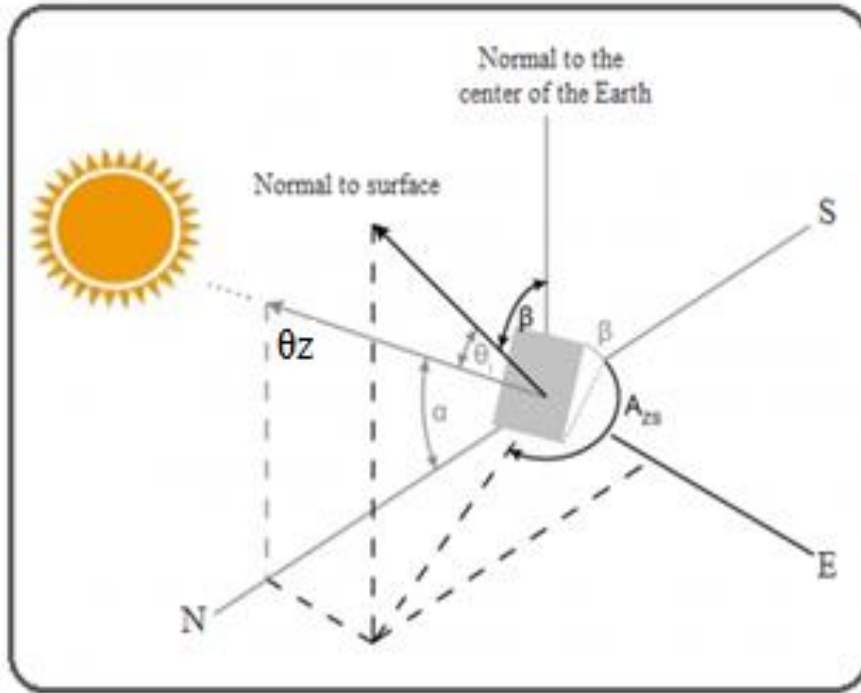


Figure 3.8: Solar angles on inclined PV panel.

These angles are given in following equations:

$$\cos\theta_i = \cos(L + \beta)\cos\delta\cos\omega + \sin(L + \beta)\sin\delta \quad (3.14)$$

$$\cos\theta_z = \cos L\cos\delta\cos\omega + \sin L\sin\delta \quad (3.15)$$

$$\delta = 23.45 \sin\left(360 \frac{284 + n}{365}\right) \quad (3.16)$$

L is the latitude of the location, with north positive, β is the tilt angle, δ is the declination angle of the sun, n the day of the year which can be obtained with the help of Table 3.1, ω is the hour angle which is given in equation 3.17.

$$\omega = 15(t - t_{noon}) \quad (3.17)$$

$$t_{noon} = 720 + 4 * longitude - (equation on time) \quad (3.18)$$

Where: t is the local time and t_{noon} is solar noon, the equation of time is expressed as following:

$$Equation\ on\ time = 9.87 \sin 2B - 7.53 \cos B - 1.5 \sin B \quad (3.19)$$

$$B = (n - 81)\left(\frac{360}{365}\right) \quad (3.20)$$

Table 3.1: Value of n

Month	n for i th
	Day of Month
January	i
February	$31 + i$
March	$59 + i$
April	$90 + i$
May	$120 + i$
June	$151 + i$
July	$181 + i$
August	$212 + i$
September	$243 + i$
October	$273 + i$
November	$304 + i$
December	$334 + i$

Adapted from (Duffie & Beckman, 2006)

3.4 Coefficient of performance of the refrigeration system

The coefficient of performance (COP) of the actual VCR shown in Figure 3.9 is calculated using equation 3.21.

$$COP = \frac{Q_{refl}}{W} \quad (3.21)$$

Where: Q_{refl} is the heat removed from the cooling space, W is the compressor input power (W).

$$Q_{refl} = \dot{m}(h_1 - h_4) \quad (3.22)$$

Where: \dot{m} is mass flow rate of the refrigerant (kg/s), h is enthalpy (kJ/kg).

$$W = \dot{m}(h_2 - h_1) \quad (3.23)$$

Therefore, equation (12) can be written as following:

$$COP = \frac{(h_1 - h_4)}{(h_2 - h_1)} \quad (3.24)$$

The values of h_1 , h_2 and h_4 are calculated from R134a tables.

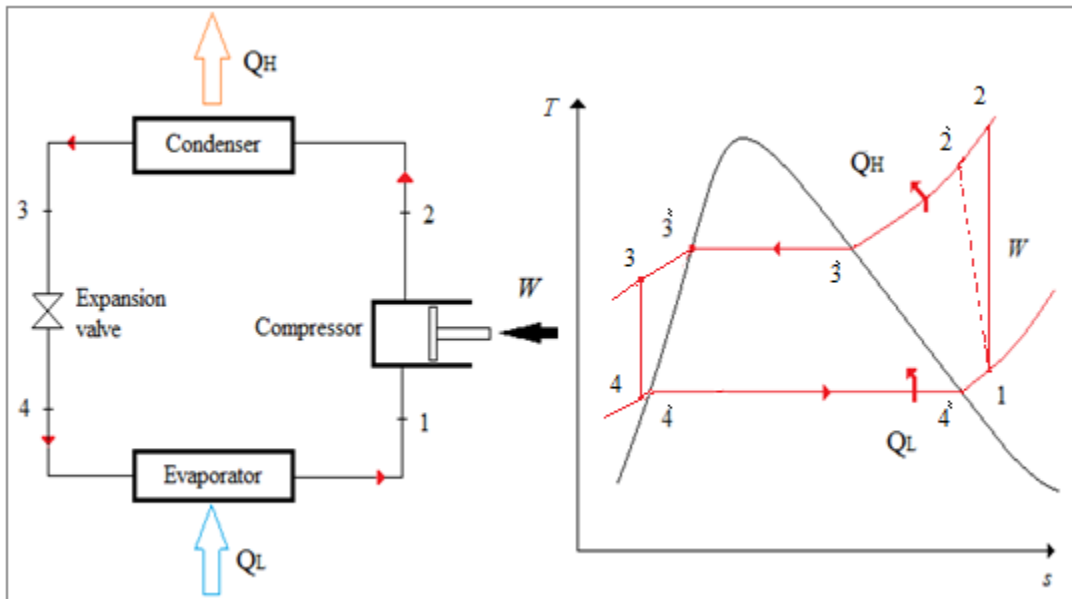


Figure 3.8: Actual vapour-compression system and its T - s diagram.

Chapter 4 RESULTS AND DISCUSSION

4.1 Introduction

This chapter presents the results of the experimental work that was performed on the solar PV refrigeration system. The model described in Chapter 2 was tested under the atmospheric condition in Bellville, Cape Town. Chapter 3 provided the experimental methodology used to obtain the necessary data for the performance analysis of the solar PV refrigeration system. The influence of the weather conditions on the Solar PV refrigeration model are discussed in this chapter. The impact of ambient temperature on the leaked and product heat load is analysed as well. The coefficient of performance of the vapour compression refrigeration cycle and the other results are described in more detail.

4.2 Solar PV refrigeration model performance

The solar PV refrigeration model was tested in the month of April. During the test period, the model was tested for five days, firstly with an empty cooling space, and then tested for another three days with a full load of 20kg of apples.

4.3 Weather conditions

The variation of solar radiation, ambient temperature and wind speed are shown in Figure 4.1. For the first day of loading cooling space, the ambient temperature ranged between 18.5 and 33.8 °C. The solar radiation on a horizontal surface ranged between 94 and 694.8 W/m². The wind speed ranged from between 0.29 and 2.24 m/s (See Appendix C-2).

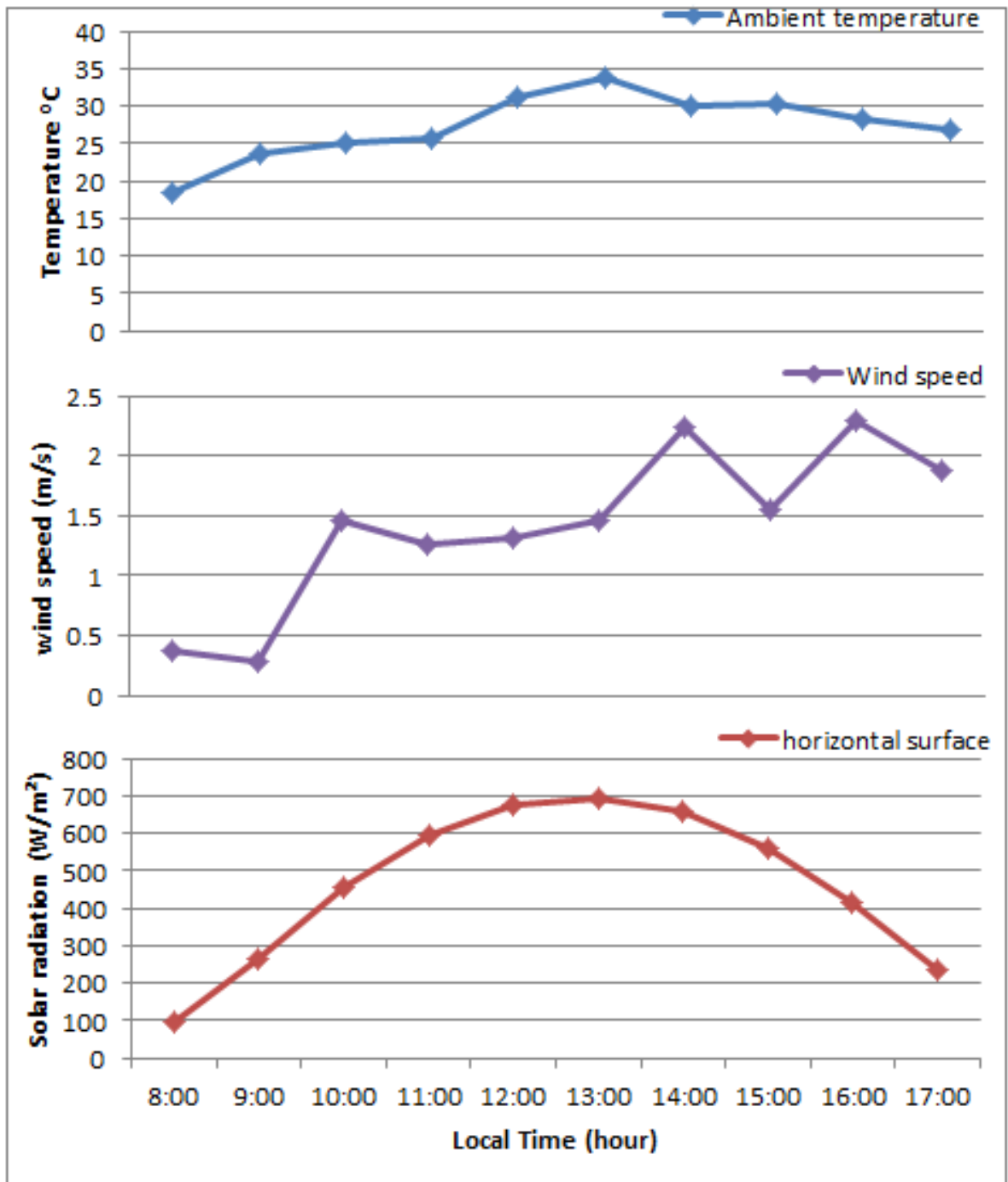


Figure 4.1: Variation of weather conditions with local time on 18 April 2016 at the Cape Peninsula University of Technology

The total solar radiation on a 30° inclined PV panel was computed using the Perez model explained in Chapter 3. The variation of solar radiation on a horizontal surface and the total solar radiation on the PV panel (18 April 2016) is shown in Figure 4.2. It was observed that the total solar radiation on the inclined PV panel was more than the solar radiation on a horizontal surface. This is in agreement with the findings from (Kanyarusoke, et al., 2012). The peak of the total solar radiation on the panel was

1022.2 W/m² while the peak of the solar radiation on horizontal surface was 694.8 W/m² as can be seen in Figure 4.2

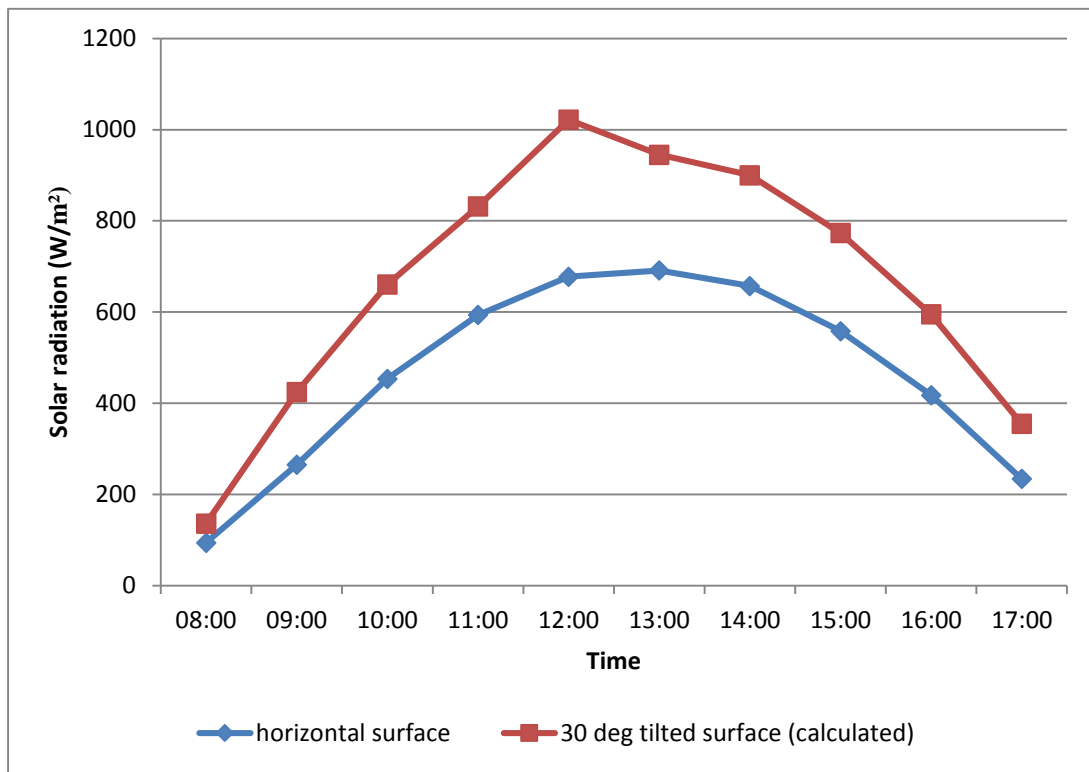


Figure 4.2: Variation of solar radiation on horizontal surface and inclined PV panel measured on 18 April 2016.

Figure 4.3 shows the solar radiation components (beam and diffuse), the total solar radiation and the solar radiation on a 30° tilted PV panel. It was observed that throughout the day, the beam radiation was always higher than the diffuse radiation.

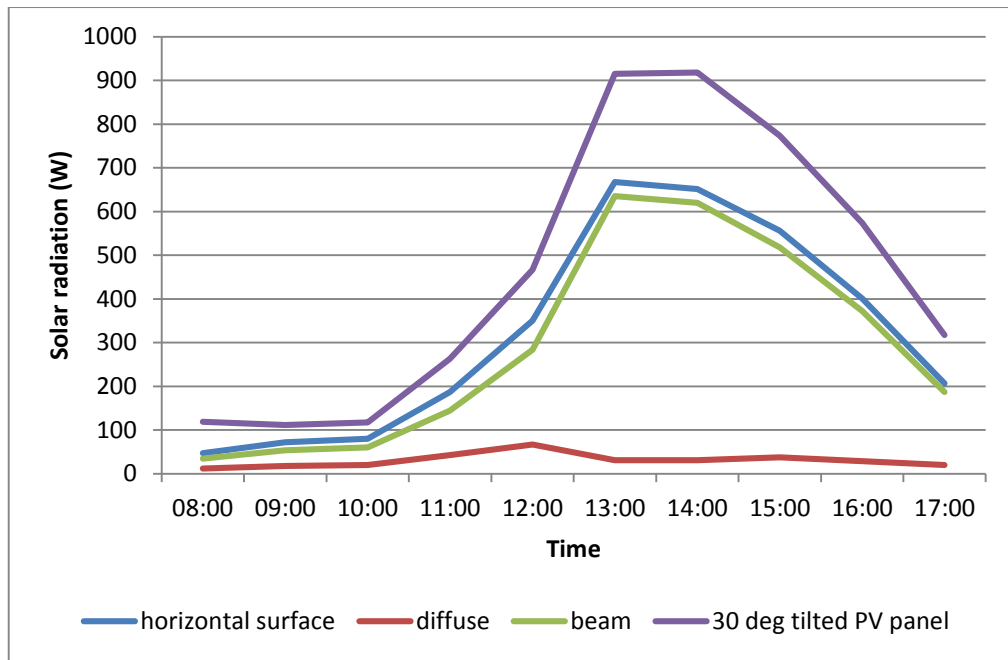


Figure 4.3: Variation of beam, diffuse and direct solar radiation with local time on 19 April 2016

The variation of the temperature of the outer surfaces of the cooling room walls during the first day of having loaded the cooling space with fruits is shown in Figure 4.4 as a typical example. See table (5) in Appendix (E).

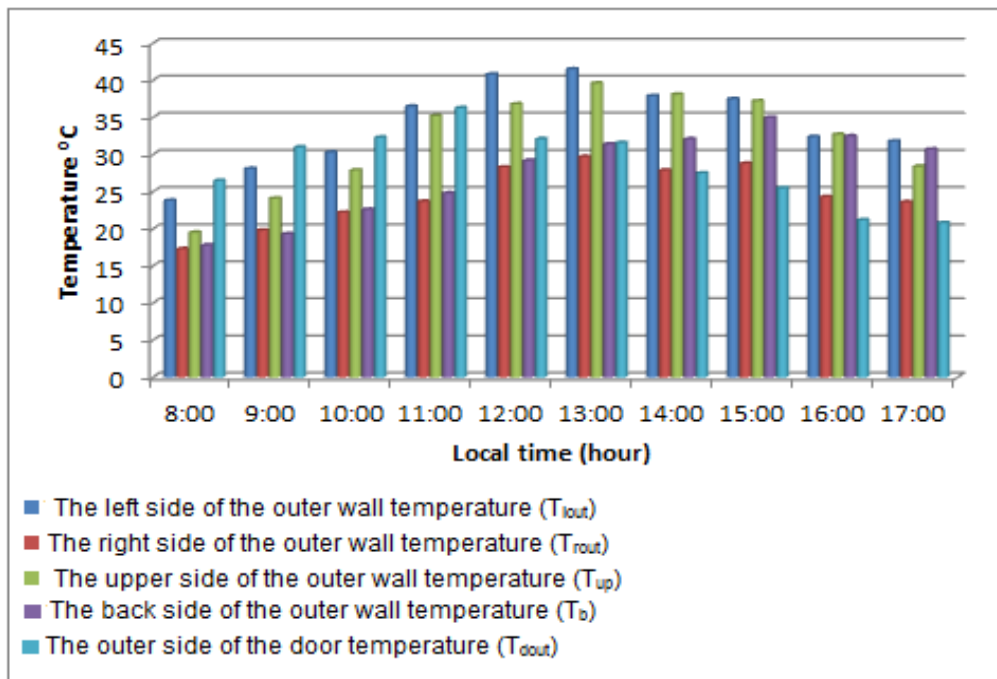


Figure 4.4: Variation of the temperature of the outer surfaces of the cooling room walls

It was observed that the left side wall had the highest temperature. Its maximum temperature reached to 41.5 °C. This is because the wall faces the sun most of the day.

The difference between ambient temperature and the average initial product temperature is shown in Figure 4.5.

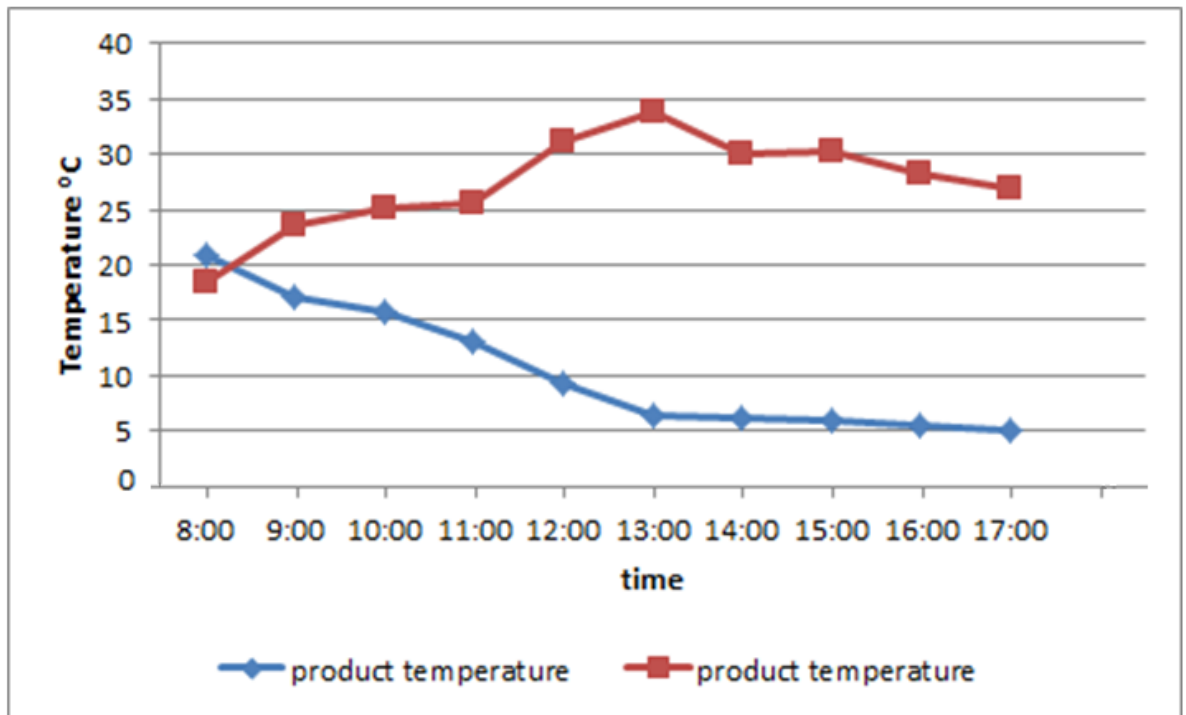


Figure 4.5: Variation of ambient and product temperature on 18 April 2016

From the graph, we can notice that the initial product was at a higher temperature than the ambient. This is what could be expected to happen on a farm because of enzymatic activity in the fruit. It was observed that the product temperature was maintained at the desirable temperature after five hours of storage.

The cooling space was loaded with 20 kg of apples at a temperature of 20 °C. The apples were loaded at 08:00 as being the appropriate time of the harvest. The fruits were stacked in two rows and columns of boxes. In order to monitor the fruit temperature in each column, two thermocouples were attached. The variation of the temperature of the stacked fruit is given in Figure 4.6.

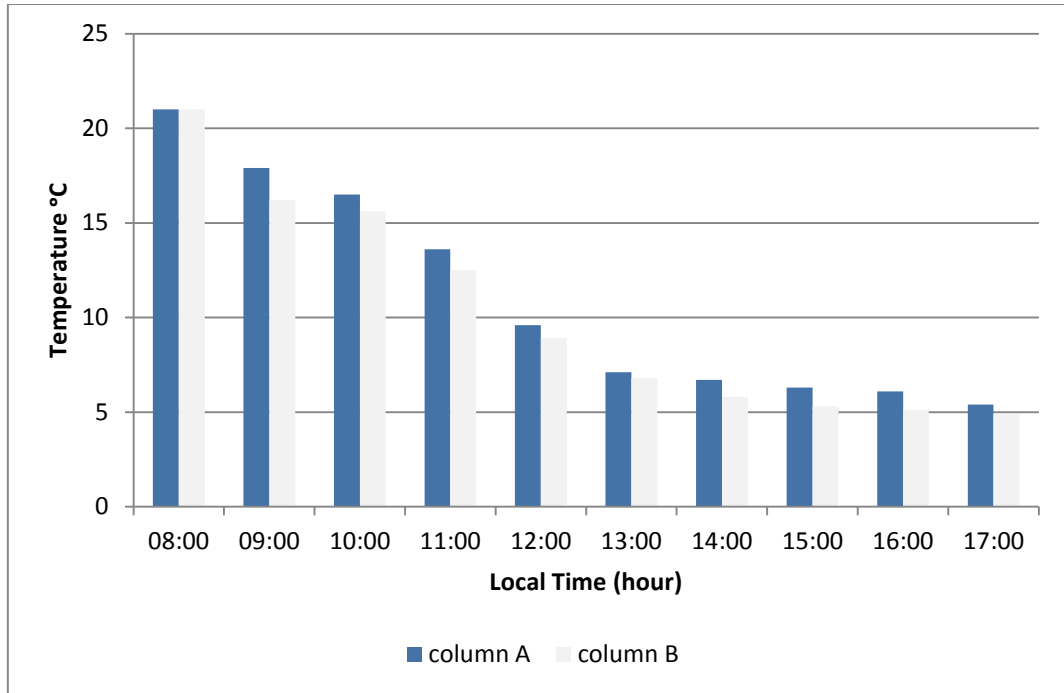


Figure 4.6: Variation of the stacked fruit at first day of storage

From the graph, Column A is a stack of six boxes of fruit which had been stacked close to the door. Column B is stack of five boxes which were stacked close to the evaporator. It was observed that there was a slight difference between the temperature distributions in the hours of storage. In the second of storage, the temperature distribution was almost even as shown in Figure 4.7.

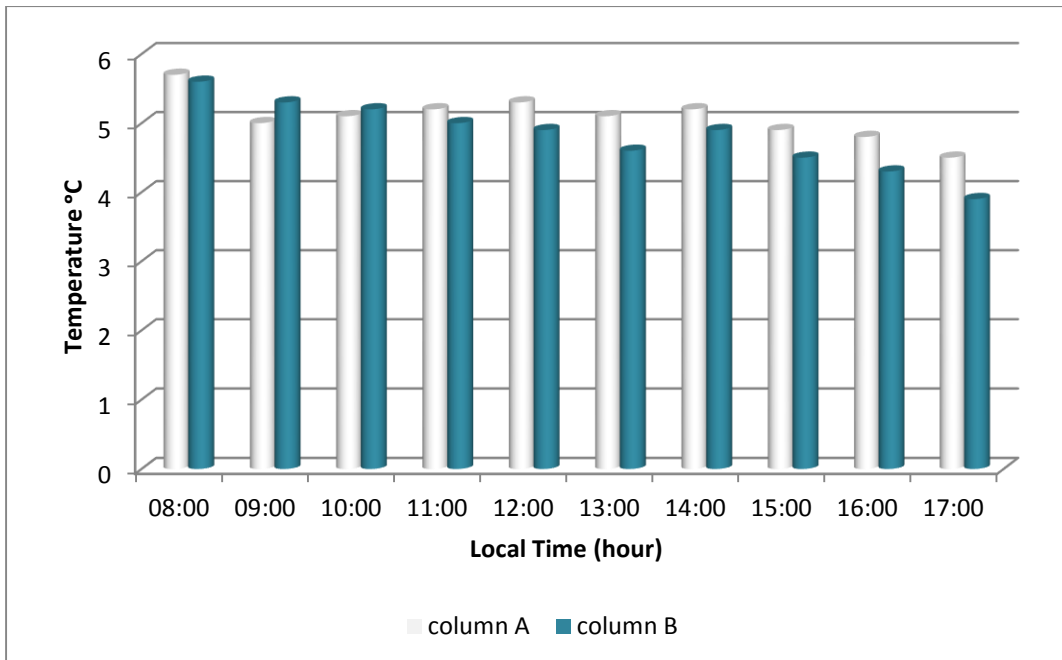


Figure 4.7: Variation of the temperature distribution in the second day of storage

The comparison between the average fruit and the ambient temperature in the second day of storage is shown in Figure 4.8. It was observed that the average fruit temperature had been maintained at about 5.01 °C while the highest ambient temperature was recorded at 31.06 °C.

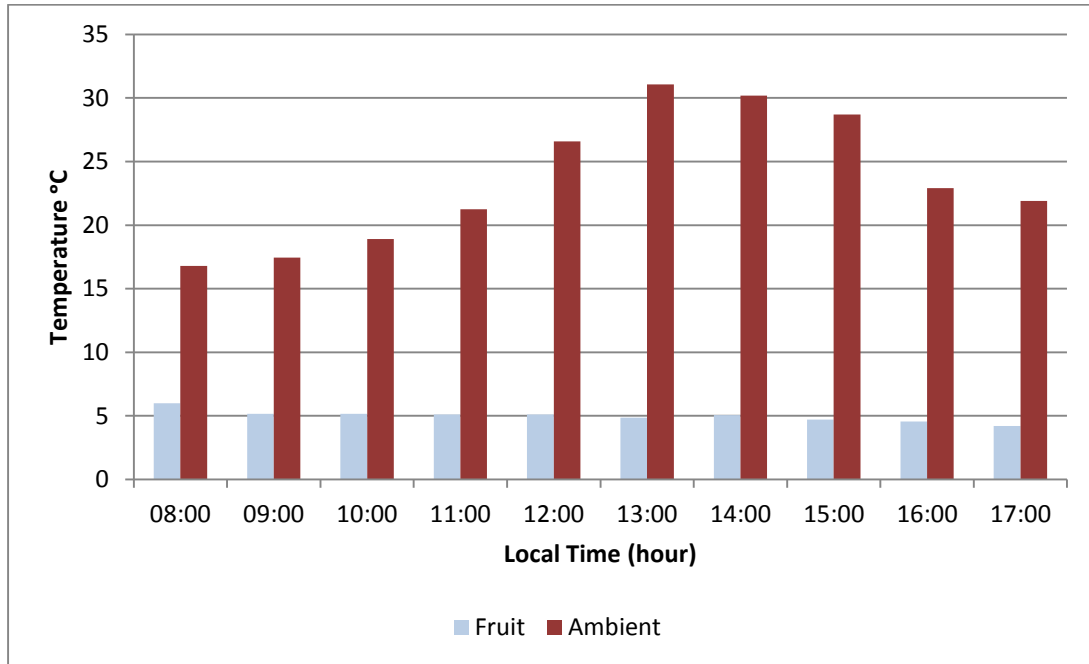


Figure 4.8: The difference between ambient and fruit temperature in the second day of storage

During the second day of loading cooling space, ambient temperature was relatively high. The highest temperature reached 31.06 °C. That increase led to the increase of the outside surface temperature of the cooling room walls. The temperature of the wall facing the sun reached 39.6 °C while the inside temperature of the cooling room was maintained at 4.6 °C as seen in Figure 4.9.

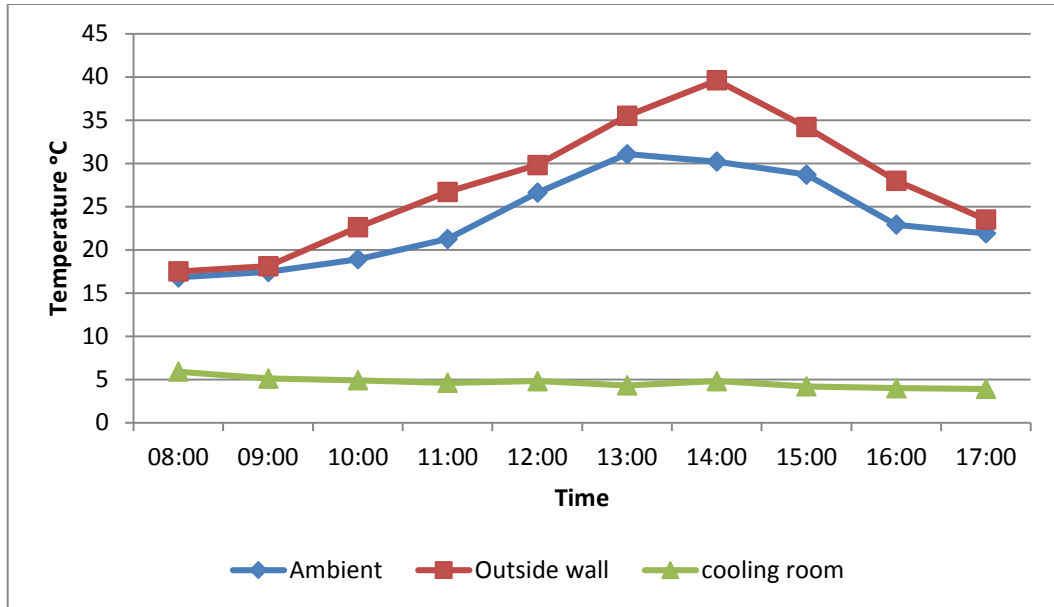


Figure 4.9: Variation of ambient, outside wall and inside cooling room temperature

The variation of the coefficient of performance COP of the system during the first day of loading the cooling space with the fruit was calculated using the temperature of the R134a at the entrance and the exit of the evaporator and the condenser. In order to get the corresponding enthalpy, R134a charts were used. The average of COP was 2.5. Figure 4.10 shows the variation of the COP of the system.

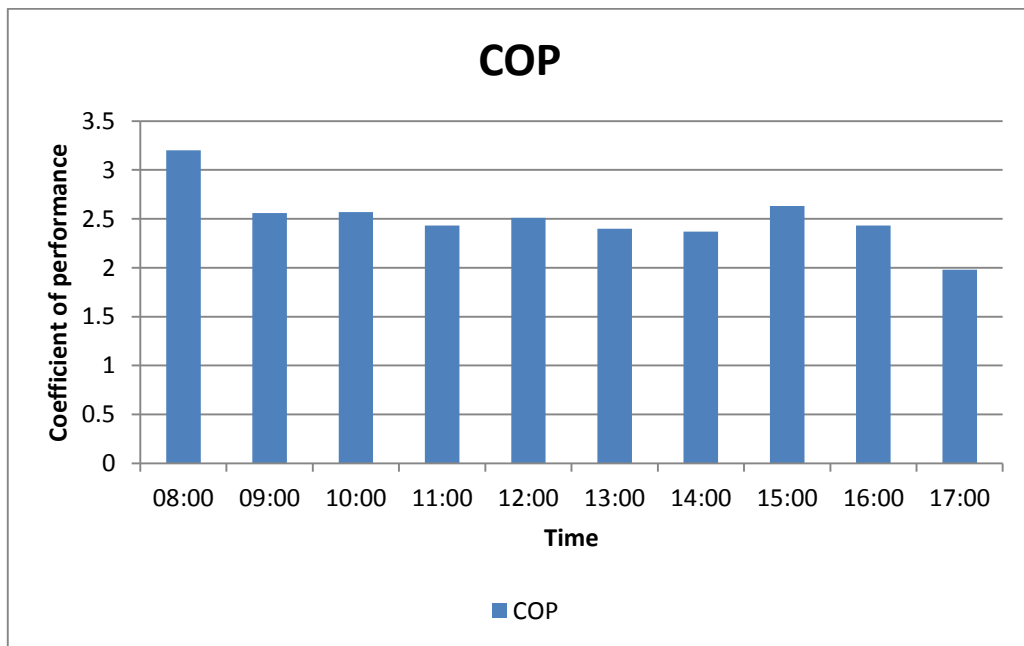


Figure 4.10: Variation of coefficient of performance of the cooling system on 18 April 2016

The total heat load of the refrigeration system model during the first day of loading a the cooling space with the fruit is given in Figure 4.11. It is observed that at the first hour of storage, the total heat load was high because the fruit temperature was high (see sample calculation of heat load in Appendix F).

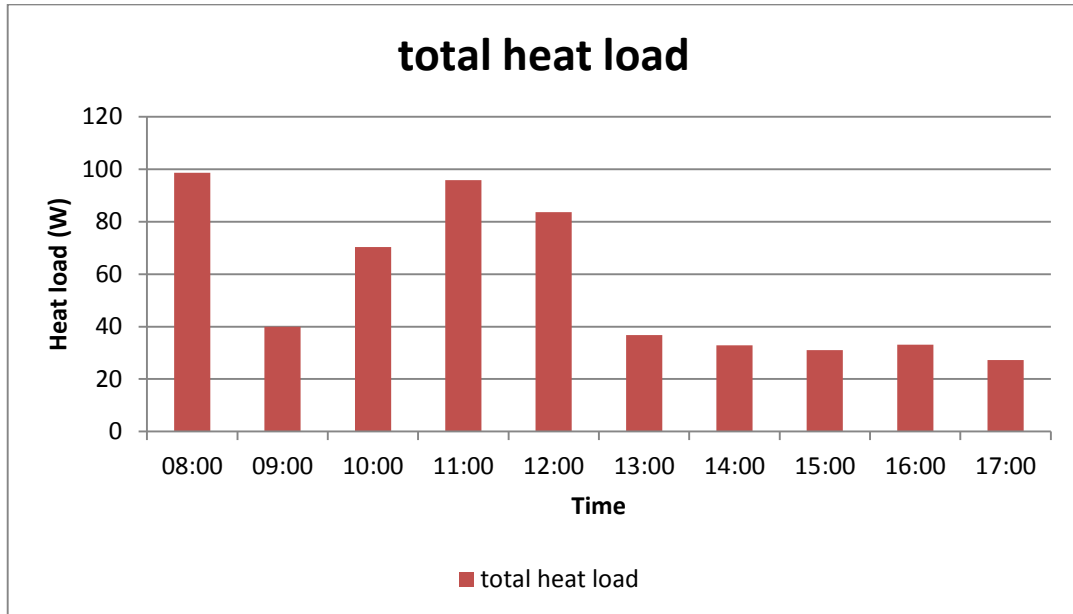


Figure 4.11: The total heat load during the first day of storage

Figure 4.12 shows the comparison between heat load of the PV refrigeration system model during the first day of loading cooling space and other day similar in weather condition but with an empty cooling space.

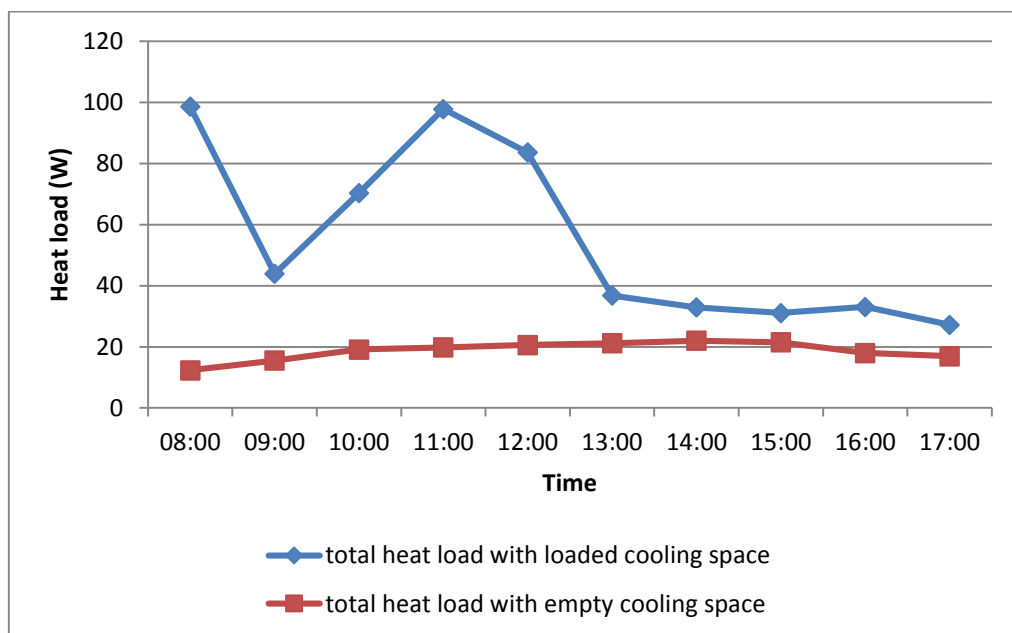


Figure 4.12: Comparison between a heat load of the PV refrigeration model with loaded and empty cooling space

From the graph, the total heat load fluctuated from 100 to 40 W during the first five hours of storage, before becoming stable. This fluctuation results from the difference in fruit temperature. See the sample of calculation in Appendix B for better understanding. It was also observed that the heat load of the cooling model with empty space was almost stable. The reason is that heat load include only heat leak from the walls.

The impact of ambient temperature and the wind speed on the total heat load of the refrigeration system is shown in Figure 4.13. It was observed that the total heat load increased with the increase in ambient temperature. But the variation of wind speed has no significant influence on the total heat load.

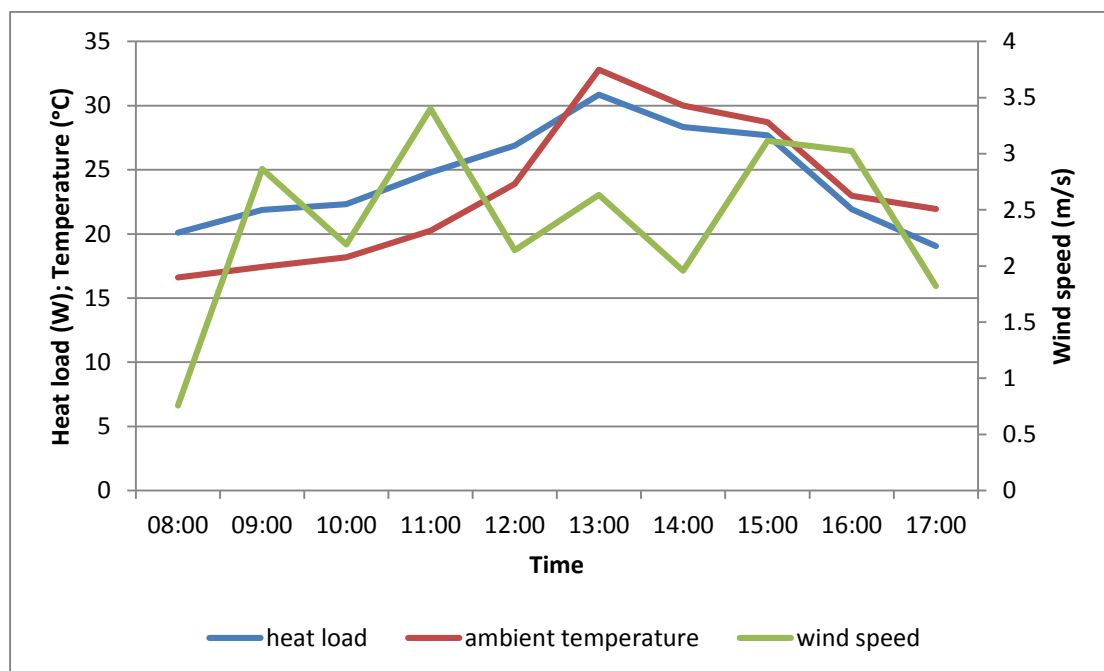


Figure 4.13: The impact of ambient temperature and wind speed on total heat load of refrigeration system

The power consumed by the refrigeration system which came from multiplying battery voltage (12) by ampere-hour is shown in Figure (4.11). It was observed that at some point, the power consumption equals zero because the compressor was at rest.

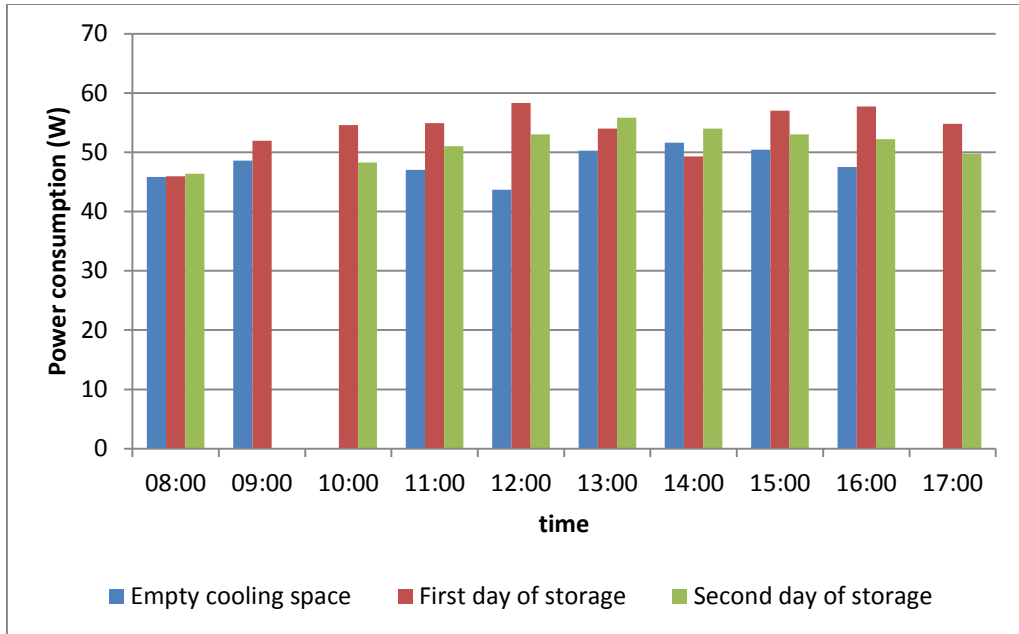


Figure 4.14: Comparison between compressor power consumption

Chapter 5 Conclusions and Recommendations

5.1 Summary

Post-harvest loss (change in edibility, availability and quality) can occur at any stage between harvesting and final delivery to the customer. Fruits and vegetables have a high rate of perishability. Therefore, preservation processes have to be undertaken soon after harvesting. A precooling process is considered to be the first stage of the preservation processes. It should apply in order to reduce the field temperature of the fruits and vegetables. Precooling is an instantaneous procedure leading to preservation. It is considered to be a short term period of storage before transportation and the long term period of storage. Applying precooling processes can make a huge impact in terms of extending the shelf life of food products.

The present study intended to make a contribution towards the efforts that address the post-harvest loss problem by developing a solar refrigeration system with the aim of using it as a precooling unit in order to reduce post-harvest losses. A solar PV refrigeration system model was designed, constructed and tested during the day time. Its performance was analysed under Cape Town weather conditions.

The solar PV refrigeration model consisted of two different systems. A solar PV system runs a conventional vapour-compression refrigeration system. 12V DC compressor is used to produce the cooling effect. In the solar PV system therefore, there is no inverter.

The test was done in April 2016. The refrigeration unit was tested with the cooling space being first empty and then full. During eight days of experiments, the climate measurements (solar radiation intensity, ambient temperature and wind speed) were collected and the refrigeration system performance was monitored as well.

5.2 Conclusion

On the basis of the results obtained in this study, the following conclusions can be drawn

- The variation of weather conditions (incident solar radiation and ambient temperature) has significant effects on the performance of a solar PV refrigeration system. The wind speed has insignificant effect on the total heat load of the refrigeration system.

- The coefficient of performance of the cooling unit varied from 1.98 to 3.2. This is comparable to ordinary of the shelf household refrigeration systems. Therefore a no electricity bills system has been designed successfully.
- The temperature of the fruits reached the desirable storage temperature after five hours of loaded cooling space.
- The cooling system was able to maintain the fruit temperature at the desirable level.
- The concept of using PV panels with a DC compressor to pre-cool farm fruit has been proved. The capacity of the refrigeration system can be increased in accordance with an appropriate PV system size.

The system is suitable for small scale farms to use as pre-cooling units. The importance of this work is that in remote areas, a solar PV refrigeration system can increase farmer income by decreasing post-harvest losses.

5.3 Recommendations for future work

- An investigation of the effect of the direct sunlight incident on the cooling compartment walls could increase the heat leakage to the system and influence the system performance. This needs to be tested
- A future work may attempt to redo the experiments using a tracking solar PV system in order to increase the energy yield.

REFERENCES

- Althouse, Andrew D. Turnquist, Carl H. Bracciano, Alfred F. Bracciano, Daniel C& Bracciano, Gloria M. 2013. *Modern Refrigeration and Air Conditioning Instructor's Resource*. 19 ed. s.l.:Goodheart-Willcox Pub.
- Arora, R. C. 2010. *Refrigeration and Air Conditioning*. reprint ed. New Delhi: PHI Learning (Pvt). Ltd.
- ASHRAE. 2002. *2002 ASHRAE Handbook: Refrigeration*. New York: American Society of Heating, Refrigeration and Air-Conditioning Engineers.
- ASHRAE. 2008. *2008 ASHRAE Handbook: heating, ventilating, and air-conditioning systems and equipment*. New York: American Society of Heating, Refrigerating, and Air-Conditioning Engineers, 2008.
- Badescu, V. (eds). 2008. *Modeling Solar Radiation at the Earth's Surface*. Bucharest: Springer Science & Business Media.
- Berk, Z. 2013. *Food Process Engineering and Technology*. 2nd ed. San Diego: ACADEMIC PRESS.
- Peter. Beck, Micheal. 2008. *Thermal Conductivity of Metal Oxide Nanofluids*.Georgia: ProQuest
- Bhattarai, R. R., Rijal, R. K. & Mishra, P. 2013. Post-harvest losses in mandarin orange: A case study of Dhankuta District, Nepal. *academicjournals*, Volume 8, pp. 763-767.
- Bilgili, M. 2011. Hourly simulation and performance of solar electric- vapor compression refrigeration system. *Solar Energy*, Issue 11, volume 85, pp. 2720-2731.
- Brown, G. V., 1976. Magnetic heat pumping near room temperature. *AIP publishing*, 47(8).
- Burden, J., Wills, R. & Smith, K. 1989. *Prevention of post-harvest food losses fruits, vegetables and root crops a training manual*. [Online]

Available at: <http://www.fao.org/docrep/t0073e/T0073E00.htm#Contents>
[Accessed 24 november 2015].

campbell, 2015. *SP Lite2*. [Online]
Available at: <https://www.campbellsci.ca/products#>
[Accessed 2 May 2016].

Compressor, D. B. 2003. *RPARTS*. [Online]
Available at: http://www.rparts.com/product_info.php?products_id=5
[Accessed 2 February 2016].

Corner, I. 2015. *Multistage refrigeration systems*. [Online]
Available at: <http://www.industrialcorner.com/refrigeration-systems-and-applications/refrigeration-cycles-and-systems/multistage-refrigeration-systems.html>
[Accessed 4 december 2015].

Devabhaktuni, Vijay., Alam, Mansoor., Shekara, Soma., Depuru, Sreenadh Reddy., Green, Robert C., Nims, Douglas.& Craig, Near. 2013. Solar Energy: Trends and enabling technologies. *Renewable and Sustainable Energy Reviews*, Volume 19, pp. 555-564.

Digi-Key, 1995. *Digi-Key*. [Online]
Available at: <http://www.digikey.com/product-search/en/fans-thermal-management/dc-fans/1179730>
[Accessed 28 october 2015].

Dincer, I. & Kanoglu, M. 2010. *Refrigeration system and applications*. 2nd ed. Channai: John wiley & Sons.

Direct, S., 1986. *SOLAR Direct*. [Online]
Available at: <http://www.solardirect.com/pv/pvlist/pvlist.htm>
[Accessed 28 October 2015].

Dossat, R. J. & Horan, T. J. 2002. *Principle of Refrigeration*. Fifth ed. New Jersey: Prentice Hall.

Duffie, J. A. & Beckman, W. A. 2006. *SOLAR ENGINEERING OF THERMAL PROCESSES*. 3rd ed. Madison: John Wiley & Sons, INC.

Duffie, J. A. & Beckman, W. A., 2013. *Solar Engineering of Thermal Processes*. 4th ed. New Jersey: John Wiley & sons.

Edenhofer. Ottmar, Pichs-Madruga. Ramon, Sokona. Youba, Seyboth. Kristin, Kadner. Susanne, Zwickel. Timm, Eickemeier. Patrick, Hansen. Gerrit, Schlömer. Steffen, Stechow. Christoph & Matschoss. Patrick. (eds). 2011. *Renewable Energy Sources and Climate Change Mitigation*. New York: Cambridge University Press.

Fang, X. & Li, D. 2013. Solar Photovoltaic and Thermal Technology and Application in China. *Renewable and Sustainable Energy Reviews*, Issue 23, pp. 330-340.

Göktun, S. & Yavuz, H. 2000. Performance of irreversible combined cycles for cryogenic refrigeration. *Energy Conversion and Management*, 41(5), pp. 449-459.

Gopala Rao, G. 2015. *Engineering for Storage of Fruits and Vegetables: Cold Storage, Controlled Atmosphere Storage, Modified Atmosphere Storage*. London: Academic Press.

Haen, H., Thomas, H., Huddleston, B. & Sharma, R. 2002. *TRADE REFORMS AND FOOD SECURITY*. [Online]
Available at: <http://www.fao.org/docrep/005/y4671e/y4671e03.htm#TopOfPage>
[Accessed 19 november 2015].

He, X. N., Gong, M. G., Zhang, H., Dai, W., Shen, J. & Wu, J. F. 2013. Design and performance of a room-temperature hybrid magnetic refrigerator combined with Stirling gas refrigeration effect. *International Journal of Refrigeration*, 36(5), pp. 1465-1471.

Heyman, D (Ed). 2007. *The world health report. A safer future: global public health security in the 21st century*. Geneva, Switzerland: WHO Press, World Health Organisation. [Online]
Available at: <http://www.who.int/whr/2007/en/>
[Accessed 4 February 2016].

Indira, V. & Sudheer, K.P. 2007. *Post Harvest Technology of Horticultural Crops*. New Delhi: New India Publishing.

Jain, V., Kachhwaha, S. S. & Sachdeva, G. 2013. Thermodynamic performance analysis of a vapor compression–absorption cascaded refrigeration system. *Energy Conversion and Management*, Issue 75, pp. 685-700.

Jones, W. P. 2011. *Air Conditioning Engineering*. Fifth ed. Abingdon: Spon press.

Kader, A. 2004. Increasing Food Availability by Reducing Postharvest Losses of Fresh Produce. *International Postharvest Symposium*, Issue 682, pp. 2169-2176.

Kanoglu, m. 2002. Exergy analysis of multistage cascade refrigeration cycle used for natural gas liquefaction. *John Wiley & Sons*, 26(8), pp. 763-774.

Kanyarusoke, K., Gryzagoridis, J. & Oliver, G. 2012. *Issues in solar tracking for sub-sahara Africa*. Stellenbosch, South Africa, Proceeding of Southern African Solar Energy Conference.

Karakurt, A. S. Gunes, M. Arda, M. & Ust, Y. 2014. *Exergetic Performance Analyses of Natural Gas Liquefaction Processes*. Turkey, ResearchGate.

Khurmi, R. S. & Gupta, J. k. 2006. *A Textbook of Refrigeration and Air Conditioning*. New Delhi: Eurasia Publishing House (P) Ltd.

Kim, D. S. & Ferreira, C. A., 2007. Solar refrigeration options - a state - of - the - art review. *International Journal of Refrigeration*, Issue 31, pp. 3-15.

Kitanovski Andrej, Jaka Tušek, Urban Tomc, Uroš Plaznik, Marko Ozbolt & Alojz Poredoš. 2014. *Magnetocaloric Energy Conversion: From Theory to Applications*. first ed. New York: Springer.

Kosmopoulos, P. et al., 2015. Solar energy prediction and verification using operational model forecasts and ground-based solar measurements. *Elsevier*, Volume 93, pp. 1918-1930.

Kreith, F. & Krumdieck, S., 2014. *PRENCIPLES OF SUSTAINABLE ENERGY SYSTEMS*. New York: Taylor & Francis Group.

Liu, J. P., Fullerton, E., Gutfleisch, O. & Sellmyer, D. J. 2010. *Nanoscale Magnetic Materials and Applications*. Second ed. New York: Springer Science & Business Media.

Loutzenhiser, P., Manz, H. Felsmann, C. Strachan, P.A., Frank, T & Maxwell, G.M. 2007. Empirical validation of models to compute solar irradiance on inclined surfaces for building energy simulation. *Solar Energy*, Issue 2, pp. 254-267.

Maehlnm, M. A. 2015. *Energy Informative*. [Online]
Available at: <http://energyinformative.org/best-solar-panel-monocrystalline->

polycrystalline-thin-film/

[Accessed 2 February 2016].

Mark, J. E. 2007. *Physical Properties of Polymers Handbook*. 2nd ed. Ohio: Springer Science & Business Media.

McDonald, B. L. 2013. *Food Security*. 3rd ed. Cambridge: John Wiley & Sons.

Mopab, M. J. & Shapiro, H. N. 2000. *Fundamentals of Engineering Thermodynamics*. 3th ed. West Sussex, England: John Wiley & Sons.

Narasimhan, V., Jiang, D. & Park, S.-Y. 2016. Design and optical analyses of an arrayed microfluidic tunable prism panel for enhancing solar energy collection. *Applied Energy*, Volume 162, pp. 450-459.

NREL, 2014. *National renewable energy laboratory*. [Online]

Available at: <http://www.nrel.gov/disclaimer.html>

[Accessed 16 february 2016].

Omni, 2009. *CMP6 Pyranometer*. [Online]

Available at: <http://www.omniinstruments.co.uk/cmp6-pyranometer.html>

[Accessed 28 April 2016].

Openelectrical, 2013. *Solar System Sizing*. [Online]

Available at: http://www.openelectrical.org/wiki/index.php?title=Solar_System_Sizing

[Accessed 15 february 2016].

Pedreschi, Romina., Lurie, Susan., Hertog, Maarten., Nicolai, Bart; Mes, Jurriaan.& Woltering, Ernst. 2013. Post-harvest proteomics and food security. *Proteomics*, Issue 13, pp. 1772-1783.

Perez, Richard., Ineichen., Pierre., Seals, Robert., Michalsky.& Stewart, Ronald. 1990. Modeling daylight availability and irradiance components from direct and global irradiance. *Solar Energy*, 44(5), pp. 271-289.

Peter Beck, M., 2008. *Thermal Conductivity of Metal Oxide Nanofluids*. USA: ProQuest.

Pimentel, D. & Peshin, R. 2014. *Integrated Pest Management: Pesticide Problems*, Vol.3. 3rd ed. London: Springer Science & Business Media.

Prasad, M. 2006. *REFRIGERATION AND AIR CONDITIONING*. Delhi: New Age international (P) Ltd.

Reddy, J. 2010. *Science and Tecnology of Photovoltaics*. Second ed. Hyderabad: BS Publication.

Rudy, S. 2000. Low temperature refrigeration. *American Society of Heating, Refrigeration and Air Conditioning Engineers, Inc.*, 42(1), p. 42.

Samlexsolar, 2004. *Samlexsolar*. [Online]

Available at: <http://www.samlexsolar.com/learning-center/solar-cell-module-array.aspx>

[Accessed 9 december 2015].

Sarbu, I. & Sebarchievici, C. 2013. Review of solar refrigeration and cooling systems. *Energy and buildings*, Volume 67, pp. 286-297.

Savary, S., Ficke, A., Aubertot, J.-N. & Hollier, C. 2012. Crop losses due to diseases and their implications for global food production losses and food security. *Springer*, Volume 4, pp. 519-537.

Scarpa, F., Tagliafico, G. & Tagliafico, L. A. 2015. A classification methodology applied to existing room temperature magnetic refrigerators up to the year 2014. *Renewable and Sustainable Energy Reviews*, Volume 50, pp. 497-503.

Schmidt, M. C. 2007. *Electric Power Research Trends*. New York: Nova Science Publishers.

Shatruk, M. *ENERGY at FSU in Chemistry & Biochemistry*. [Online]

Available at: <http://www.chem.fsu.edu/energy>

[Accessed 5 November 2015].

Silbrestein, E. 2015. *Heat Pumps*. 2nd ed. Boston: Cengage learning.

Solarcraft, 2014. *PWM vs MPPT Solar Charge Controllers*. [Online]

Available at: <http://solarcraft.net/articles/comparing-pwm-and-mppt-charge-controllers/>

[Accessed 3 February 2016].

- Sonnenenergie, D. G. f. 2013. *Planning and Installing Photovoltaic Systems: A Guide for Installer, Architects*. Second ed. London: Routledge.
- Sun, Da-W. 2012. *Handbook of Frozen Food Processing and Packaging*. 2nd ed. New York: CRC Press.
- Tefera, T. 2012. Post-harvest losses in African maize in the face of increasing food shortage. *Springer Science*, Volume 4, pp. 267-277.
- Ullah, K R. Saidur, R. Ping, H w. Akikikur, R & Shuvo, N H . 2013. A review of solar thermal refrigeration and cooling methods. *Renewable and Sustainable Energy Reviews*, Issue 24, pp. 499-513.
- Vader, R., 2014. *victronenergy*. [Online]
Available at: <https://www.victronenergy.com/upload/documents/White-paper-Which-solar-charge-controller-PWM-or-MPPT.pdf>
[Accessed 25 April 2016].
- Wang, M., Zhang, J. & Xu, Q. 2012. Optimal design and operation of a C3MR refrigeration system for natural gas liquefaction. *Computers & Chemical Engineering*, Volume 39, pp. 84-95.
- Whitman, W. C., Johnson, W. M. & Tomczyk, J. A. 2005. *Refrigeration & Air Conditioning Technology*. Fifth ed. New York: Cengage Learning.
- Whitman, B., Johnson, B., Tomczyk, J. & Silberstein, E. 2012. *Refrigeration and Air Conditioning Technology*. Seventh ed. New York: Cengage Learning.
- WHO, 2007. *Fresh fruits and vegetables*. First ed. Rome: Food & Agriculture Org.
- WHO, 2007. *THE WORLD HEALTH REPORT*. [Online]
Available at: <http://www.who.int/whr/2007/en/>
[Accessed 4 February 2016].
- Zhi, Q. X; Han, L; Dietrich, M; Gan, Z. H; Qiu, L. M; Thummes, G. 2013. A three-stage Stirling pulse tube cryocooler reached 4.26 K with He-4 working fluid. *Cryogenics*, Volume 58, pp. 93-96.

Zimm, C; Boede, A; Chell, J; Sternberg, A; Fujita, A; Fujieda, S; Fukamichi, k. 2006. Design and performance of a permanent-magnet rotary refrigerator. *International Journal of Refrigeration*, 29(8), pp. 1302-1306.

Zimm, C; Jastrab, A; Sternberg, A; Pecharsky, V; Jr, K. Gschneider; Osborne, M; Anderson, I. 1998. *Advances in Cryogenic Engineering*. New York, Plenum Press

APPENDICES

Appendix A: Technical specification of experimental applications.

Appendix A-1: 12 V DC Danfoss compressor specifications.

Code numbers

BD50F without electronic unit	101Z1220
Electronic unit 12-24V DC - standard	single: 101N0210, 30 pcs: 101N0211
Electronic unit 12-24V DC - w. metal shielding	single: 101N0220, 30 pcs: 101N0221
Electronic unit 12-24V DC - with AEO	single: 101N0300, 30 pcs: 101N0301

Application

Application	LBP/MBP/(HBP)
Evaporating temperature range °C	-30 to 0 (10)
Voltage range / max. voltage	12 - 24V DC / 31.5V DC
Max. machine compartment temperature °C	55
Comp. cooling at ambient temp. 43°C	S or F ₁ *

Design * depending on application

Displacement	cm ³	2.50
Oil quantity	cm ³	150
Maximum refrigerant charge	g	300
Free gas vol. in compressor	cm ³	870
Weight: Compressor/Electronic unit	kg	4.3/0.25

Motor

Motor type	Variable speed	
Resistance, all 3 windings (25°C)	Ω	2.0
Approvals (electronic unit)	E4 72/245 95/54 0277 00	

Dimensions

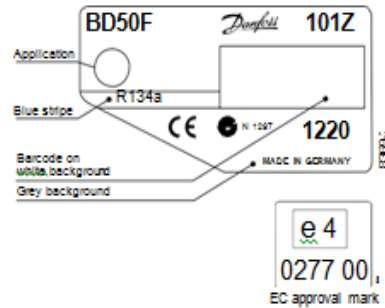
Height	mm	A	137
		B	135
		B1	128
		B2	73
Suction connector	location/I.D. mm	C	6.2 ±0.09
Process connector	location/I.D. mm	D	6.2 ±0.09
Discharge connector	location/I.D. mm	E	5.0 +0.12/+0.20
Compressors on a pallet	pcs.	150	

Standard battery protection settings (no connection C - P)

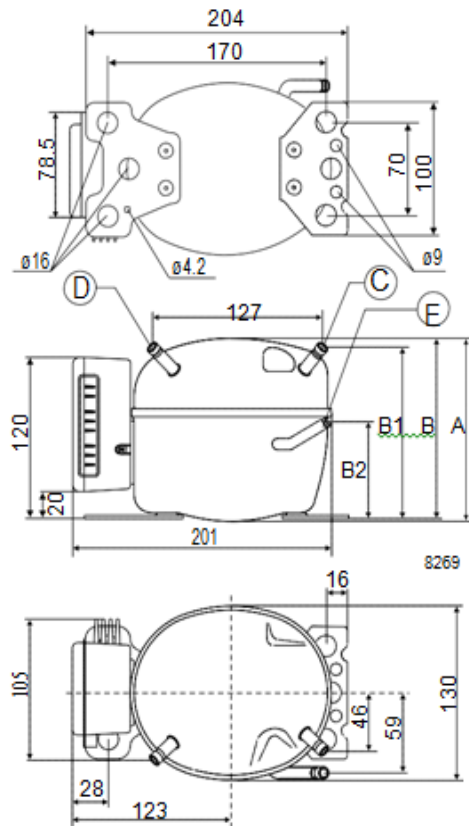
12V cut-out [V]	12V cut-in [V]	24V cut-out [V]	24V cut-in [V]
10.4	11.7	22.8	24.2

Optional battery protection settings

Resistor (R2) [kΩ]	12V cut-out [V]	12V cut-in [V]	12V max. Voltage	24V cut-out [V]	24V cut-in [V]	24V max. Voltage
0	9.6	10.9	17.0	21.3	22.7	31.5
1.6	9.7	11.0	17.0	21.5	22.9	31.5
2.4	9.9	11.1	17.0	21.8	23.2	31.5
3.6	10.0	11.3	17.0	22.0	23.4	31.5
4.7	10.1	11.4	17.0	22.3	23.7	31.5
6.2	10.2	11.5	17.0	22.5	23.9	31.5
8.2	10.4	11.7	17.0	22.8	24.2	31.5
11	10.5	11.8	17.0	23.0	24.5	31.5
14	10.6	11.9	17.0	23.3	24.7	31.5
18	10.8	12.0	17.0	23.6	25.0	31.5
24	10.9	12.2	17.0	23.8	25.2	31.5
33	11.0	12.3	17.0	24.1	25.5	31.5
47	11.1	12.4	17.0	24.3	25.7	31.5
82	11.3	12.5	17.0	24.6	26.0	31.5
220	9.6	10.9				31.5



- S = Static cooling normally sufficient
- O = Oil cooling
- F₁ = Fan cooling 1.5 m/s
(compressor compartment temperature equal to ambient temperature)
- F₂ = Fan cooling 3.0 m/s necessary



Capacity (EN 12900/CECOMAF)

rpm \ °C	-30	-25	-23.3	-20	-15	-10	-5	0	5	10
2,000	20.1	31.0	34.9	42.8	56.3	72.2	91.6	115	144*	178*
2,500	27.0	39.0	43.4	52.7	68.9	88.9	113	144*	181*	
3,000	31.0	45.4	50.6	61.5	80.7	104	134*	171*		
3,500	38.1	53.2	59.1	71.9	95.0	124*	159*			

Capacity (ASHRAE)

rpm \ °C	-30	-25	-23.3	-20	-15	-10	-5	0	5	10
2,000	24.7	38.3	43.1	52.9	69.5	89.3	113	143	178*	221*
2,500	33.3	48.1	53.6	65.0	85.1	110	140	178*	224*	
3,000	38.2	56.0	62.5	75.9	100	129	166*	212*		
3,500	47.0	65.7	72.9	88.7	117	153*	196*			

Power consumption

rpm \ °C	-30	-25	-23.3	-20	-15	-10	-5	0	5	10
2,000	25.1	31.8	34.0	38.2	44.7	51.3	58.3	65.8	74.2*	83.5*
2,500	34.1	40.5	42.9	47.8	55.8	64.7	74.3	84.8*	96.1*	
3,000	39.9	49.2	52.2	57.8	66.5	76.4	88.4*	104*		
3,500	50.2	59.3	62.5	69.0	80.2	93.4*	109*			

Current consumption (for 24V applications the following must be halved)

rpm \ °C	-30	-25	-23.3	-20	-15	-10	-5	0	5	10
2,000	2.2	2.6	2.8	3.1	3.8	4.4	5.1	5.8	6.4*	6.9*
2,500	2.9	3.4	3.6	4.0	4.7	5.4	6.2	7.0*	7.8*	
3,000	3.5	4.2	4.4	4.9	5.6	6.5	7.4*	8.5*		
3,500	4.2	4.9	5.2	5.8	6.7	7.8*	9.0*			

COP (EN 12900/CECOMAF)

rpm \ °C	-30	-25	-23.3	-20	-15	-10	-5	0	5	10
2,000	0.80	0.98	1.03	1.12	1.26	1.41	1.57	1.75	1.94*	2.13*
2,500	0.79	0.96	1.01	1.10	1.24	1.37	1.53	1.70*	1.88*	
3,000	0.78	0.92	0.97	1.06	1.21	1.37	1.51*	1.65*		
3,500	0.76	0.90	0.95	1.04	1.19	1.32*	1.45*			

COP (ASHRAE)

rpm \ °C	-30	-25	-23.3	-20	-15	-10	-5	0	5	10
2,000	0.99	1.21	1.27	1.38	1.56	1.74	1.94	2.16	2.40*	2.65*
2,500	0.98	1.19	1.25	1.36	1.53	1.70	1.89	2.10*	2.33*	
3,000	0.96	1.14	1.20	1.31	1.50	1.69	1.87*	2.04*		
3,500	0.94	1.11	1.17	1.28	1.46	1.64*	1.80*			

Test conditions EN 12900/CECOMAF
 ASHRAE Condensing temperature 55°C 55°C
 Ambient and suction gas temp. 32°C 32°C
 Liquid temperature 55°C 32°C
 Static cooling, 12V DC
 * Fan cooling of electronic unit compulsory
 1 Watt = 0.86 kcal/h

Compressor speed

Electronic unit	Resistor (R1) Ω	Motor speed rpm	Contr. circ. current mA
101N0210 101N0220	0	2,000	5
	277	2,500	4
	692	3,000	3
	1523	3,500	2
101N0300 with AEO	0	AEO	6
	173	2,000	5
	450	2,500	4
	865	3,000	3
	1696	3,500	2

In AEO (Adaptive Energy Optimizing) speed mode the BD compressor will always adapt its speed to the actual cooling demand.

Wire dimensions

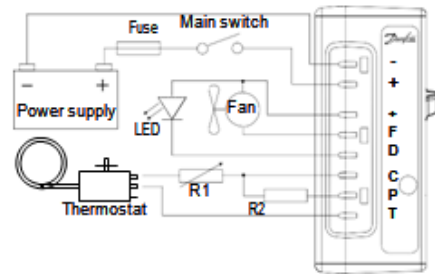
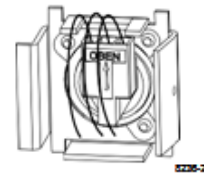
Cross section mm²	Max length* m 12V operation	Max length* m 24V operation
2.5	2.5	5
4	4	8
6	6	12
10	10	20

*Length between battery and electronic unit

Accessories

Devices	BD50F
Standard automobile fuse DIN 7258 12V: 15A 24V: 7.5A	Not deliverable from Danfoss
Mounting accessories	
Bolt joint for one compressor	118-1917
Bolt joint in quantities	118-1918
Snap on in quantities	118-1919

Terminal plug



Operational errors shown by LED (optional)

Number of flashes	Error type
5	Thermal cut-out of electronic unit (If the refrigeration system has been too heavily loaded, or if the ambient temperature is high, the electronic unit will run too hot).
4	Minimum motor speed error (If the refrigeration system is too heavily loaded, the motor cannot maintain minimum speed at approximately 1,850 rpm).
3	Motor start error (The rotor is blocked or the differential pressure in the refrigeration system is too high (>5 bar)).
2	Fan over-current cut-out (The fan loads the electronic unit with more than 1A _{max}).
1	Battery protection cut-out (The voltage is outside the cut-out setting).

Appendix A-2: Deep cycle solar battery specification.

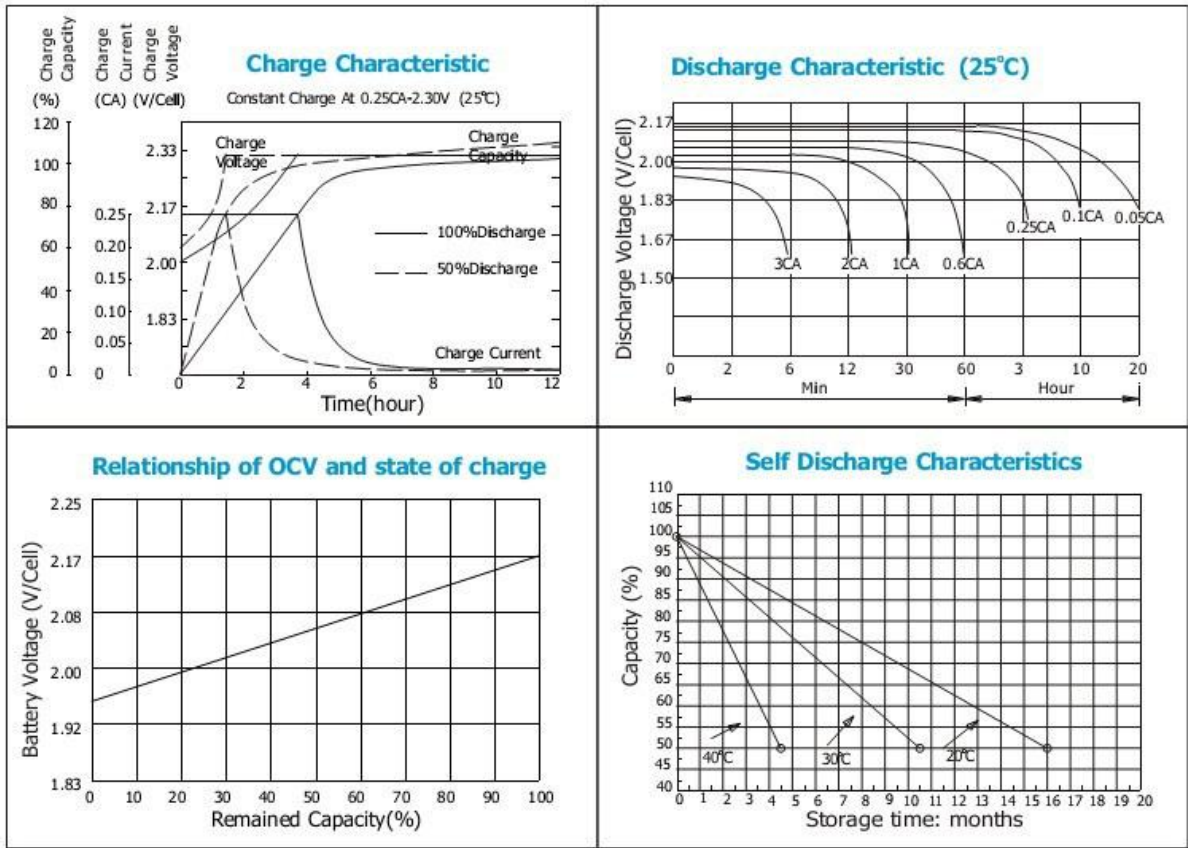
Battery Model			Maximus 105
Nominal Voltage			12V
Nominal Capacity (20Hr)			105Ah
Nominal Capacity (5Hr)			85Ah
Reserve Capacity (Min)			170
CCA (-18°C) A / IEC	490		A
Operating Temperature (°C)			[-40°C to +50°C]
Dimensions ± 0.5mm	Length		332mm
	Width		171mm
	Height		220mm
	Total Height		230mm
Cell Layout and Type	1		
Terminals	C		
Approx. Weight	Wet Charged		24.5Kgs

Constant current discharge ratings-amperes at 25°C


F. V/Time	5 MIN	10 MIN	15 MIN	30 MIN	1 HR	3 HR	5 HR	10 HR	20 HR
1. 60V	350	240	175	105	66.0	27.3	19.1	10.6	5.27
1. 67V	315	219	170	102	65.9	27.2	18.9	10.4	5.25
1. 70V	299	211	164	100	65.7	27.2	18.9	10.4	5.25
1. 75V	266	195	155	98.0	65.0	27.0	18.8	10.2	5.23
1. 80V	240	181	148	95.0	64.2	26.9	18.6	10.0	5.04
1. 85V	182	149	128	87.4	63.5	26.8	18.5	9.83	4.74

Constant power discharge ratings-watts at 25°C

F. V/Time	5 MIN	10 MIN	15 MIN	30 MIN	1 HR	3 HR	5 HR	10 HR	20 HR
1. 60V	577	398	310	198	130	52.4	36.5	21.2	10.5
1. 67V	547	393	307	194	126	52.4	36.5	20.9	10.5
1. 70V	511	383	302	189	122	52.4	36.5	20.7	10.5
1. 75V	476	358	284	184	121	51.6	36.1	20.4	10.5
1. 80V	427	333	267	179	119	50.9	35.5	20.0	10.1
1. 85V	342	276	233	164	118	50.7	35.0	19.7	9.48



Appendix A-4: T-type thermocouple quality inspection certificate

	7 Vuurelag Avenue Spartan Est 7, Kempton Park 1619 T: 011 986 9800 F: 011 392 5235	Temperature Sensor Quality Inspection Certificate
	47 Flamingo Crescent, Lansdown, Cape Town, 7779 T: 021 7628995 F: 021 762 8996	

Temperature Sensor - Quality Inspection Certificate

Customer: CPUT

Job Number: C317883 A

Drawing/Part No: STY 020441

Date of Inspection: 2/4/15

Sampling Table		
Order Quantity		Quantity to inspect
From	To	
1	3	All (100%)
5	10	3 off
10	50	6 off
50	100	10 off
100 +	100	15 off

	NOMINAL	ACTUAL
Sensor type, class:	T	
Stem Length L1, L2 (min):	L1: L2:	L1: L2:
Stem Diameter D1, D2 (mm):	D1: D2:	D1: D2:
Termination Type:		
Mounting Type:		
Cable Option:	Teflon	
Cable Length:	200m	200m
Grounded or Ungrounded:	E	


Sensor Accuracy Inspection					
Sample No.	Tolerance Spec. #	Calibrator Temp.	Sample Temp.	Variance	Accepted?
1	-20.13 TS.13	98.51	99.09	-0.58	✓
2	"	98.49	98.63	-0.14	✓
3	"	98.50	97.8	0.7	✓
4	"	98.47	97.9	0.57	✓
5	"	98.51	99.15	-0.64	✓

- | | | | | |
|---|---|-----|---|----|
| 1. Are all weld seams in a good condition? | ✓ | YES | | NO |
| 2. Are there any mechanical defects on the sensor? | | YES | ✓ | NO |
| 3. Is the colour coding & polarity according to Sensor Ref. chart (U-IMS-MFR-DF-007)? | ✓ | YES | | NO |
| 4. Have the label details been checked and are they acceptable? | ✓ | YES | | NO |
| 5. Do the sensor response times correspond with the Tolerance Reference Chart* ? | | YES | | NO |
| 6. Is the insulation of ungrounded sensors higher than 1000mΩ at 100V ? | | YES | | NO |
| 7. Is the jobcard and drawing (if applicable) updated and correct? | ✓ | YES | | NO |

* Refers to Tolerance Reference Chart- Sensors U-IMS-MFR-D-003 Rev 03

Remarks

The above sensors were found: Acceptable Rejected

QA Inspector: Jan Signed:  Date: 2/4/15

Appendix A-5: Testo 926 digital thermometer certificate of conformity and digital technical data

		<p>Kalibrier-Protokoll Certificate of conformity • Protocole d'étalonnage Protocollo di collaudo • Informe de calibración</p>
<p>Gerät / Module type / Modèle / Modelo:</p>		<p>testo 926</p>
<p>Meßbereich / Measuring range / Etendue de mesure / Rango de medición:</p>		<p>-50...+400°C</p>
<p>Serien-Nr. / Serial no. / No. de série / Número de serie:</p>		<p>33835720</p>
<p>Segmenttest / Display test / Test d'affichage / Test del visualizador:</p>		<p><input checked="" type="checkbox"/> OK</p>
<p>Meßwerte / Measured values / Valeurs mesurées / Valores medidos:</p>		
<p>Sollwert / Reference / Référence / Referencia:</p>		<p>Istwert / Actual Value / Valeur réelle / Valor medido:</p>
<p>+80.0 °C</p>		<p>+79.9 °C</p>
<p><i>J. Yeung</i></p>		
<p>Prüfer / Inspector / Responsable / Verificador</p>		

9. Technical data

Characteristic	Value
Parameters	Temperature (°C/°F / °R)
Measuring range	-50.0...+400°C / -58.0...+752.0°F / -40.0...+320°R
Resolution	0.1°C / 0.1°F / 0.1°R (-50.0...+199.9°C / -58.0...+391.8°F / -40.0...+159.9°R) 1°C / 1°F / 1°R (rest of range)
Accuracy (± 1 Digit)	±0.3°C / ±0.6°F / ±0.2°R (-20.0...+70.0°C / -4.0...+158.0°F / -16.0...+56.0°R) ±0.7°C+0,5% o.r. / ±1.3°F+0,5% o.r. / ±0.6°R + 0,5% o.r. (rest of range)
Probe connections	1x Omega TC socket for temperature probe type T (Cu-CuNi), radio module (accessory part)
Measuring rate	2/s
Operating temperature range	-20 ... +50°C / -4 ... +122°F / -16 ... +40°R
Storage temperature	-40 ... +70°C / -40 ... +158°F / -32 ... +56°R
Voltage supply	1x 9 V monobloc battery/rech. battery
Running time (display lighting off / on)	with probe connected: approx. 200h / approx. 68h, with radio probe: approx. 45h / 33h
Protection class	with TopSafe (accessory part) and probe connected: IP65
EC Directive	2004/108/EC
Warranty	2 years, warranty conditions: see www.testo.com/warranty

With TopSafe and the following probes, this product complies with guidelines in accordance with the EN 13485 standard:

Part no.	Measuring range
0613 1001	-50...+275°C / -58.0...+527°F
0603 1293	-50...+350°C / -58.0...+662°F
0603 1793	-50...+350°C / -58.0...+662°F
0603 2192	-50...+350°C / -58.0...+662°F
0603 2492	-50...+350°C / -58.0...+662°F
0603 3292	-50...+350°C / -58.0...+662°F

Suitability: S, T (storage, transport)
Environment: E (transportable thermometer)
Accuracy class: 0.5
Measurement range: see table above

According to EN 13485, the measuring instruments should be checked and calibrated regularly under the terms of EN 13486 (Recommended: Yearly).
Contact us for more information: www.testo.com

Appendix B: Technical specification of experimental instrumentation.

Appendix B-1: Kipp & Zonen CMP06 pyranometer specification. Adapted from (Omni, 2009)

Specifications	CMP 3	CMP 6	CMP10 & CMP 11	CMP 21	CMP 22
Classification to ISO 9060:1990	Second Class	First Class	Secondary Standard	Secondary Standard	Secondary Standard
Spectral range (50 % points)	300 to 2800 nm	285 to 2800 nm	285 to 2800 nm	285 to 2800 nm	200 to 3600 nm
Sensitivity	5 to 20 $\mu\text{V}/\text{W}/\text{m}^2$	5 to 20 $\mu\text{V}/\text{W}/\text{m}^2$	7 to 14 $\mu\text{V}/\text{W}/\text{m}^2$	7 to 14 $\mu\text{V}/\text{W}/\text{m}^2$	7 to 14 $\mu\text{V}/\text{W}/\text{m}^2$
Impedance	20 to 200 Ω	20 to 200 Ω	10 to 100 Ω	10 to 100 Ω	10 to 100 Ω
Expected output range (0 to 1500 W/m^2)	0 to 30 mV	0 to 30 mV	0 to 20 mV	0 to 20 mV	0 to 20 mV
Maximum operational irradiance	2000 W/m^2	2000 W/m^2	4000 W/m^2	4000 W/m^2	4000 W/m^2
Response time (63 %)	< 6 s	< 6 s	< 1.7 s	< 1.7 s	< 1.7 s
Response time (95 %)	< 18 s	< 18 s	< 5 s	< 5 s	< 5 s
Zero offsets					
(a) thermal radiation (at 200 W/m^2)	< 15 W/m^2	< 12 W/m^2	< 7 W/m^2	< 7 W/m^2	< 3 W/m^2
(b) temperature change (5 K/h)	< 5 W/m^2	< 4 W/m^2	< 2 W/m^2	< 2 W/m^2	< 1 W/m^2
Non-stability (change/year)	< 1%	< 1%	< 0.5%	< 0.5%	< 0.5%
Non-linearity (100 to 1000 W/m^2)	< 1.5%	< 1%	< 0.2%	< 0.2%	< 0.2%
Directional response (up to 80° with 1000 W/m^2 beam)	< 20 W/m^2	< 20 W/m^2	< 10 W/m^2	< 10 W/m^2	< 5 W/m^2
Spectral selectivity (350 to 1500 nm)	< 3%	< 3%	< 3%	< 3%	< 3%
Temperature response	< 5% (-10°C to +40°C)	< 4% (-10°C to +40°C)	< 1% (-10°C to +40°C)	< 1% (-20°C to +50°C)	< 0.5% (-20°C to +50°C)
Tilt response (0° to 90° at 1000 W/m^2)	< 1%	< 1%	< 0.2%	< 0.2%	< 0.2%
Field of view	180°	180°	180°	180°	180°
Accuracy of bubble level	< 0.2°	< 0.1°	< 0.1°	< 0.1°	< 0.1°
Temperature sensor output				10K Thermistor (optional Pt-100)	10K Thermistor (optional Pt-100)
Detector type	Thermopile	Thermopile	Thermopile	Thermopile	Thermopile
Operational temperature range	-40°C to +80°C	-40°C to +80°C	-40°C to +80°C	-40°C to +80°C	-40°C to +80°C
Storage temperature range	-40°C to +80°C	-40°C to +80°C	-40°C to +80°C	-40°C to +80°C	-40°C to +80°C
Humidity range	0 to 100% non-condensing	0 to 100% non-condensing	0 to 100% non-condensing	0 to 100% non-condensing	0 to 100% non-condensing
Ingress Protection (IP) rating	67	67	67	67	67
Recommended applications	Economical solution for routine measurements in weather stations, field testing	Good quality measurements for hydrology networks, greenhouse climate control	Meteorological networks, PV panel and thermal collector testing, materials testing	Meteorological networks, reference measurements in extreme climates, polar or arid	Scientific research requiring the highest level of measurement accuracy and reliability

Appendix B-2: SP-LITE silicon pyranometer specification. Adapted from (campbell, 2015)

SP-LITE Silicon Pyranometer

2. Sensor Specifications

Electrical

Nominal Impedance:	<50 Ω
Response Time:	<1 second
Sensitivity:	10 $\mu\text{V}/(\text{W m}^{-2})$
Expected signal range: (under atmospheric conditions)	0 – 15 mV
Stability:	<±2% per year
Non-linearity:	<±1% up to 1000 W m^{-2}
Temperature dependence of sensitivity:	<±0.15% /°C

Spectral

Spectral range:	400 to 1100 nm
Detector type:	BPW 34

Directional

Cosine corrected between 80° angle of incidence, error:	within ±10%
Cosine errors averaged over opposite azimuth error (at 60° angle of incidence):	within ±10%
Tilt response:	zero error

Mechanical

Housing material:	Anodized aluminum
Cable material:	Polyurethane
Weight:	110 g
Cable length:	5 m (can be extended up to 100 m)
Physical Dimensions:	See Figure 5

Environmental

Working temperature:	-30 to +70°C
----------------------	--------------

Dimensions



DIMENSIONS IN MM

FIGURE 5. Dimensions of SP-LITE with Leveling Device

Appendix B-3: 03101 R.M Young three cup anemometer. Adapted from (campbell, 2015).

Range:	0 to 50 m s ⁻¹ (112 mph), gust survival 60 m s ⁻¹ (134 mph)
Sensor:	12 cm diameter cup wheel assembly, 40 mm diameter hemispherical cups
Accuracy:	±0.5 m s ⁻¹ (1.1 mph)
Turning Factor:	75 cm (2.5 ft)
Distance Constant (63% recovery):	2.3 m (7.5 ft)
Threshold:	0.5 m s ⁻¹ (1.1 mph)
Transducer:	Stationary coil, 1300 ohm nominal resistance
Output:	AC sine wave signal induced by rotating magnet on cup wheel shaft 100 mV peak-to-peak at 60 rpm; 6 V peak-to-peak at 3600 rpm
Output Frequency:	1 cycle per cup wheel revolution; 0.75 m s ⁻¹ per Hz
Cup Wheel Diameter:	12 cm (4.7 in)
Weight:	113 g (4 oz)

Appendix C-1: Brightness coefficient for Perez Anisotropic Sky

ε	f_{11}	f_{12}	f_{13}	f_{21}	f_{22}	f_{23}
1-1.065	-0.008	0.588	-0.062	-0.06	0.072	-0.022
1.065-1.23	0.130	0.683	-0.151	-0.019	0.066	-0.029
1.23-1.5	0.330	0.487	-0.221	0.055	-0.064	-0.026
1.5-1.95	0.568	0.187	-0.295	0.109	-0.152	0.014
1.95-2.8	0.873	-0.392	-0.221	0.226	-0.462	0.001
2.8-4.5	1.132	-1.237	-0.412	0.288	-0.823	0.056
4.5-6.2	1.060	-1.6	-0.359	0.264	-1.127	0.131
6.2-∞	0.678	-0.327	-0.250	0.156	-1.377	0.251

Adapted from (Perez et al., 1990)

Appendix D: The weather condition

Table D-1: The measured data on 11 April 2016

Local Time	Solar radiation (total horizontal) I_h [W/m ²]	Solar radiation (diffuse) I_d [W/m ²]	Air temperature [°C]	Wind speed [m/s]
8:00	107.1	90.5	16.22	0.029
8:15	154.7	77.95	17.02	0.032
8:30	205.7	45.73	18.26	0.254
8:45	159.3	44.76	17.54	0.803
9:00	108.7	27.77	16.5	0.774
9:15	118.9	31.11	16.57	0.397
9:30	140.8	36.64	17.05	0.674
9:45	158	41.36	17.57	0.139
10:00	152.7	40.71	17.37	0.467
10:15	256.1	70.27	18.76	0.207
10:30	459.5	65	20.97	0.265
10:45	567.9	38.58	23.68	0.042
11:00	615.8	35.54	26.36	0.072
11:15	631.1	33.52	25.92	0.011
11:30	669.8	32.55	26.87	0.101
11:45	695.3	32.37	27.42	0.333
12:00	714.5	32.76	26.92	0.173
12:15	734.2	32.85	24.93	0.637
12:30	746.2	32.82	25.02	0.585
12:45	756.8	32.62	25.04	0.911
13:00	757.8	31.92	26.86	0.606
13:15	761.3	32.05	27.01	2.13
13:30	759.3	32.89	27.14	2.571
13:45	751.9	33.69	27.31	2.506
14:00	736.8	34.56	27.8	2.564
14:15	718.5	34.76	28.11	2.462
14:30	693.8	34.76	28.86	1.684
14:45	665.8	34.2	28.74	2.002
15:00	637	33.35	28.41	2.352
15:15	602.7	32.24	27.33	2.045
15:30	565.1	31.01	26.95	1.767
15:45	524	29.88	26.48	2.287
16:00	477	28.79	25.64	1.979
16:15	421.1	27.62	25.31	1.772
16:30	365.9	26.06	25.2	1.377
16:45	323.6	24.16	25.06	1.862
17:00	275.4	20.17	25.86	1.433

Table D-2: The measured data on 12 April 2016

Local Time	Solar radiation (total horizontal) I_h [W/m ²]	Solar radiation (diffuse) I_d [W/m ²]	Air temperature [°C]	Wind speed [m/s]
8:00	35.91	9.16	16	0
8:15	59.64	17.25	16.31	0.053
8:30	86.6	24.48	16.46	0.147
8:45	170.6	49.24	17.04	0.116
9:00	285.2	60.92	19.3	0.029
9:15	351.7	32.92	22.32	0
9:30	396.2	29	24.15	0
9:45	443.5	27.62	26.71	0.072
10:00	487.9	27.05	27.88	0.341
10:15	527.7	27.13	28.8	0.124
10:30	561.4	28	29.68	0.192
10:45	597.6	28.91	30	0.353
11:00	621.1	29.24	29.77	0.677
11:15	650.4	29.32	29.77	1.022
11:30	689.8	30.09	31.46	1.086
11:45	708.3	32.27	30.87	1.368
12:00	701.9	31.53	30.26	1.482
12:15	744	31.86	28.65	1.471
12:30	752.6	31.86	28.66	2.154
12:45	759.8	31.86	28.79	1.958
13:00	759	31.85	29.29	1.572
13:15	756	32.41	29.52	1.994
13:30	749	33.23	29.09	2.299
13:45	737.6	34.01	28.86	2.149
14:00	721.1	34.71	28.93	2.024
14:15	703.8	35.21	28.84	2.112
14:30	682	34.97	28.71	2.398
14:45	653.3	34.36	28.51	2.199
15:00	621.2	33.43	28.83	1.597
15:15	585.8	32.28	27.44	1.841
15:30	547.1	30.87	26.23	2.462
15:45	506.9	29.71	25.69	2.199
16:00	465.1	28.44	25.08	1.91
16:15	419.6	26.65	24.09	2.537
16:30	371.6	24.67	23.49	2.833
16:45	321.2	22.39	22.96	2.396
17:00	269.5	19.35	23.87	2.418

Table D-3: The measured data on 13 April 2016

Local Time	Solar radiation (total horizontal) I_h [W/m ²]	Solar radiation (diffuse) I_d [W/m ²]	Air temperature [°C]	Wind speed [m/s]
8:00	44.38	11.67	13.77	0.021
8:15	59.31	15.72	13.88	0.032
8:30	68.82	17.28	14.21	0
8:45	78.23	19	14.73	0.093
9:00	102.9	25.12	14.8	1.1
9:15	124.7	31.57	14.84	0.814
9:30	132.4	33.9	15.3	0.346
9:45	146.9	37.88	15.84	0.596
10:00	188.7	48.7	16.69	0.513
10:15	259.8	67.05	17.91	0.32
10:30	317.2	79.79	18.98	0.272
10:45	455.8	88	21.28	0.309
11:00	565.5	40.84	22.94	0.261
11:15	649.3	30.16	24.46	0.042
11:30	674	30.34	26.43	0.011
11:45	688.1	30.94	27.17	0
12:00	710.2	31.66	27.63	0
12:15	720.1	31.98	24.47	0.021
12:30	724.8	32.33	24.76	0.626
12:45	734.9	32.3	25.19	0.498
13:00	735.7	32.77	25.83	0.586
13:15	730	34.13	26.12	0.559
13:30	696.5	34.28	26.42	0.887
13:45	698.8	35.89	27.01	1.072
14:00	681.7	36.71	27.11	2.01
14:15	670.2	38.28	26.98	2.063
14:30	645.3	38.97	26.75	1.674
14:45	625.9	39.33	26.7	1.287
15:00	596.4	37.44	26.52	1.156
15:15	566	34.66	25.7	2.128
15:30	527.7	33.44	25.69	2.21
15:45	475.4	32.29	26.69	0.798
16:00	446.1	32.61	25.81	1.784
16:15	316.1	28.12	25.28	2.172
16:30	270	26.9	25.35	1.321
16:45	237.8	24.31	24.49	1.731
17:00	189.7	22.09	24.48	1.5

Table D-4: The measured data on 14 April 2016

Local Time	Solar radiation (total horizontal) I_h [W/m ²]	Solar radiation (diffuse) I_d [W/m ²]	Air temperature [°C]	Wind speed [m/s]
8:00	43.02	14.37	14.42	0
8:15	125.3	46.11	16.27	0
8:30	182	38.97	17.84	0
8:45	238.7	39.36	19.4	0
9:00	241.2	46.49	19.76	0.072
9:15	243.5	36.31	21.36	0
9:30	370.4	45.23	21.94	0
9:45	333.2	56.41	22.1	0.568
10:00	403.9	36.11	20.6	1.569
10:15	550.1	63.92	22.93	1.561
10:30	303.3	62.9	20.21	1.787
10:45	232.9	37.18	17.94	3.421
11:00	526	38.08	19.76	1.879
11:15	691.1	39.69	22.25	1.876
11:30	529.2	66.33	22.14	2.366
11:45	133.6	32.66	19.36	3.393
12:00	670.7	44.49	20.16	3.371
12:15	754	44.83	20.46	3.371
12:30	575.5	44.06	20.73	3.196
12:45	444	60.41	20.32	2.808
13:00	269.2	38.84	20.12	3.658
13:15	502.1	59.95	20.67	3.533
13:30	442.3	78.34	21.24	3.021
13:45	197.7	58.22	19.83	4.056
14:00	296.2	65.36	19.79	4.042
14:15	419.4	80.6	19.31	4.125
14:30	230.6	59.54	19.1	3.514
14:45	149.7	41.5	18.68	3.298
15:00	195.1	40.68	18.68	3.097
15:15	245.3	46.66	18.91	2.631
15:30	258.4	50.56	19.42	1.527
15:45	324.1	48.06	19.77	2.241
16:00	238	51.94	19.7	1.801
16:15	157.4	38.8	19.11	2.347
16:30	104.7	21.97	18.12	3.827
16:45	67.32	17.93	16.94	3.285
17:00	125	28.47	17.52	2.249

Table D-5: The measured data on 15 April 2016

Local Time	Solar radiation (total horizontal) I_h [W/m ²]	Solar radiation (diffuse) I_d [W/m ²]	Air temperature [°C]	Wind speed [m/s]
9:00	119	31.54	15.41	1.18
9:15	142.5	38.18	15.7	1.496
9:30	179.5	47.6	16.08	1.214
9:45	204.6	54.77	17.08	1.114
10:00	280.5	67.64	17.78	1.451
10:15	344.8	74.11	18.89	1.527
10:30	524.1	49.48	19.67	1.447
10:45	593.9	28.39	20.12	1.304
11:00	631.2	26.11	20.53	1.738
11:15	656.6	25.59	21.52	1.943
11:30	674.9	25.6	22.23	2.118
11:45	688.6	26.23	24.18	1.618
12:00	703.7	26.57	26.19	1.756
12:15	716.4	26.53	29.25	1.728
12:30	723.9	26.7	30.48	1.849
12:45	719	26.76	29.68	2.116
13:00	725.2	26.99	30.6	1.781
13:15	725.8	28.01	31.59	1.513
13:30	718.2	29.05	31.01	1.417
13:45	706.6	29.89	29.48	1.279
14:00	691	30.42	26.7	1.115
14:15	672.2	30.55	25.99	1.515
14:30	654.2	30.94	25.53	2.07
14:45	628.3	31.38	25.67	1.977
15:00	597.5	31.86	25.48	2.312
15:15	565.7	30.89	25.02	2.748
15:30	533	29.72	24.71	2.374
15:45	499.9	27.64	24.19	2.625
16:00	460.4	25.7	23.58	2.648
16:15	414.2	23.67	23.19	2.739
16:30	367	21.85	22.76	2.837
16:45	316.1	20	22.37	2.433
17:00	263.5	17.93	21.99	2.435

Table D-6: The measured data on 18 April 2016

Local Time	Solar radiation (total horizontal) I_h [W/m ²]	Solar radiation (diffuse) I_d [W/m ²]	Solar radiation on 30° PV panel [W/m ²]	Air temperature [°C]	Wind speed [m/s]
8:00	94	47.97	136.11	18.53	0.367
8:15	126.9	29.05		20.88	0.042
8:30	170.3	21.62		23.37	0.228
8:45	220.9	20.32		25.15	0.158
9:00	265.1	21.12	437.55	25.24	0.291
9:15	315.2	21.06		24.94	0.672
9:30	361.9	21.26		28.51	0.776
9:45	409.9	21.45		26.4	1.756
10:00	453.7	21.56	660.42	23.63	1.462
10:15	494.8	22.12		23.89	1.346
10:30	530.8	22.5		24.73	1.076
10:45	564.9	23.18		25.35	1.123
11:00	593.8	23.78	831.85	25.68	1.263
11:15	618.1	24.16		26.64	1.251
11:30	644.6	24.36		27.47	1.356
11:45	663.8	25.07		29.11	1.166
12:00	677.5	25.43	1022.22	31.57	1.321
12:15	682.8	25.94		35.16	1.181
12:30	690.2	26.27		35.08	1.645
12:45	694.8	26.07		35.75	1.432
13:00	691.4	26.78	945.17	35.89	1.467
13:15	685.5	27.37		35.69	1.68
13:30	681.2	28.24		34.49	2.012
13:45	672.1	28.8		32.04	2.256
14:00	657.4	28.96	900.36	29.97	2.246
14:15	644.4	29.16		29.94	1.747
14:30	621.9	29.48		30.41	1.328
14:45	603.9	30.35		30.51	1.526
15:00	558.4	32.76	773.32	30.26	1.551
15:15	496.5	26.85		30.16	1.846
15:30	530.3	34.37		29.93	2.55
15:45	461.1	27.26		29.28	2.249
16:00	417.8	23.91	595.21	28.18	2.3
16:15	376	22.35		27.82	2.206
16:30	330.9	20.78		27.47	1.966
16:45	283.4	19.22		27.1	2.064
17:00	234.1	17.58	354.8	26.87	1.877

Table D-7: The measured data on 19 April 2016

Local Time	Solar radiation (total horizontal) I_h [W/m ²]	Solar radiation (diffuse) I_d [W/m ²]	Solar radiation on 30° PV panel [W/m ²]	Air temperature [°C]	Wind speed [m/s]
8:00	46.78	12.04	118.7	16.8	0.757
8:15	79.53	20.67		17.15	1.041
8:30	82.7	21.34		17.84	1.432
8:45	86.2	22.27		17.82	1.964
9:00	71.74	17.99	111.7	17.44	2.864
9:15	129.4	33.92		17.61	3.292
9:30	90.6	22.86		17.62	3.933
9:45	82.7	20.74		17.58	2.673
10:00	80.1	20.18	117.42	18.17	2.193
10:15	89.3	22.38		18.62	2.329
10:30	125.7	32.34		19.12	2.706
10:45	201.3	50.25		20.16	2.692
11:00	186.6	42.36	263.18	20.26	3.4
11:15	183.3	44.35		20.16	2.289
11:30	390.5	68.62		21.96	2.229
11:45	483.2	72.21		24.14	2.464
12:00	350.2	66.63	466.55	23.65	2.142
12:15	626.8	53.35		27.4	1.519
12:30	641.1	37.99		30.69	0.942
12:45	621.5	31.54		31.06	0.923
13:00	667.1	31.17	915.14	33.86	0.617
13:15	671.5	30.59		34.78	0.916
13:30	663.8	30.59		35.5	0.691
13:45	662	30.59		32.14	1.884
14:00	651.1	31.46	917.77	30.02	1.73
14:15	611.3	31.01		30.2	1.194
14:30	605.3	33.07		30.64	1.707
14:45	523.5	30.31		30.76	2.057
15:00	556	37.68	773.86	28.74	3.116
15:15	515.3	33.84		25.18	3.633
15:30	483	31.98		23.81	4.05
15:45	442.4	30.39		23.53	4.008
16:00	400.6	28.5	573.79	22.97	4.117
16:15	350.2	26.19		22.66	3.142
16:30	300.7	24		22.67	2.414
16:45	254.2	22.08		22.3	2.592
17:00	207	20.15	317.03	21.94	1.82

Table D-8: The measured data on 20 April 2016

Local Time	Solar radiation (total horizontal) I_h [W/m ²]	Solar radiation (diffuse) I_d [W/m ²]	Solar radiation on 30° PV panel [W/m ²]	Air temperature [°C]	Wind speed [m/s]
8:00	75.84	33.71	213.9	20.2	0.175
8:15	113	26.95		21.11	1.279
8:30	143.7	22.74		21.46	1.099
8:45	197.4	23.22		23.7	0.702
9:00	243.8	24.34	402.76	23.81	1.302
9:15	289.2	25.13		24.34	1.386
9:30	333.8	25.38		26.96	1.579
9:45	383.8	24.63		25.02	2.492
10:00	423.4	24.62	625.58	23.97	1.53
10:15	459.7	24.82		25.2	1.283
10:30	504.8	24.73		25.92	1.378
10:45	539	24.91		26.66	2.185
11:00	571.4	25.56	818.83	27.09	1.633
11:15	598.7	26.26		26.84	2.687
11:30	618.4	27.27		26.94	2.378
11:45	608.4	28.39		26.86	3.062
12:00	419.6	38.04	580.46	24.88	4.008
12:15	502.5	48.72		23.15	4.392
12:30	644.3	47.53		23.86	4.383
12:45	639.5	40.48		22.77	6.292
13:00	598.5	44.11	823.7	21.87	5.35
13:15	591.2	38.04		22.32	4.658
13:30	635.2	34.48		22.46	4.4
13:45	591.6	32.97		21.15	4.5
14:00	646.3	40.95	891.88	20.06	5.367
14:15	472.7	36.95		20.03	5.3
14:30	424.6	36.97		19.3	4.767
14:45	267.2	35.56		19.37	5.333
15:00	257.4	41.9	361.74	19.95	5.167
15:15	430.4	40.21		20.52	5.275
15:30	275.6	30.08		20.54	5.608
15:45	171.4	36.17		20.42	5.158
16:00	141.8	27.49	205.49	20.12	4.133
16:15	112.9	26.49		19.86	4.408
16:30	125.1	33.17		20.09	4.375
16:45	162.8	32.44		20.38	4.258
17:00	188.2	28.39	288.6	20.83	4.45

Appendix E: Measured data from cooling system

Table E-1: Measured data on 11 April 2016 (empty cooling space)

Time	T _{lin}	T _{rin}	T _{din}	T _{in}	T _{ein}	T _{eout}	T _{lou} t	T _{rout}	T _{dout}	T _{bout}	T _{up}	T _{cin}	T _{cout}
8:00	17.2	17.4	18.8	18.0	-9.1	12.4	19.5	17.4	19.6	17.1	17.2	20.6	19.1
9:00	7.6	8.2	9.0	7.5	-3	5.4	18.9	17.5	19.8	19	18.3	26.6	20.6
10:00	4.9	4.7	6.1	4.5	-3.9	3.2	22	18.5	20	20.3	21.1	29.9	21
11:00	4.5	4.4	5.8	4.2	-7.1	1.2	25.3	18.6	20.7	27	28.3	32.5	24.8
12:00	4.8	4.3	5.1	4.1	-0.4	3.0	38	25.9	26.1	30	33.7	33.7	29.1
13:00	4.5	4.8	5.3	4.4	-3.1	2.6	38.3	25	29.1	31	28.4	31.9	27.2
14:00	5.8	5.9	6.1	5.2	-3.4	2.2	38.8	26.3	30	35.6	29.1	38.9	31.1
15:00	6.2	6.5	6.8	5.8	-1.3	3.1	34	28.1	31.4	35.5	22.5	33	24.8
16:00	5.4	5.2	5.9	4.6	-3.6	2.3	27.4	26.1	27.2	26.9	22.4	30	23.4
17:00	5.0	5.1	5.8	4.5	-5.2	0.9	23.7	21	22.2	22.6	22.1	33.1	28.3

Table E-2: Measured data on 12 April 2016 (empty cooling space)

Time	T _{lin}	T _{rin}	T _{din}	T _{in}	T _{ein}	T _{eout}	T _{lou} t	T _{rout}	T _{dout}	T _{bout}	T _{up}	T _{cin}	T _{cout}
8:00	7.2	6.8	7.9	6.2	0.9	5.0	22.2	20.8	18.2	27.2	21.5	32.7	24.2
9:00	8.2	8.0	9.0	7.2	-4.5	4.7	29.7	21.2	20.7	29.7	25.3	30.2	26.3
10:00	6.4	6.2	7.2	5.7	-3.9	2.3	30	22.0	21	28.2	28.7	38	26.6
11:00	6.5	6.3	6.8	6.0	-2.2	2.5	30.4	21	21.3	29.6	30.2	34	28.2
12:00	5.5	5.3	6.2	5.0	-0.4	3.7	30.1	22.5	23.3	27.2	28.4	31	26.1
13:00	5.5	5.4	5.8	4.9	-4.1	2.3	29.1	20.4	22.2	22.1	29	29	23.1
14:00	5.3	4.9	6.1	4.5	-5.2	1.9	26.4	23.5	25	19.1	29.3	32	26.5
15:00	4.2	3.9	5.2	4.0	-6.3	0.8	17.9	15.7	17	15.2	18.9	26.2	21.0
16:00	4.0	3.6	4.9	3.5	-4.6	1.3	16.6	17.1	17.1	16.3	18	23.6	20.3
17:00	3.9	3.5	4.2	3.2	-2.2	1.1	16.2	16.6	16.2	15.9	17.2	24.4	21.3

Table E-3: Measured data on 13 April 2016 (empty cooling space)

Time	T _{lin}	T _{rin}	T _{din}	T _{in}	T _{ein}	T _{eout}	T _{lou} t	T _{rout}	T _{dout}	T _{bout}	T _{up}	T _{cin}	T _{cout}
8:00	4	3.8	4.5	3.1	-6	-1.9	17.6	17.1	16.5	21.8	15.9	26.7	21.1
9:00	3.9	3.7	4.3	3	-0.8	1.6	21.2	17.3	16.7	28.2	19.2	24	20.8
10:00	4.7	4.6	5.1	3.9	-2.1	0.5	29.3	18.7	17.5	25.8	22.1	28.5	22.3
11:00	4.5	4.3	4.9	3.7	-3.6	-1.0	30.4	21.7	19.6	26.7	26.8	35.6	30.9
12:00	5.1	4.9	5.5	4.1	-4.4	-0.5	34.2	22.5	22.8	28.5	29.1	35.4	28.1
13:00	4.8	4.2	5.1	3.9	-5.0	-1.2	31.8	20.8	23.9	22.2	30.2	33.4	26.2
14:00	5.3	5.1	5.8	4.6	-4.5	-0.8	33	22.5	24.7	22.0	30.8	32	26.8
15:00	5.0	4.4	5.3	3.9	0.9	2.6	25.2	19.2	22.9	17.8	21.1	27.1	25.1
16:00	4.9	4.2	5.1	3.8	-5.2	-1.6	28.2	16.8	24.4	16.7	20.8	34.3	27.5
17:00	4.2	4.5	4.8	3.4	-0.7	1.0	24.3	16.5	25.7	15.8	20.3	23	20.5

Table E-4: Measured data on 14 April 2016 (empty cooling space)

Time	T _{lin}	T _{rin}	T _{din}	T _{in}	T _{ein}	T _{eout}	T _{lou} t	T _{rout}	T _{dout}	T _{bout}	T _{up}	T _{cin}	T _{cout}
8:00	4.1	3.8	4.2	3.1	-6.6	-1.9	16.7	14.5	13.5	20.5	16.8	23.5	17.6
9:00	4.5	3.9	4.6	3.0	-5.8	-1.3	23.7	15.4	15.8	25.6	19.8	26.5	22.1
10:00	4.1	3.9	4.2	3.1	-1.7	0.8	29.2	19	20.4	25.8	26.5	32.1	24.4
11:00	4.2	3.7	4.4	3.0	-4.3	-1.3	29.7	20.2	20.9	27.2	26.4	35.3	28.6
12:00	4.5	3.8	4.8	3.2	-4.5	-0.9	30.4	20.9	21.3	27.9	29.6	33.2	27.3
13:00	5.6	5.2	6.1	4.6	-3.2	-0.3	34.2	24	25.5	24.3	31.3	32.5	26.3
14:00	5.3	4.9	5.4	4.1	-3.8	-0.5	36.7	23.9	28.2	21.0	32.1	30.5	27.4
15:00	5.2	4.7	5.5	4.0	3.6	0.5	34.8	23.3	28.9	20.1	31.7	36.0	30.7
16:00	5.1	4.8	5.2	4.1	-4.2	-0.8	27.9	19.7	27.1	17.1	26.9	31.9	27.3
17:00	4.3	4.1	4.9	3.6	0.5	1.8	27	17.7	24.6	17.0	22.0	26.4	22.4

Table E-5: Measured data on 18 April 2016 (full cooling space)

Time	T _{lin}	T _{r in}	T _{din}	T _{in}	T _{ein}	T _{eout}	T _{lout}	T _{rout}	T _{dout}	T _{bout}	T _{up}	T _{cin}	T _{c out}	T _p
8:00	6.7	6.5	6.8	6	-5.3	1.6	23.8	17.3	17.8	26.5	19.5	28.5	24.3	21
9:00	11.9	11.5	12.6	10	-4.2	2.5	28.1	19.8	19.3	31	24.1	37.9	31.3	17.1
10:00	10.4	10.2	11.4	9.8	-5.1	1.9	30.3	22.2	22.6	32.3	27.9	39.5	35.4	15.8
11:00	10.3	9.7	10.8	8.8	-5.2	2.3	36.5	23.7	24.8	36.3	35.2	42.9	38.1	13.0
12:00	9.8	9.3	10.2	6.7	-5.3	2.0	40.8	28.3	29.2	31.6	36.8	40.4	36.2	9.2
13:00	8.1	7.5	8.5	5.4	-5.1	2.4	41.5	29.7	31.4	32.1	39.6	44.5	38.7	6.8
14:00	7.8	6.5	8.0	4.5	-6.2	0.9	37.9	27.9	32.1	27.5	38.1	39.7	32.3	6.2
15:00	7.6	6.4	7.9	4.9	-5.8	2.1	37.5	28.8	35	25.8	37.1	38.9	32.5	5.9
16:00	7.1	6.2	7.3	4.6	-6.5	0.5	32.4	24.3	32.5	21.2	32.7	38	30.8	5.1
17:00	6.8	5.9	6.8	4.5	-6.7	-0.9	31.8	23.6	30.7	20.8	28.4	37.5	29.3	5.0

Table E-6: Measured data on 19 April 2016 (full cooling space)

Time	T _{lin}	T _{r in}	T _{din}	T _{in}	T _{ein}	T _{eout}	T _{lout}	T _{rout}	T _{dout}	T _{bout}	T _{up}	T _{cin}	T _{c out}	T _p
8:00	6.8	6.7	6.9	6.1	-1.9	3.8	17.5	16.5	16	19.7	17.8	28.3	21.4	5.6
9:00	5.9	5.3	6.5	4.9	1.1	4.2	18.1	16.8	16.2	18.3	17.3	20	18.9	5.2
10:00	5.6	5.2	6.1	4.7	-0.7	2.9	22.6	17.3	17.3	23.4	21.7	27.8	21.6	5.2
11:00	5.6	5.3	5.9	4.6	-1.5	2.7	26.7	19.8	20.5	25.4	24.3	36.5	29.6	5.1
12:00	5.7	5.4	6.2	4.8	-2.0	2.4	29.8	23.2	22.1	28.6	26.8	37.7	28.9	5.0
13:00	6.1	5.5	6.8	4.3	-2.5	1.7	34.5	26.3	25.6	26.6	35.7	38.2	29.8	4.8
14:00	6.4	5.7	6.7	4.8	-2.9	1.2	39.6	30.4	31.2	26.2	38.8	36.5	29.3	5.1
15:00	5.8	4.9	6.4	4.2	-2.8	0.9	34.2	26.7	31.7	24.1	30.3	37.8	27.5	4.7
16:00	5.4	4.7	5.8	4.0	-4.5	-0.5	28.0	22.4	28.4	19.3	26.8	29.5	23.1	4.5
17:00	4.9	3.9	5.2	3.5	-4.6	-0.8	23.5	18	24.1	19.8	23.1	31.5	24.1	4.2

Table E-7: Ampere-hour consumed by the DC compressor

Time\Date	12 April	13 April	14 April	18 April	19 April	20 April
8:00	3.95	3.7	3.82	3.83	3.87	0
9:00	3.91	0	4.05	4.33	0	4.23
10:00	4.3	3.8	0	4.55	4.02	4.54
11:00	3.9	3.95	3.92	4.58	4.25	4.61
12:00	3.6	3.84	3.64	4.86	4.42	4.15
13:00	3.7	3.94	4.19	4.50	4.65	3.85
14:00	3.91	3.85	4.3	4.11	4.5	4.16
15:00	3.45	0	4.2	4.75	4.42	4.07
16:00	3.56	3.98	3.96	4.81	4.35	3.95
17:00	3.53	0	0	4.57	4.15	4.10

Appendix F: sample calculations

F-1: solar radiation incident on PV panels

Day: 18 April 2016

Latitude: $L = -33.93^\circ$,

Longitude: $Long = 18.46^\circ$,

Solar constant: $I_{SC} = 1367 \text{ W/m}^2$

PV panel inclination angle: $\beta = 30^\circ$

Ground reflectance: $\rho = 0.2$

Local time 9:00

The horizontal radiation incident $I_h = 265.1 \text{ W/m}^2$

The diffuse radiation incident $I_d = 21.12 \text{ W/m}^2$

The beam radiation $I_b = I_h - I_d$
 $= 265.1 - 21.12 = 243.98 \text{ W/m}^2$

From equation (3.17):

Hour angle: $\omega = 15(t - t_{\text{noon}})$

$t = 9 \text{ h}$

$t_{\text{noon}} = 720 + 4 \times \text{longitude}$ - equation of time Eq (3.18)

Equation of time = $9.87 \sin 2B - 7.53 \cos B - 1.5 \sin B$ Eq (3.19)

$B = 360 \times (n - 81) / 365$ Eq (3.20)

On the 18 April, $n = 108$ from Table 3.2

Therefore:

$B = 360 \times (108 - 81) / 365 = 26.63$

Equation of time = $9.87 \sin (2 \times 26.63) - 7.53 \cos (26.63) - 1.5 \sin (26.63)$
 $= 0.509$

$t_{\text{noon}} = 720 + 4 \times 18.46 - 0.509$
 $= 793.33 \text{ minutes} = 13.22 \text{ h}$

$\omega = 15 (9 - 13.22)$
 $= -63.3$

From equation (3.16), declination angle: $\delta = 23.45 \times \sin [360 \times (284 + n) / 365]$
 $= 23.45 \times \sin [360 \times (284 + 108) / 365]$
 $= 10.51^\circ$

From equation (3.14), Incident angle of beam radiation $\theta_i = \cos^{-1} [\cos (L + \beta) \times \cos \delta \times \cos \omega + \sin (L + \beta) \times \sin \delta]$

$\theta_i = \cos^{-1} [\cos (-33.93 + 30) \times \cos 10.51 \times \cos -63.3 + \sin (-33.93 + 30) \times \sin 10.51]$
 $\theta_i = 64.64^\circ$

From equation (3.15), Zenith angle $\theta_z = \cos^{-1} [\cos L \times \cos \delta \times \cos \omega + \sin L \times \sin \delta]$
 $\theta_z = \cos^{-1} [\cos -33.93 \times \cos 10.51 \times \cos -63.3 + \sin -33.93 \times \sin 10.51]$

$$= 74.65^\circ$$

From equation (3.13), the beam radiation ratio $R_b = \cos \theta_i / \cos \theta_z$

$$= \cos 64.64 / \cos 74.65$$

$$= 1.66$$

From equations (3.11) and (3.12), $F_1 = \max [0; (f_{11} + \Delta f_{12} + \pi \theta_z f_{13} / 180)]$,

$$F_2 = f_{21} + \Delta f_{22} + \pi \theta_z f_{23} / 180$$

$$\Delta = m \times I_d / I_{on} \quad \text{Eq (3.8)}$$

$$m = 1 / \cos \theta_z \quad \text{Eq (3.9)}$$

$$= 1 / \cos 74.65$$

$$= 3.779$$

$$I_{on} = I_{sc} (1 + 0.033 \cos (360n/365) \times \cos \theta_z) \quad \text{Eq (3.10)}$$

$$= 1367(1 + 0.033 \cos (360 \times 108/365) \times \cos 74.65)$$

$$= 1264 \text{ W/m}^2$$

$$\Delta = 3.779 \times 21.12 / 1264$$

$$= 0.063$$

$$\varepsilon = [(I_d + I_{b,n}) / I_d + 5.535 \times 10^{-6} \times \theta_z^3] / (1 + 5.535 \times 10^{-6} \times \theta_z^3) \quad \text{Eq (3.6)}$$

$$I_{b,n} = I_b / \cos \theta_z \quad \text{Eq(3.7)}$$

$$= 243.98 / \cos 74.65$$

$$= 922.07$$

$$\varepsilon = [(21.12 + 922.07) / 21.12 + 5.535 \pi 10^{-6} \times 74.65^3] / (1 + 5.535 \times 10^{-6} \times 74.65^3)$$

$$= 14.21$$

Therefore from appendix C-1,

$$f_{11} = 0.678, f_{12} = -0.327, f_{13} = -0.250,$$

$$f_{21} = 0.156, f_{22} = -1.377, f_{23} = 0.251$$

$$F_1 = [0.678 + (0.063 \times -0.327) + (\pi \times 74.65 \times -0.25 / 180)]$$

$$= -0.331$$

$$F_2 = [0.156 + (0.063 \times -1.377) + (\pi \times 74.65 \times 0.251 / 180)]$$

$$= 0.396$$

From equation (3.3), the total solar radiation incident on 30° PV panel is:

$$I_T = R_b \times I_b + I_d [(1 - F_1) \times (1 + \cos \beta) / 2 + F_1 (a/b) + F_2 \sin \beta] + I_h \rho_g (1 - \cos \beta) / 2$$

$$a = \max (0; \cos \theta_i) \quad \text{Eq (3.4)}$$

$$= \max (0 ; 0.4407)$$

$$b = \max (0; \cos \theta_z) \quad \text{Eq (3.5)}$$

$$= \max (0 ; 0.264)$$

Therefore:

$$\begin{aligned}
I_T &= R_b \times I_b + I_d [(1 - F_1) \times (1 + \cos \beta)/2 + F_1 (a/b) + F_2 \sin \beta] + I_n \rho_g (1 - \cos \beta)/2 \\
&= 1.66 \times 243.98 + 21.12[(1 - 0.331) (1 + \cos 30)/2 + 0.331(0.4407/0.2646) + 0.396 \\
&\cos 30] + 265.1 \times 0.2 \times (1 - \cos 30)/2 \\
&= 437.55 \text{ W/m}^2
\end{aligned}$$

F-2: Coefficient of performance (COP) of the cooling system

From equation (3.21), the coefficient of performance is

$$\text{COP} = Q_{\text{refl}}/W$$

$$Q_{\text{refl}} = \dot{m} (h_1 - h_4) \quad \text{Eq (3.22)}$$

$$W = \dot{m} (h_2 - h_1) \quad \text{Eq (3.23)}$$

$$\text{Therefore, COP} = (h_1 - h_4) / (h_2 - h_1)$$

From table E-5 in appendix E at 14:00, $T_{\text{ein}} = -6.2 \text{ }^\circ\text{C}$

From R-134a tables,

$$-8 \longrightarrow 204.52$$

$$-6.2 \longrightarrow h_4$$

$$-6 \longrightarrow 203.07$$

$$h_4 = 204.52 + [(-6.2-8) / (-6-8)] (203.07 - 204.54)$$

$$= 203.049 \text{ kJ/kg}$$

To get h_1 at $T_{\text{eout}} = 0.9 \text{ }^\circ\text{C}$

$$0 \longrightarrow 250.45$$

$$0.9 \longrightarrow h_1$$

$$1 \longrightarrow 251.61$$

$$h_1 = 250.45 + (0.9/2) (251.61 - 250.45)$$

$$= 250.972 \text{ kJ/kg}$$

To get h_2 at $T_{\text{cin}} = 39.7 \text{ }^\circ\text{C}$

$$38 \longrightarrow 270.39$$

$$39.7 \longrightarrow h_2$$

$$40 \longrightarrow 271.27$$

$$h_2 = 270.39 + [(39.7-38)/(40-38)](271.27 - 270.39)$$

$$= 271.138 \text{ kJ/kg}$$

$$\text{COP} = (250.972 - 203.049) / (271.138 - 250.972)$$

$$\text{COP} = 2.37$$

F-3: Total heat load of the refrigeration model

From equation (2.0), the sensible heat through the surface is:

$$Q_{\text{leak}} = UA\Delta T$$

$$U = 1 / [(x_1/k_1) + (x_2/k_2) + (x_3/k_3)]$$

$$= 1 / [(0.003/0.23) + (0.045/0.02) + (0.002/205)] \quad \text{table 2.1}$$

$$0.522 \text{ W/m}^2 \cdot \text{k}$$

The size of the cooling model is 0.6m x 0.45m x 0.65m

From table E-5 in appendix E,

At 8:00 heat leak from left side wall is

$$Q_{leak} = 0.522 \times 0.6 \times 0.65 \times (23.8 - 6.7)$$

$$= 3.48 \text{ W}$$

Right side wall

$$Q_{leak} = 0.522 \times 0.6 \times 0.65 \times (17.3 - 6.5)$$

$$= 2.19 \text{ W}$$

Door

$$Q_{leak} = 0.522 \times 0.45 \times 0.65 \times (17.8 - 6.8)$$

$$= 1.67 \text{ W}$$

Up side

$$Q_{leak} = 0.522 \times 0.45 \times 0.6 \times (19.5 - 6.8)$$

$$= 1.789 \text{ W}$$

Back side

$$Q_{leak} = 0.522 \times 0.45 \times 0.65 \times (26.5 - 6.7)$$

$$= 3.02 \text{ W}$$

The total heat leaked to the system is:

$$Q_{leak} = 12.15 \text{ W}$$

From equation (2.5), the sensible heat from 20kg of apples is

$$Q_{p-res} = mC_p(T_1 - T_2)$$

$$= 20 \times 3.82 (21 - 17.1)$$

$$= 297.96 \text{ kJ}$$

$$Q_{p-res} = 297.96 \times 1000 / 3600$$

$$= 82.76 \text{ W}$$

From table 2.5 the respiration load is

$$Q_{p-res} = 20 \times 0.329$$

$$= 0.658$$

The heat from fan is

$$Q_{fan} = 2 \text{ W} \quad (\text{fan specification})$$

Therefore, the total heat load is

$$Q_{ref} = \sum Q_{leak} + \sum Q_{p-sen} + \sum Q_{fan} + \sum Q_{p-res}$$

$$= 12.15 + 82.76 + 2 + 0.658$$

$$= 97.56 \text{ W}$$